Eph Receptor Clustering by Chondroitin Sulfate Inhibits Axon Regeneration

Thesis by

Gregory Martin Miller

In Partial Fulfillment of the Requirements for

the degree of

Doctor of Philosophy

CALIFORNIA INSTITUTE OF TECHNOLOGY

Pasadena, California

2018

(Defended December 18, 2017)

ACKNOWLEDGEMENTS

For my family, Lon, MaryAnne, Murissa, Tiffany, Darla, and Norman.

PUBLISHED CONTENT AND CONTRIBUITIONS

Chapter 1: Sugar-Dependent Modulation of Neuronal Development, Regeneration, and Plasticity by Chondroitin Sulfate Proteoglycans

Miller, Gregory M., and Linda C. Hsieh-Wilson. “Sugar-dependent modulation of neuronal development, regeneration, and plasticity by chondroitin sulfate proteoglycans.” *Experimental Neurology* 274 (2015): 115-125. doi: 10.1016/j.expneurol.2015.08.015

G.M.M participated in the writing of the manuscript.

ABSTRACT

Chondroitin sulfate proteoglycans (CSPGs) play important roles in the developing and mature nervous system, where they guide axons, maintain stable connections, restrict synaptic plasticity, and prevent axon regeneration following CNS injury. The chondroitin sulfate glycosaminoglycan (CS GAG) chains that decorate CSPGs are essential for their functions. Through these sugar chains, CSPGs are able to bind and regulate the activity of a diverse range of proteins and through these interactions can regulate neuronal growth. These CS-protein interactions depend on specific sulfation patterns within the CS GAG chains, and accordingly, particular CS sulfation motifs are upregulated during development, in the mature nervous system, and in response to CNS injury. Thus, spatiotemporal regulation of CS GAG biosynthesis may provide an important mechanism to control the functions of CSPGs and modulate intracellular signaling pathways. Here, we will discuss these sulfation-dependent processes and highlight how the CS sugars on CSPGs contribute to neuronal growth, axon guidance, and plasticity in the nervous system.

Chondroitin sulfate proteoglycans (CSPGs) are a major barrier to regenerating axons in the central nervous system (CNS), exerting their inhibitory effect through their polysaccharide side chains. Chondroitin sulfate (CS) potently inhibits axon regeneration through modulation of inhibitory signaling pathways induced by carbohydrate binding to protein ligands and receptors. Here, we identify a novel carbohydrate-protein interaction between CS and EphA4 that inhibits axon regrowth. We characterize the mechanism of activation and demonstrate how carbohydrate binding induces phosphorylation of the intracellular kinase domain through clustering of cell surface EphA4. Collectively, our studies present a novel mechanism of EphA4 activation by CS independent of the canonical ephrin ligands and uncover the role of this interaction in inhibition of neurite regrowth after

injury. Our results underscore a mechanism of action by which carbohydrates can function as direct, activating ligands for protein receptors and provide mechanistic insights into the inhibition of axon growth by CS following injury to the CNS.

Chondroitin sulfate proteoglycans (CSPGs) regulate neuronal plasticity, as well as axon regeneration and guidance through their ability to bind protein ligands and cell surface receptors. In this way, extracellular CSPGs can modulate the activity of intracellular signaling pathways. Here, a computational analysis of EphA4-CS interactions is performed to characterize the importance of key arginine and lysine residues towards CS binding, and to identify structural differences in CS-A, CS-C, CS-D, and CS-E docking to EphA4. Carbohydrate-induced Eph receptor clustering could be a general mechanism of Eph receptor activation. To identify additional Eph receptors that interact with CS, CS-E was docked to all EphA and EphB family members to predict relative binding affinities. The relative strengths of the predicted binding energies are: EphB4 > EphA8 > EphA1 > EphA3 > EphB1 > EphB3 > EphA7 > EphA5 > EphA4 > EphA6 > EphB2 > EphB6 > EphA2. In addition, the arginine and lysine residues that mediate CS binding are identified for each Eph receptor. These computational predictions provide mechanistic insights into Eph receptor activation by chondroitin sulfate and have implications for inhibition of axon regeneration following injury to the nervous system and axon guidance during development.

Table of Contents

Acknowledgements…….. iii

Published Content and Contributions…… iv

Abstract……....…… v

Table of Contents…….. vii

List of Figures……....……... viii

Chapter 1:	Sugar-Dependent Modulation of Neuronal Development, Regeneration, and Plasticity by Chondroitin Sulfate Proteoglycans	1
Chapter 2:	Carbohydrate-Induced Eph Receptor Clustering Inhibits Neurite Growth	44
Chapter 3:	Computational Characterization of Eph Receptor Interactions with Chondroitin Sulfate	80
Appendix A:	Retinal Axon Guidance by Synthetic Chondroitin Sulfate Polymers	120
Appendix B:	Disaccharide Analysis of the Visual Cortex of Sulfotransferase Knockout Mice	126

List of Figures

Chapter 1: **Sugar-Dependent Modulation of Neuronal Development, Regeneration, and Plasticity by Chondroitin Sulfate Proteoglycans**

Figure 1.1 Biosynthesis of Chondroitin Sulfate motifs 5

Figure 1.2 Modulation of intracellular signaling pathways by chondroitin sulfate 13

Chapter 2: **Carbohydrate Induced Eph Receptor Clustering Inhibits Neurite Growth**

Figure 2.1 EphA4 binds the glycosaminoglycan side chains of CSPGs 48

Figure 2.2 CS expression and EphA4 binding to Neu7 astrocytes 50

Figure 2.3 DRGs lacking EphA4 show improved neurite outgrowth when cultured on a substratum of inhibitory CS 51

Figure 2.4 CS clusters cell surface EphA4 53

Figure 2.5 CS induces tyrosine phosphorylation of EphA4 54

Figure 2.6 Receptor clustering and phosphorylation is independent of the ligand binding domain 57

Figure 2.7 Computational docking of CS-E hexasaccharide 58

Figure 2.8 Loss of carbohydrate binding attenuates EphA4 phosphorylation 60

Figure 2.9 Microfluidic Axotomy Assay 61

Figure 2.10 Lentivirus expression of mutant EphA4 receptor 62

Figure 2.11 Loss of CS-E binding promotes axon regeneration 64

Chapter 3: **Computational Characterization of Eph Receptor Interactions with Chondroitin Sulfate**

Figure 3.1	CS-A, CS-C, CS-D, and CS-E hexasaccharide docking to site 1 of EphA4	84
Figure 3.2	CS-A, CS-C, CS-D, and CS-E hexasaccharide docking to site 2 of EphA4	85
Figure 3.3	Summarized docking data for CS-A, CS-C, CS-D, and CS-E hexasaccharide docking to EphA4	87
Figure 3.4	CS-E docking to EphA4 mutants	89
Figure 3.5	Per-Residue Energy Decomposition for site 1	91
Figure 3.6	Per-Residue Energy Decomposition for site 2	92
Figure 3.7	Per-Residue Energy Decomposition for site 1 and site 2	93
Figure 3.8	Summarized docking data CS-E hexasaccharide docking to EphA and EphB family members	95
Figure 3.9	CS-E hexasaccharide docking to EphA1	96
Figure 3.10	CS-E hexasaccharide docking to EphA2	97
Figure 3.11	CS-E hexasaccharide docking to EphA3: site1	98
Figure 3.12	CS-E hexasaccharide docking to EphA3: site 2	99
Figure 3.13	CS-E hexasaccharide docking to EphA4: site 1	100
Figure 3.14	CS-E hexasaccharide docking to EphA4: site 2	101
Figure 3.15	CS-E hexasaccharide docking to EphA5	102
Figure 3.16	CS-E hexasaccharide docking to EphA6	103
Figure 3.17	CS-E hexasaccharide docking to EphA7	104

Figure 3.18 CS-E hexasaccharide docking to EphA8 105

Figure 3.19 CS-E hexasaccharide docking to EphB1: site 1 106

Figure 3.20 CS-E hexasaccharide docking to EphB1: site 2 107

Figure 3.21 CS-E hexasaccharide docking to EphB2 108

Figure 3.22 CS-E hexasaccharide docking to EphB3 109

Figure 3.23 CS-E hexasaccharide docking to EphB4 110

Figure 3.24 CS-E hexasaccharide docking to EphB6 111

Appendix A: **Retinal Axon Guidance by Synthetic Chondroitin Sulfate Polymers**

Figure A.1 Stripe Assay, Assessment of Axon Guidance of Retinal Neurons 121

Figure A.2 Retinal Axon Guidance by CS Mimetic Polymers 123

Appendix B: **Disaccharide Analysis of the Visual Cortex of Sulfotransferase Knockout Mice**

Figure B.1 Disaccharide Analysis of Chst11 and Chst15 Knockout Mice 128

Figure B.2 Disaccharide Analysis of Visual Cortex 129

Figure B.3 Disaccharide Analysis of Visual Cortex as Molar Percentage 131

Chapter 1: Sugar-Dependent Modulation of Neuronal Development, Regeneration, and Plasticity by Chondroitin Sulfate Proteoglycans

Abstract

Chondroitin sulfate proteoglycans (CSPGs) play important roles in the developing and mature nervous system, where they guide axons, maintain stable connections, restrict synaptic plasticity, and prevent axon regeneration following CNS injury. The chondroitin sulfate glycosaminoglycan (CS GAG) chains that decorate CSPGs are essential for their functions. Through these sugar chains, CSPGs are able to bind and regulate the activity of a diverse range of proteins. CSPGs have been found both to promote and inhibit neuronal growth. They can promote neurite outgrowth by binding to various growth factors such as midkine (MK), pleiotrophin (PTN), brain-derived neurotrophic factor (BDNF), and other neurotrophin family members. CSPGs can also inhibit neuronal growth and limit plasticity by interacting with transmembrane receptors such as protein tyrosine phosphatase σ (PTPσ), leukocyte common antigen-related (LAR) receptor protein tyrosine phosphatase, and the Nogo receptors 1 and 3 (NgR1 and NgR3). These CS-protein interactions depend on specific sulfation patterns within the CS GAG chains, and accordingly, particular CS sulfation motifs are upregulated during development, in the mature nervous system, and in response to CNS injury. Thus, spatiotemporal regulation of CS GAG biosynthesis may provide an important mechanism to control the functions of CSPGs and to modulate intracellular signaling pathways. Here, we will discuss these sulfation-dependent processes and highlight how the CS sugars on CSPGs contribute to neuronal growth, axon guidance, and plasticity in the nervous system.

Introduction

Chondroitin sulfate proteoglycans (CSPGs) play critical roles in the developing central nervous system (CNS) and in response to adult CNS injury. During embryonic development, axons must elongate, navigate specific paths, and form synapses with their target neurons. To establish precise patterns of connectivity, a range of attractive or repulsive cues guide axons to their proper targets. Several families of extracellular receptors and their ligands are known to attract or repel growth cones, including netrins, ephrins, semaphorins, and slits.[1,2] In addition to these prototypical axon guidance molecules, increasing evidence suggests that the chondroitin sulfate (CS) sugars on CSPGs can serve as guidance cues for growth cones and contribute to the formation of neuronal boundaries in the developing CNS.[3–5] CSPGs are also major components of perineuronal nets (PNNs), where they play crucial roles in the maturation of synapses and the closure of critical periods by limiting synaptic plasticity.[6–9] In the adult CNS, CSPGs are dramatically upregulated in the glial scar around injury sites, where they restrict synaptic and anatomical plasticity, neuronal regeneration, and repair.[10–13] Enzymatic digestion of the CS GAG chains on CSPGs can promote axon regeneration, sprouting, and functional recovery in *in vivo* models of CNS injury, underscoring again critical roles for CS sugars. In this review, we will highlight the various functions of the CS sugars on CSPGs and how they contribute to neuronal growth, axon guidance, and plasticity in the nervous system. We will also discuss strong evidence that specific sulfated motifs within CS chains can serve as ligands for extracellular receptors, thereby enabling CSPGs to activate key signaling pathways important for neuronal development and function.

Structure of chondroitin sulfate proteoglycans

CSPGs are composed of a core protein with one or more covalently attached CS GAG chains.[11,14] They are major components of the extracellular matrix (ECM), where they provide structural support and modulate neuronal activity.[8,11,15] In addition, some CSPGs are inserted into the membrane via a single membrane-spanning domain or a glycosylphosphatidylinositol (GPI) anchor, or are localized to secretory granules. The most abundant CSPGs in the CNS are members of the lectican family, which is composed of aggrecan, brevican, neurocan, and versican.[16] Lecticans contain an N-terminal G1 domain, C-terminal G3 domain, and a central region decorated with varying numbers of CS chains (ranging from 1 to >100). Aggrecan, unlike the other lecticans, also contains a G2 domain following the N-terminal G1 domain.[16] The phosphacan or receptor-type protein-tyrosine phosphatase zeta (PTPζ/RPTPβ) family, which consists of both transmembrane and soluble secreted forms, is expressed predominantly in the CNS and is found in neurons and astrocytes throughout development and adulthood.[17,18] The small leucine-rich proteoglycans (SLRPs) such as decorin and biglycan have N-terminal binding sites for 1 or 2 CS chains and leucine-rich repeats flanked by cysteine residues in their central domain.[19] Another prominent CSPG in the nervous system is NG2, a transmembrane proteoglycan with a CS chain attached to its large extracellular domain.[20]

Structure of chondroitin sulfate sugars

Proteoglycan core proteins are decorated at certain serine residues with CS GAG chains via a tetrasaccharide linker. CS GAGs are linear polysaccharides comprosed of a repeating disaccharide unit containing *N*-acetyl-D-galactosamine (GalNAc) and D-glucuronic acid (GlcA).[21,22] Each chain contains up to 100 disaccharide units and

undergoes extensive sulfation in the Golgi by chondroitin sulfotransferases.[23,24] The commonly occurring CS disaccharide units are characterized by the number and position of their sulfate modifications (Fig. 1.1a). For instance, the monosulfated CS-A and CS-C motifs contain sulfate groups at the 4-*O* and 6-*O* positions of the GalNAc residue, respectively, and are generated by the sulfotransferases chondroitin 4-*O*-sulfotransferase (C4ST) and chondroitin 6-*O*-sulfotransferase (C6ST), respectively (Fig. 1.1b). The disulfated CS-D unit is synthesized from the CS-C precursor via 2-*O* sulfation of the GlcA residue by uronyl 2-*O*-sulfotransferase (UST), while the CS-E unit is generated from a CS-A unit by 6-*O* sulfation of the GalNAc residue by the sulfotransferase *N*-acetylgalactosamine 4-sulfate 6-*O*-sulfotransferase (GalNAc4S-6ST). Thus, a suite of sulfotransferase enzymes works in concert to produce a structurally complex, heterogeneously sulfated polysaccharide. This non-template driven process results in diverse patterns of sulfation that allow CS GAGs to interact with a wide range of proteins, including different growth factors, cytokines, and transmembrane receptors.

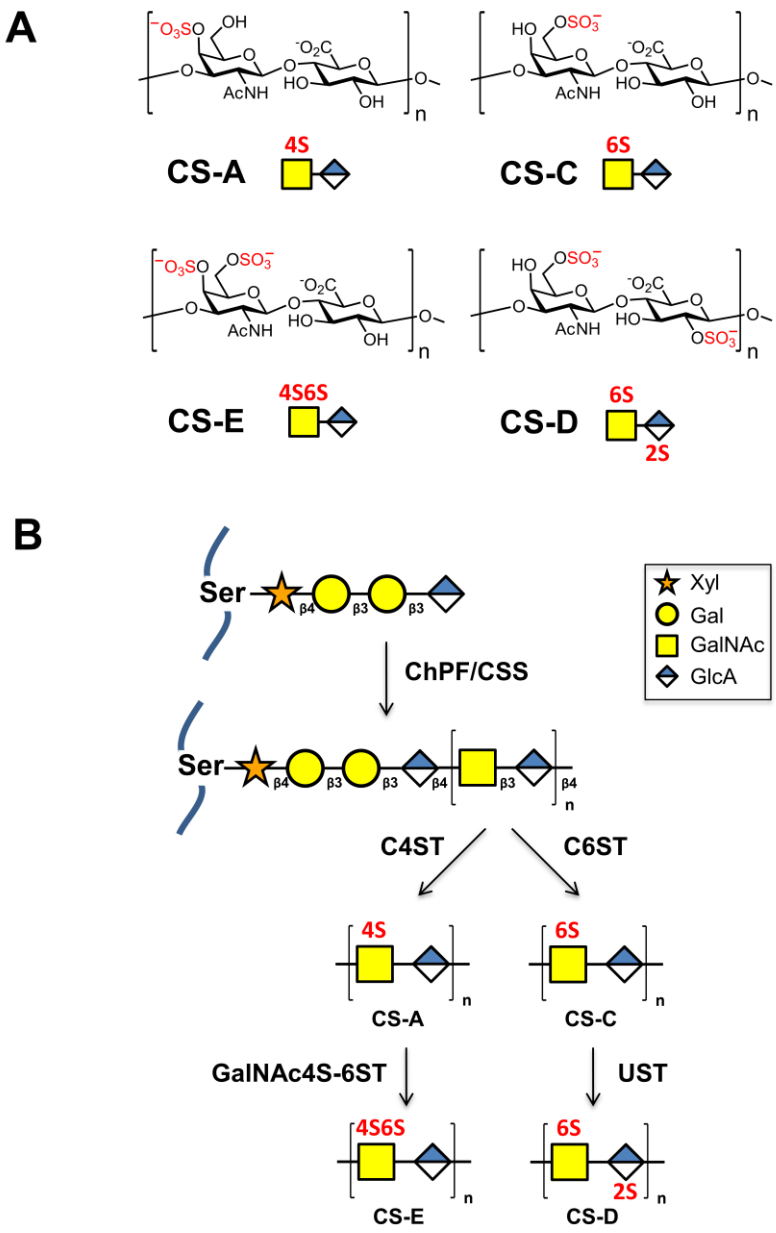

Figure 1.1: Biosynthesis of Chondroitin Sulfate motifs (**a**) Common sulfation motifs of chondroitin sulfate, which consists of the repeating disaccharide *N*-acetyl-D-galactosamine-β(1,3)-D-glucuronic acid. n = 20-100. CS-A and CS-C are monosulfated at the 4-*O* and 6-*O* positions of GalNAc, respectively. CS-D is sulfated at the 2-*O* position of GlcA and 6-*O* position of GalNAc. CS-E is sulfated at the 4-*O* and 6-*O* positions of GalNAc. (**b**) Biosynthesis of chondroitin sulfate. A core tetrasaccharide (xylose (Xyl)-galactose (Gal)-galactose (Gal)-glucuronic acid (GlcA)) is appended to serine residues of the core proteoglycan. Chain extension is performed by chondroitin sulfate synthase (CSS) and chondroitin polymerizing factor (ChPF). The polysaccharide chains are then elaborated through sulfation by C4ST to generate CS-A or C6ST to generate CS-C, followed by GalNAc4S-6ST or UST to form CS-E or CS-D, respectively.

CSPG receptors

Many of the diverse functions of CSPGs arise from their ability to bind a large number of protein partners. CSPGs interact with various proteins in the ECM, including fibronectin, laminin, neural cell adhesion molecule (NCAM), and neural glial cell adhesion molecule (NgCAM).[25–27] Through these interactions, CSPGs can block laminin-mediated integrin activation, as well as cell adhesion molecules important for promoting neuronal migration and growth.[28–30] CSPGs are also known to interact with a variety of growth factors, such as midkine (MK), pleiotrophin (PTN), nerve growth factor (NGF), and brain-derived neurotrophic factor (BDNF), and in some cases can help assemble growth factor-receptor complexes.[31–35] In this way, CSPGs can modulate growth factor signaling pathways by presenting soluble factors to their cell surface receptors and/or potentially sequestering them from their cell surface receptors. It is becoming increasing clear that CSPGs can also interact with and modulate the activity of many membrane-associated proteins, including the protein tyrosine phosphatases PTPσ and leukocyte common antigen-related (LAR) and the Nogo receptors NgR1 and NgR3.[36–39] For example, the interaction of CS and heparan sulfate (HS) GAGs with the thrombospondin repeats of semaphorin 5A (Sema5A) guides neurons in the developing diencephalon fiber tract, with each interaction resulting in different functional outcomes. While HS is required for Sema5A-mediated attraction, the interaction with CS converts Sema5A to a repulsive guidance cue, suggesting that neuronal responses to axon guidance cues can depend on their GAG binding status.[40] We will highlight additional examples below where the CS sugar chains mediate the interactions and activity of CSPGs toward their protein partners.

Regulation of the 'sulfation code'

The sulfation profiles of CS are spatially and temporally regulated in a tissue-specific and cell type-specific manner. In the nervous system, particular CS sulfation motifs are upregulated during early and postnatal development.[33,41–44] For example, distinct immunohistochemical patterns are exhibited by monoclonal antibodies that recognize sulfated CS chains (antibodies CS-56, 2H6 and MO-225). Although these antibodies recognized a varied set of overlapping epitopes, each revealed distinct CS expression patterns in the brain.[45] For example, the CS-56 and 2H6 epitopes were highly expressed in the postnatal day 7 (P7) mouse cortex and showed decreased expression in P12 and P20 cortical tissue.[22,33] In the cerebellum, CS-56 immunoreactivity was detected at P7 and P12 but was absent at P20. Interestingly, the MO-225 epitope was not observed in the cortex but showed strong expression in the cerebellum at P7, P12, and P22.[33,45]

Additional insights into the expression dynamics of CS motifs were obtained from high-performance liquid chromatography (HPLC) analysis of CS disaccharides following digestion of the GAG chains. The monosulfated CS-A motif was the most abundant motif in the embryonic mouse cortex and cerebellum, and its levels increased as development progressed.[42,44,46] Expression of the CS-C motif was highest during embryonic development and steadily decreased through development, but it remained the second most abundant CS motif.[42,44,46] Interestingly, the disulfated CS-E motif exhibited its highest expression in the embryonic mouse cortex, and its levels decreased into adulthood but remained higher in the cortex than in the cerebellum.[42,44,46] In contrast, expression of the disulfated CS-D motif was highest in the cerebellum and peaked around P10.[42,46] Notably, deletion of these highly sulfated motifs by genetic knockdown of the sulfotransferases UST

and GalNAc4S-6ST via *in utero* electroporation resulted in impaired migration of cortical neurons *in vivo*.[42] Electroporated neurons accumulated in the lower intermediate zone and the subventricular zone and did not migrate radially in the neocortex.

In addition to dynamic changes in CS sulfation, the expression of specific CS sulfotransferases is spatially and temporally regulated.[42,43,45–48] Widespread mRNA expression of *C4ST* and *GalNAc4S-6ST* was observed in the cortex, hippocampus, cerebellum, striatum, and the olfactory bulb during postnatal development and into adulthood, while *UST* was preferentially expressed in the developing cerebellum.[44,48] In the cerebellum, expression of *GalNAc4S-6ST* shifted during postnatal development from the external to the internal granular layer.[46,48] This change in sulfotransferase mRNA expression profile matched the levels of CS-E expression observed by immunostaining and coincided with the migration and maturation of granular cells.[48]

Interestingly, studies suggest that proteoglycans possess well-defined GAG sequences. For example, early studies demonstrated that the CS chains of phosphacan purified from P20 mouse brains contained a higher abundance of the CS-D motif compared to those of phosphacan purified from P7 and P12 brains, and accordingly, they exhibited higher binding affinity for the growth factor PTN.[33] More recently, GAG fragments of similar size and charge were isolated from the heparan sulfate proteoglycan bikunin, and mass spectrometry sequencing revealed a single, defined sequence motif.[49]

Together, multiple lines of evidence indicate that the sulfation patterns on CS chains are specific and highly controlled. Spatiotemporal regulation of CS GAG biosynthesis could provide an important mechanism to modulate the interactions and functions of CSPGs and activate intracellular signaling pathways. Moreover, the concerted

expression of particular sulfation motifs on different proteoglycan core proteins could provide an elegant mechanism to coordinate the activities of various CSPGs. In this review, we will discuss current hypotheses regarding CSPGs and evidence supporting an important role for the sulfated CS chains in mediating the diverse activities of CSPGs toward neurons.

CSPGs as stimulatory cues for neuronal growth

Although CSPGs are traditionally considered inhibitory molecules, they are sometimes expressed in growth-permissive regions, such as the neocortical subplate where thalamocortical afferent axons grow.[50,51] As such, CSPGs do not always constitute a barrier to axon initiation or outgrowth and may also participate in axon extension and pathfinding. In fact, numerous studies have established the ability of CSPGs to stimulate neurite outgrowth *in vitro*, and their growth-promoting activity depends on the CS sugar chains.

Role of CS sulfation patterns

The stimulatory effects of CSPGs on cultured neurons vary with the CS sulfation pattern and neuron type. CS chains enriched in highly sulfated motifs have been shown to promote neurite outgrowth of embryonic neurons *in vitro*.[52–59] For example, the phosphacan variant DSD-1-PG contains a specific sugar epitope, DSD-1, that stimulates the outgrowth of embryonic day 18 (E18) rat hippocampal neurons and E14 mesencephalic neurons.[55,56] The growth-promoting effects of DSD-1-PG were blocked by removal of the sugar chains or by the monoclonal antibody (mAb) 473HD, which recognizes the DSD-1 sugar epitope.[53,55,57] Polysaccharides enriched in the disulfated CS-D sulfation motif inhibited the interaction of mAb 473HD and DSD-1-PG, suggesting that CS-D may compose part of the DSD-1 epitope.[53,54,58] Further characterization of mAb 473HD demonstrated that it recognized the tetrasaccharide sequence A-D or D-A.[60] Both CS-D

and DSD-1 interacted strongly with PTN (also known as HB-GAM) and promoted neurite outgrowth, at least in part, through those interactions.[33,52] PTN induced cortical cell migration *in vitro* through the proteoglycan receptor RPTPβ, and this activity was blocked by the addition of RPTPβ antibodies, the tyrosine phosphatase inhibitor sodium vanadate, or exogenous CS.[61]

Interestingly, while CS-D-enriched polysaccharides promoted the outgrowth of dendrite-like extensions in cultured embryonic hippocampal neurons, polysaccharides enriched in the disulfated CS-E motif promoted the outgrowth of a single, axon-like extension.[57] Moreover, the activity of CS-E was not blocked by mAb 473HD, suggesting that a structurally distinct epitope from DSD-1 is responsible for the growth-promoting effects.[54,58] Both CS-D- and CS-E-enriched polysaccharides bound preferentially to a variety of growth factors. MK and PTN appeared to have similar affinities for DSD-1, CS-D, and CS-E but did not interact strongly with CS-A- or CS-C-enriched polysaccharides.[31,33,62] Similarly, other neurotrophic factors such as NGF, BDNF, neurotrophin-3 (NT-3), and neurotrophin-4/5 (NT-4/5) showed preferential binding to CS-E compared to CS-A or CS-C polysaccharides.[32,34]

In addition to CS, GAGs such as HS and dermatan sulfate (DS) can also bind to growth factors, including MK, PTN, FGF, and BDNF, and promote neurite outgrowth.[45,63–65] Heparan sulfate proteoglycans (HSPGs) stimulated neurite outgrowth of cultured rat sympathetic neurons, spinal cord neurons, chick retinal neurons, and motor neurons in a GAG-dependent manner.[66–69] Hybrid CS/DS chains, which are synthesized from CS through the action of chondroitin-glucuronate 5-epimerase to convert GlcA to L-iduronic acid (IdoA),[22] have been shown to promote the outgrowth of embryonic hippocampal

neurons.[57,59,64,70] Moreover, DS chains enriched in the disulfated DS-D and DS-E motif, but not the disulfated DS-B motif (sulfated at the 2-*O* position of IdoA and 4-*O* position of GalNAc), stimulated neurite outgrowth, highlighting the importance of the sulfate group position for the activity of GAGs.[57,70] Interestingly, the DS-D and DS-E motifs also promoted the formation of an increased number of neurites per cell compared to CS-D and CS-E, respectively.[57,64] Thus, CS and DS structures with the same sulfation patterns can exhibit different activities towards developing neurons. In the future, comparative analyses of various GAG families and their distinct functions or mechanisms will be important for understanding the physiological roles of GAGs during development and in the mature nervous system.

Pure synthetic molecules for assessing structure-function relationships

The structural complexity of CS GAGs renders it difficult to purify well-characterized, homogeneous oligosaccharides and polysaccharides from natural sources. For instance, the CS-D polysaccharide used in the literature contains only ~20% of the CS-D sulfation motif, with the CS-C motif constituting the majority of the polysaccharide.[57] Thus, from a purity and selectivity standpoint, chemically-synthesized GAG structures with defined sulfation motifs are crucial for studying the structure–function relationships of CS GAGs.[21] To determine whether the growth-promoting activity of CS-E-enriched polysaccharides (which contain only ~60% CS-E) was due to the CS-E sulfation motif, defined tetrasaccharides were chemically synthesized.[32,71] Interestingly, a tetrasaccharide structure was sufficient to promote neurite outgrowth, and only a tetrasaccharide containing the CS-E motif (E-E), not the CS-A (A-A) or CS-C motifs (C-C), strongly promoted the outgrowth of embryonic hippocampal, cortical, and dopaminergic

neurons.[32,71,72] A different CS tetrasaccharide containing the same number of sulfate groups as CS-E had no appreciable effect on neuronal growth, indicating that the precise position of the sulfate groups was important.[32] The CS-E tetrasaccharide bound preferentially to specific growth factors, including BDNF and MK, and the growth-promoting activity of the tetrasaccharide was abolished by the addition of function-blocking antibodies against these growth factors or their cell surface receptors (TrkB and RPTPβ/ζ, respectively).[32,34] Together, these results demonstrate that the specific sequence of the sulfate groups along the sugar backbone, rather than electrostatics alone, modulates GAG–protein interactions and can direct important neuronal signaling events.

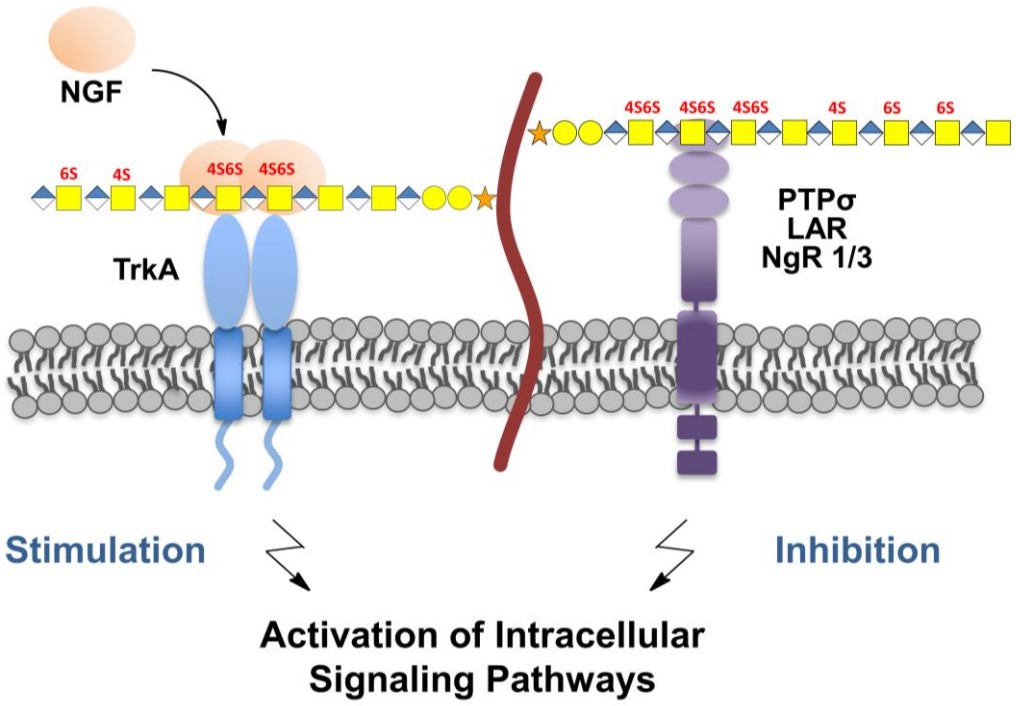

Figure 2.2: Modulation of intracellular signaling pathways by chondroitin sulfate. (left) CS chains can localize soluble ligands such growth factors to the cell surface and facilitate interactions with their cognate receptors. For example, nerve growth factor (NGF) signaling and neurite outgrowth are enhanced when CS-E is presented on the cell surface. (right) Alternatively, CS chains can directly interact with transmembrane receptors such PTPσ, LAR, NgR1, and NgR3, and affect intracellular signaling. For example, CS interacts with lysine-rich IgG domains of PTPσ and inhibits neurite outgrowth.

Mechanisms of growth promotion

Studies suggest that the CS chains on CSPGs promote neuronal growth *in vitro* by recruiting growth factors to the cell surface and facilitating interactions with their cell surface receptors (Fig. 2). CS-E polysaccharides can enhance the formation of neurotrophin-Trk complexes in a sulfation-dependent manner.[34] For instance, CS-E-enriched polysaccharides presented on a substratum increased NT-4/5-mediated TrkA activation in PC12 cells, while removal of endogenous CS chains by chondroitinase ABC (ChABC) reduced TrkA activation. A complex of CS-E with neurotrophins and their

cognate Trk receptors was observed on CS GAG microarrays, and the colocalization of CS-E and TrkA increased in PC12 cells upon treatment with the neurotrophin NGF. On the other hand, the addition of exogenous CS-E polysaccharides into the culture medium inhibited NT-4/5- and NGF-mediated TrkA activation, consistent with the mechanism that CS-E polysaccharides in solution can sequester neurotrophins away from the cell surface and prevent them from activating TrkA receptors. In addition to neutrophin-Trk complexes, contactin-1 (CNTN-1) has been identified as a receptor for CS-E.[73] CNTN-1 regulates neurite outgrowth through the non-receptor-type tyrosine kinase Fyn. Phosphorylation and activation of Fyn was induced upon treatment with CS-E, but not CS-A or CS-C, polysaccharides. Antibodies against CNTN-1 inhibited CS-E-induced neurite outgrowth of embryonic hippocampal neurons. This stimulation was further inhibited when MK or BDNF antibodies were used in combination with CNTN-1 antibodies. Although it remains to be determined whether CSPGs modulate neurotrophin and CNTN-1 signaling *in vivo*, heparan sulfate proteoglycans utilize similar mechanisms for the regulation of numerous growth factors such as fibroblast growth factors, Sonic Hedgehog, and epidermal growth factor.[74–76]

As CS GAGs can modulate growth factor activation at the cell surface, the ability to engineer cells to express specific GAG structures would provide a novel means to control cell growth pathways. Recent studies have explored the ability to promote neuronal growth through the cell surface presentation of particular sulfated GAGs.[77] For example, liposomal-mediated delivery of CS-E, but not CS-A or CS-C, polysaccharides to cultured cortical neurons enhanced neurite outgrowth mediated by NGF.[77] The presentation of CS-E at neuronal cell membranes also stimulated NGF-mediated phosphorylation of Akt. The

observed sulfation-dependent results are consistent with the high affinity of NGF for the disulfated CS-E motif.[34] In other studies, pluripotent embryonic stem cells engineered to display highly sulfated heparan sulfate underwent accelerated exit from self-renewal and differentiation into mature neuronal populations through increased activation of fibroblast growth factor/extracellular signal-regulated kinase (FGF/ERK)-mediated signaling pathways.[78] These studies lend strong support to the mechanism that specific sulfation motifs on GAG chains can recruit soluble factors to the cell surface and facilitate activation of their receptors (Fig. 2). Thus, controlled expression of GAG sulfation patterns at the cell surface may afford regulation of growth factor binding sites and tune intracellular signaling in a cell-type specific manner.

CSPGs as inhibitory cues for neuronal growth

CSPGs have been well documented to act as inhibitory cues in a variety of neuronal contexts. During development, CSPGs delineate boundaries that prevent extending axons from crossing.[3–5] In the mature system, CSPGs have been shown to restrict synaptic plasticity and help stabilize existing connections.[9,10] Following CNS injury, CSPGs prevent axons from regenerating past the injury site to form functional connections.[10–13] Although CSPGs were originally thought to function as non-specific, electrostatic or physical barriers to neuronal growth, it is becoming evident that the CS sugar chains on CSPGs can engage and modulate the activity of many inhibitory cell surface receptors. We will highlight recent studies that have demonstrated the importance of specific sulfation motifs in these systems.

Inhibition of neurite growth and axon elongation

While many studies have noted the stimulatory effects of CSPGs on embryonic hippocampal neurons, other studies have reported that CSPGs can inhibit the outgrowth of dorsal root ganglion (DRG), retinal ganglion cell (RGC) and cerebellar granule neurons (CGN).[5,36,56,79–83] The seemingly paradoxical activity of CSPGs appears to depend on the neuronal lineage, neuronal age, and expression of specific CSPG receptors. For example, certain CSPGs exhibit both stimulatory and inhibitory effects on neurons, depending on the neuron type. Whereas DSD-1-PG promoted the outgrowth of embryonic hippocampal neurons as described above, it potently inhibited the outgrowth of neonatal DRG explants.[56] In addition to their effects on neurite outgrowth, CSPGs also form an inhibitory barrier to elongating DRG, RGC, and CGN axons *in vitro*.[5,36,84] This activity depends on the CSPG concentration: neurons grown on a step gradient of immobilized CSPGs extended their axons at a reduced rate for each successively increasing CSPG concentration.[82] Interestingly, RGC neurons extended axons further than DRG neurons on these CSPG step gradients, highlighting cell type-specific responses.

Many studies have established that CSPG-mediated inhibition occurs through activation of the small GTPase RhoA and its effector protein, Rho-associated, coiled-coil containing protein kinase ROCK.[36,81,85] Activation of the Rho/ROCK pathway leads to phosphorylation of LIM domain kinase 2 (LIMK2), myosin light chain (MLC), and other downstream proteins that induce cytoskeletal rearrangements such as neurite retraction and growth cone collapse.[86,87] CSPGs are also known to activate epidermal growth factor receptor (EGFR) pathways, and blocking the kinase activity of EGFR or mitogen-activated protein kinase (MAPK) reversed the inhibition by CSPGs.[36,80,88]

The CS GAG chains on CSPGs are essential for the inhibitory activity of CSPGs. Enzymatic removal of the CS chains with ChABC rendered CSPGs significantly less inhibitory toward cultured DRG, RGC, and CGN neurons in neurite outgrowth and boundary assays.[79,83,84,89] Genetic disruption of CS biosynthesis by deletion of chondroitin polymerizing factor (ChPF) also reduced the inhibitory activity of CSPGs.[84] Specifically, CSPGs isolated from ChPF-deficient astrocytes failed to repel cultured CGN axons. Notably, decreasing the sulfation levels of CSPGs using the general sulfotransferase inhibitor chlorate reduced the ability of CSPGs to inhibit neurite outgrowth of DRG neurons.[90] Although the inhibitory activity of CSPGs resides primarily in their sugar chains, some core proteins also exhibit inhibitory properties.[66,91–93] For instance, the proteoglycan NG2 inhibited the outgrowth of neonatal CGN and embryonic DRG neurons even after ChABC treatment.[79,83] Three independent domains within the extracellular portion of NG2 each exhibited comparable inhibitory activity as the full extracellular domain of NG2.[83] Notably, only the activity of the central domain containing CS attachment sites was affected by enzymatic digestion with ChABC. In some cases, the interaction of CSPGs with cell surface receptors does not require the GAG chains. For example, the binding of phosphacan to N-CAM and Ng-CAM was not significantly reduced by ChABC treatment, and phosphacan lacking GAG chains still bound to neurons and inhibited neurite growth comparable to intact phosphacan.[94,95] Thus, the core protein, in addition to the GAG chains, can contribute to the inhibitory functions of certain CSPGs. Below, we will focus on the importance of the CS chains and specific sulfation motifs in mediating the inhibitory effects of CSPGs in the context of visual plasticity and CNS injury.

CSPGs and visual plasticity

During the critical period of development, the brain is most plastic, and experience-dependent activity shapes neuronal connections.[6,96,97] Sensory input during the critical period is required for the formation of functional neural circuits. In the mouse visual cortex, monocular deprivation during the critical period leads to a shift in the responsiveness of neurons toward the non-deprived eye.[6,97] This shift in ocular dominance (OD) is not observed if monocular deprivation is performed after the close of the critical period, which is accompanied by a marked reduction in plasticity and the formation of perineuronal net (PNN) structures.[98,99] PNNs, which consist of CSPGs, tenascin, link-proteins, and hyaluronic acid, surround the cell body and extend along the dendrites of inhibitory neurons expressing the calcium-binding protein parvalbumin (PV). They serve to restrict synaptic plasticity and stabilize the network of existing neuronal connections.[6–9] The CSPGs in PNNs, and in particular, their CS sugar chains, are essential to the structure and function of PNNs. Digestion of the CS sugars by ChABC in the visual cortex reactivated critical period plasticity following monocular deprivation in adult mice.[98,99] ChABC treatment also increased dendritic spine dynamics and density in the visual cortex *in vivo* and in hippocampal organotypic slices.[99–101] These effects were prevented by pretreatment with β1-integrin blocking antibodies, suggesting that the increase in dendritic spine dynamics occurred through disruption of CSPG interactions with integrin and activation of β1-integrin signaling pathways (Orlando et al., 2012).[101] Interestingly, CSPG interactions with hyaluronic acid (HA) chains are also required for the formation and stabilization of PNN structures. The N-terminal and C-terminal domains of lecticans allow these CSPGs to interact with HA and tenascins, two key components of PNNs.[102,103] CSPG-HA

interactions are stabilized by link protein, and genetic deletion of link protein or enzymatic digestion of HA or CS resulted in the loss of PNNs.[11,98,104,105]

Specific sulfation motifs on CSPGs have been shown to regulate PNN formation and critical period plasticity.[9] The sulfation patterns of CSPGs are tightly regulated during postnatal development in the mouse visual cortex. While 6-*O* sulfation of CS (CS-C) decreases, 4-*O* sulfation (CS-A) increases as the critical period comes to a close, resulting in an increase in the 4-*O* to 6-*O* sulfate (4S/6S) ratio.[106] Transgenic mice overexpressing C6ST-1 retain a low 4S/6S ratio and develop fewer PNNs around PV neurons.[106] Their PNNs are rich in CS-C and display a diffuse structure that is unable to tightly enwrap thalamocortical synaptic contacts. Importantly, the mice also exhibit persistent cortical plasticity into adulthood. When subjected to monocular deprivation, adult mice overexpressing C6ST-1 show ocular dominance plasticity similar to juvenile wild-type mice. Thus, the change from low to high 4S/6S sulfation ratio on CSPGs coincides with the close of the critical period when plasticity is restricted, and reducing this ratio can modulate PNN structure and enhance cortical plasticity.

CSPGs are believed to regulate plasticity in a sulfation-dependent manner by localizing plasticity-restricting factors to PNNs.[9,107] The transcription factor orthodenticle homeobox 2 (Otx2) is a key regulator of visual cortex plasticity.[108,109] The localization of Otx2 to PV neurons occurs through binding of Otx2 to sulfated CS GAG chains. In transgenic mice overexpressing C6ST-1, Otx2 was not incorporated in PV neurons surrounded by PNNs enriched in CS-C.[106] Otx2 fragments interact preferentially with highly sulfated CS-D- and CS-E-enriched polysaccharides.[110] The localization of Otx2 to PV neurons was disrupted by blocking Otx2-CS interactions through intracortical infusion

of a CS-E hexasaccharide or an arginine-lysine rich N-terminal Otx2 fragment that interacts with CS-D and CS-E polysaccharides.[110,111] Infusion of this N-terminal Otx2 fragment, but not an alanine-containing mutant, also reopened critical period plasticity in adult mice.[110] Thus, the accumulation of Otx2 within PV neurons is sulfation pattern-dependent and appears to be mediated by highly sulfated CS sequences. Interestingly, the CS-E motif was also recently shown to interact with semaphorin 3A (Sema3A), a chemorepulsive guidance protein.[112] Sema3A is enriched in PNNs, and ChABC treatment disrupted the localization of Sema3A to PNNs.[113] Importantly, the abundance of Sema3A was reduced in PNNs during periods of enhanced synaptic remodeling in regions undergoing structural reorganization.[114] These examples suggest important roles for CS sugars in the regulation of synaptic plasticity and highlight the potential to modulate plasticity by altering the sulfation patterns of CSPGs and their sulfation-dependent interactions.

CSPGs and CNS injury

CSPGs are dramatically upregulated in the glial scar, which forms in response to CNS injury.[12,13,115] Comprised of reactive astrocytes, microglia, and ECM molecules, the glial scar serves as a major barrier to regenerating axons.[11–13,115] It also functions to restrict anatomical plasticity by inhibiting collateral sprouting and synaptic reorganization.[10–12] Within 24 h after injury, reactive astrocytes begin to synthesize and secrete CSPGs in high concentrations into the glial scar, where they persist for months.[116–118] One well-established strategy for overcoming the inhibition of the glial scar is localized delivery of the enzyme ChABC.[119] ChABC digestion of the CS sugars on CSPGs induced axon regeneration following injury to the nigrostriatal, serotoninergic, or reticulospinal axon pathways.[120–122]

ChABC treatment also resulted in improved regeneration and functional recovery in several models of spinal cord injury.[123–127] For example, mice treated with ChABC after a dorsal column crush injury exhibited growth of ascending sensory projections and descending corticospinal tract axons.[124] Enhanced functional recovery of locomotor and proprioceptive behaviors was also observed. In other studies, ChABC treatment increased conduction through intact fibers in the ventrolateral funiculus following unilateral hemisection of adult rat spinal cord.[128] The remarkable effects of ChABC have been proposed to occur both through regeneration of corticospinal tract axons, as well as enhanced plasticity and sprouting of spared axons.

Interestingly, enzymatic digestion of keratan sulfate (KS) GAGs using keratanase II (K-II) also led to axon regeneration and improved recovery of motor and sensory function following injury.[129,130] KS, another component of the glial scar, is composed of repeating disaccharide units of galactose (Gal) and *N*-acetyl-D-glucosamine (GlcNAc), and it can be sulfated at the 6-*O* position of Gal and GlcNAc residues.[131,132] KS digestion by K-II led to comparable effects on axon regeneration and sprouting as CS digestion by ChABC.[129,130] The effects of digestion with K-II and ChABC on axon regeneration were not additive, as treatment with both K-II and ChABC did not result in improved axon recovery compared to either treatment alone.[129,130] It is unclear whether CS and KS inhibit axon regeneration through common receptors or if KS-specific receptors also exist.

In addition to enzymatic digestion of GAGs, genetic manipulation of CS sugar chains indicates a critical role for the sugars in inhibiting axon regeneration and plasticity after CNS injury. Mice lacking the enzyme chondroitin sulfate *N*-acetylgalactosaminyltransferase-1 (CSGalNAcT-1), which appends the first GalNAc

residue to the core tetrasaccharide linker on CSPGs, synthesized less CS and exhibited reduced scar formation after a spinal cord compression injury.[133] The mice also displayed enhanced axon growth and a larger area encompassing serotonin-positive (5HT(+)) terminals beyond the lesion site. Notably, *CSGalNAcT-1* knockout mice showed improved motor function and more complete, faster recovery in motor function assays compared to mice treated with ChABC. Likewise, genetic deletion of *N*-acetylglucosamine 6-*O*-sulfotransferase-1, an enzyme required for KS chain elongation, resulted in reduction of glial scar formation and promoted axonal regrowth of the corticospinal tract.[134,135]

Given the importance of the CS sugars, understanding the functions of different CS sulfation patterns in the glial scar and characterizing their mechanisms of action may provide new therapeutic strategies for promoting neuronal repair. Several studies indicate that particular CS sulfation patterns are upregulated in response to CNS injury. In addition to enhanced expression of CSPGs, the sulfotransferases C4ST, C6ST, and GalNAc4S-6ST are upregulated at the injury site following cortical lesions in mice and rats.[136–138] Consistent with these observations, disaccharide analysis of CS polysaccharides isolated from injured issue showed increased levels of the CS-A, CS-C, and CS-E motifs.[89,139] For instance, a large increase in total CS and CS-A expression was observed one day after dorsal hemisection injury in mice.[89] Others studies revealed an increase in CS-C and CS-E levels, but a decrease in CS-A levels, one week and one month after cortical lesion in rats.[138] Increased CS-E expression was also observed by immunohistochemistry 2 weeks after an optic nerve crush injury, as well as 24 h after cortical stab and dorsal spinal cord injuries in mice.[36] Comparison of these results are confounded by differences in the methods of CS analysis, the timing post injury, and the type of injury model. Nonetheless,

these studies all observe an increase in the total amount of CS and in general, an increase in the CS-E sulfation motif. Systematic investigations into the CS patterns in different injury models and at various times points post injury are required for a better understanding of the temporal dynamics of CS sulfation following CNS injury.

Studies suggest that specific sulfation motifs within long CS polysaccharide chains enable CSPGs to interact with inhibitory receptors, possibly modulating the clustering and/or activation of those receptors (Fig. 1.2). Until recently, CSPGs were widely believed to inhibit axon growth through relatively non-specific mechanisms, such as steric blockage of the extracellular space, arrays of negatively charged sulfate, or steric hindrance of adhesive matrix molecules.[139–141] However, recent studies suggest that CSPGs can interact directly with cell surface receptors expressed on injured axons and thereby activate growth-inhibitory signaling pathways.[142] Several important CSPG receptors have been identified, including the protein tyrosine phosphatases PTPσ and LAR and the Nogo receptors NgR1 and NgR3.[36,38,39,143] DRG neurons from *PTPσ*-deficient mice crossed CSPG-rich boundaries and exhibited improved neurite outgrowth in response to CSPGs *in vitro*.[36,39,143] Axons from *PTPσ*-deficient mice also extended further from the lesion site following a dorsal column crush injury. In a similar manner, modulating the activity of PTPσ using a peptide mimetic blocked CSPG-mediated inhibition and allowed DRG neurons to cross CSPG-rich barriers.[144] Systemic treatment with this peptide following contusion spinal cord injury resulted in axon regeneration and recovery of locomotor function. It's worth noting that PTPσ also binds to HS and this interaction promotes neurite outgrowth of cultured DRG neurons.[143] Like Sema5A, PTPσ is another example where the neuronal response is dependent on its GAG binding status. Similarly, DRG and CGN neurons from

LAR-deficient mice exhibited increased neurite outgrowth when grown on a CSPG substratum compared to neurons from wild-type mice.[38] As with PTPσ, blocking the activity of LAR using a peptide reversed the CSPG-mediated inhibition of neurite outgrowth *in vitro* and promoted axon growth and improved locomotor recovery *in vivo* following dorsal transection in mice. Likewise, genetic deletion of *NgR1* and *NgR3* resulted in improved neurite outgrowth of CGN neurons grown on a CSPG substratum and enhanced axon regeneration in mice following an optic nerve crush injury.[37] However, complete recovery was not observed in either $PTP\sigma^{-/-}$ or $NgR1^{-/-}$; $NgR2^{-/-}$; $NgR3^{-/-}$ triple knockout mice, and $NgR1^{-/-}$; $NgR3^{-/-}$; $PTP\sigma^{-/-}$ triple knockout mice displayed increased optic nerve regeneration compared to knockout of *NgR1*, *NgR3*, or *PTPσ* alone, suggesting that the inhibitory effects of CSPGs in the glial scar are mediated through multiple different receptors.

Importantly, the disulfated CS-E sulfation motif is critical for engaging these inhibitory CSPG receptors. PTPσ bound selectively to CS-E, but not to CS-A or CS-C, polysaccharides through its lysine-rich IgG domain.[36] Moreover, the ability of CS-E polysaccharides to inhibit the outgrowth of DRG neurons was significantly attenuated in neurons from *PTPσ*-deficient mice.[36] Interestingly, however, residual inhibition by CS-E (~22%) remained in *PTPσ*-deficient neurons, consistent with the idea that multiple different receptors interact with CSPGs to inhibit neuronal growth. NgR1 and NgR3 also interacted preferentially with CS chains containing the CS-E or CS-D motifs, but not those enriched in CS-A or CS-C, suggesting that these receptors also engage the CS-E structure on CSPGs.[37]

Additional evidence indicates that the CS-E sulfation motif is critical for the inhibitory activity of CSPGs. The CS-E motif has been shown to exert strong inhibitory effects on sensory neurons both *in vitro* and *in vivo*.[36,136,139,145] Studies using CS-E-enriched polysaccharides and pure synthetic polymers containing CS-E showed that the CS-E motif was sufficient to inhibit CGN and DRG neurons in neurite outgrowth, growth cone collapse, and boundary assays.[36,139,145] In contrast, CS-A- and CS-C-enriched polysaccharides and synthetic polymers had no appreciable inhibitory effects even when used at 10-fold higher concentrations or when combined with CS-E. Notably, CSPGs isolated from mice lacking GalNAc4S-6ST, the sulfotransferase that produces CS-E, showed significantly less inhibition of DRG neurite outgrowth.[36] Similar effects were observed upon knockdown of C4ST or GalNAc4S-6ST in astrocytes: CSPGs isolated from these astrocytes lacked either CS-A and CS-E or CS-E alone, respectively, and were less inhibitory towards CGN and cortical neurons in neurite outgrowth and boundary assays.[89,136] In contrast, reduced inhibition by CSPGs was not observed when C6ST-1, which produces CS-C, was knocked down.[89] Importantly, blocking the CS-E, but not the CS-A, motif using a specific monoclonal antibody rescued the CSPG-mediated inhibition of DRG neurite outgrowth *in vitro* and promoted axon regeneration *in vivo* following an optic nerve crush injury.[36] Interestingly, the CS-E-blocking antibody promoted regeneration in mice to a similar extent as complete digestion of CS chains using ChABC, suggesting that CS-E represents the major inhibitory determinant on CSPGs. The number of regenerating axons and the distance of regeneration was further enhanced by combining the CS-E antibody treatment with a small-molecule cyclic AMP analogue to activate intrinsic neuronal growth pathways. Given that CSPGs interact with several different

receptors, blocking the CS-E motif may be an effective means to target multiple inhibitory receptors simultaneously.

Summary and conclusions

CSPGs are key components of the developing and mature nervous system, where they guide developing axons, restrict synaptic plasticity, and prevent axon regeneration following CNS injury. The functions of CSPGs are mediated largely by the CS sugar chains that decorate them and the ability of these sugars to engage various protein receptors in a sulfation-dependent manner. The different sulfation patterns on CS chains are tightly regulated, and the spatiotemporal expression of sulfation motifs offers a means to modulate a diverse range of neuronal processes in a cell type- and tissue-specific manner. Highly sulfated motifs, such as CS-E and CS-D, are important for modulating the functions of CSPGs and their interactions with stimulatory growth factors and inhibitory cell surface receptors. Further studies of the spatiotemporal expression of CS sulfation patterns and the identification of their interacting protein partners will provide new insights into many important neural processes. This understanding, coupled with the development of methods to disrupt CS sugars and specific sulfation motifs, such as blocking antibodies or pharmacological agents, should provide novel approaches for promoting neuronal growth, regeneration, and CNS plasticity.

References

1. Bashaw, G. J. & Klein, R. Signaling from axon guidance receptors. *Cold Spring Harb. Perspect. Biol.* **2,** a001941 (2010).
2. Tessier-Lavigne, M. & Goodman, C. S. The molecular biology of axon guidance. *Science (80-.).* **274,** 1123–1133 (1996).
3. Brittis, P. A., Canning, D. R. & Silver, J. Chondroitin sulfate as a regulator of neuronal patterning in the retina. *Science (80-.).* **255,** 733–736 (1992).
4. Carulli, D., Laabs, T., Geller, H. M. & Fawcett, J. W. Chondroitin sulfate proteoglycans in neural development and regeneration. *Curr. Opin. Neurobiol.* **15,** 116–120 (2005).
5. Snow, D. M., Lemmon, V., Carrino, D. A., Caplan, A. I. & Silver, J. Sulfated Proteoglycans in Astroglial Barriers Inhibit Neurite Outgrowth in Vitro. *Exp. Neurol.* **109,** 111–130 (1990).
6. Berardi, N., Pizzorusso, T., Ratto, G. M. & Maffei, L. Molecular basis of plasticity in the visual cortex. *Trends Neurosci.* **26,** 369–378 (2003).
7. Dityatev, A., Schachner, M. & Sonderegger, P. The dual role of the extracellular matrix in synaptic plasticity and homeostasis. *Nat. Rev. Neurosci.* **11,** 735–746 (2010).
8. Kwok, J. C., Dick, G., Wang, D. & Fawcett, J. W. Extracellular matrix and perineuronal nets in CNS repair. *Dev. Neurobiol.* **71,** 1073–1089 (2011).
9. Miyata, S. & Kitagawa, H. Mechanisms for modulation of neural plasticity and axon regeneration by chondroitin sulphate. *J. Biochem.* **157,** 13–22 (2015).
10. Bartus, K., James, N. D., Bosch, K. D. & Bradbury, E. J. Chondroitin sulphate

proteoglycans: key modulators of spinal cord and brain plasticity. *Exp. Neurol.* **235,** 5–17 (2012).

11. Galtrey, C. M. & Fawcett, J. W. The role of chondroitin sulfate proteoglycans in regeneration and plasticity in the central nervous system. *Brain Res. Rev.* **54,** 1–18 (2007).
12. Silver, J. & Miller, J. H. Regeneration beyond the glial scar. *Nat. Rev. Neurosci.* **5,** 146–156 (2004).
13. Yiu, G. & He, Z. Glial inhibition of CNS axon regeneration. *Nat. Rev. Neurosci.* **7,** 617–627 (2006).
14. Kjellén, L. & Lindahl, U. Proteoglycans: Structures and Interactions. *Annu. Rev. Biochem.* **60,** 443–475 (1991).
15. Busch, S. A. & Silver, J. The role of extracellular matrix in CNS regeneration. *Curr. Opin. Neurobiol.* **17,** 120–127 (2007).
16. Yamaguchi, Y. Lecticans: organizers of the brain extracellular matrix. *Cell. Mol. Life Sci.* **57,** 276–289 (2000).
17. Hayashi, N., Miyata, S., Yamada, M., Kamei, K. & Oohira, A. Neuronal expression of the chondroitin sulfate proteoglycans receptor-type protein-tyrosine phosphatase β and phosphacan. *Neuroscience* **131,** 331–348 (2005).
18. Maurel, P., Rauch, U., Flad, M., Margolis, R. K. & Margolis, R. U. Phosphacan, a chondroitin sulfate proteoglycan of brain that interacts with neurons and neural cell-adhesion molecules, is an extracellular variant of a receptor-type protein tyrosine phosphatase. *Proc. Natl. Acad. Sci. U.S.A.* **91,** 2512–2516 (1994).
19. Hocking, A. M., Shinomura, T. & McQuillan, D. J. Leucine-rich repeat

glycoproteins of the extracellular matrix. *Matrix Biol.* **17,** 1–19 (1998).

20. Stallcup, W. B. The NG2 proteoglycan: Past insights and future prospects. *J Neurocytol.* **31,** 423–435 (2002).

21. Gama, C. I. & Hsieh-Wilson, L. C. Chemical approaches to deciphering the glycosaminoglycan code. *Curr. Opin. Chem. Biol.* **9,** 609–619 (2005).

22. Sugahara, K. *et al.* Recent advances in the structural biology of chondroitin sulfate and dermatan sulfate. *Curr. Opin. Struct. Biol.* **13,** 612–620 (2003).

23. Kusche-Gullberg, M. & Kjellen, L. Sulfotransferases in glycosaminoglycan biosynthesis. *Curr. Opin. Struct. Biol.* **13,** 605–611 (2003).

24. Mikami, T. & Kitagawa, H. Biosynthesis and function of chondroitin sulfate. *Biochim. Biophys. Acta - Bioenerg.* **1830,** 4719–4733 (2013).

25. Friedlander, D. R. *et al.* The neuronal chondroitin sulfate proteoglycan neurocan binds to the neural cell adhesion molecules Ng-CAM/L1/NILE and N-CAM, and inhibits neuronal adhesion and neurite outgrowth. *J. Cell Biol.* **125,** 669–680 (1994).

26. Grumet, M., Flaccus, A. & Margolis, R. U. Functional characterization of chondroitin sulfate proteoglycans of brain: interactions with neurons and neural cell adhesion molecules. *J. Cell Biol.* **120,** 815–824 (1993).

27. Wu, Y. J., LA PIERRE, D. P., Jin, W. U., Albert, J. Y. E. E. & Burton, B. Y. The interaction of versican with its binding partners. *Cell Res.* **15,** 483–494 (2005).

28. Muir, D., Engvall, E., Varon, S. & Manthorpe, M. Schwannoma cell-derived inhibitor of the neurite-promoting activity of laminin. *J. Cell Biol.* **109,** 2353–2362 (1989).

29. Tan, C. L. *et al.* Integrin activation promotes axon growth on inhibitory chondroitin

sulfate proteoglycans by enhancing integrin signaling. *J. Neurosci.* **31,** 6289–6295 (2011).

30. Zuo, J., Ferguson, T. A., Hernandez, Y. J., Stetler-Stevenson, W. G. & Muir, D. Neuronal matrix metalloproteinase-2 degrades and inactivates a neurite-inhibiting chondroitin sulfate proteoglycan. *J. Neurosci.* **18,** 5203–5211 (1998).

31. Deepa, S. S., Umehara, Y., Higashiyama, S., Itoh, N. & Sugahara, K. Specific molecular interactions of oversulfated chondroitin sulfate E with various heparin-binding growth factors. Implications as a physiological binding partner in the brain and other tissues. *J. Biol. Chem.* **277,** 43707–43716 (2002).

32. Gama, C. I. *et al.* Sulfation patterns of glycosaminoglycans encode molecular recognition and activity. *Nat. Chem. Biol.* **2,** 467–473 (2006).

33. Maeda, N. *et al.* Heterogeneity of the chondroitin sulfate portion of phosphacan/6B4 proteoglycan regulates its binding affinity for pleiotrophin/heparin binding growth-associated molecule. *J. Biol. Chem.* **278,** 35805–35811 (2003).

34. Rogers, C. J. *et al.* Elucidating glycosaminoglycan–protein–protein interactions using carbohydrate microarray and computational approaches. *Proc. Natl. Acad. Sci.* **108,** 9747–9752 (2011).

35. Zou, P. *et al.* Glycosaminoglycan structures required for strong binding to midkine, a heparin-binding growth factor. *Glycobiology* **13,** 35–42 (2003).

36. Brown, J. M. *et al.* A sulfated carbohydrate epitope inhibits axon regeneration after injury. *Proc. Natl. Acad. Sci.* **109,** 4768–4773 (2012).

37. Dickendesher, T. L. *et al.* NgR1 and NgR3 are receptors for chondroitin sulfate proteoglycans. *Nat. Neurosci.* **15,** 703–712 (2012).

38. Fisher, D. *et al.* Leukocyte common antigen-related phosphatase is a functional receptor for chondroitin sulfate proteoglycan axon growth inhibitors. *J. Neurosci.* **31,** 14051–14066 (2011).

39. Shen, Y. *et al.* PTPσ is a receptor for chondroitin sulfate proteoglycan, an inhibitor of neural regeneration. *Science (80-.).* **326,** 592–596 (2009).

40. Kantor, D. B. *et al.* Semaphorin 5A is a bifunctional axon guidance cue regulated by heparan and chondroitin sulfate proteoglycans. *Neuron* **44,** 961–975 (2004).

41. Fernaud-Espinosa, I., Nieto-Sampedro, M. & Bovolenta, P. Developmental distribution of glycosaminoglycans in embryonic rat brain: relationship to axonal tract formation. *J. Neurobiol.* **30,** 410–424 (1996).

42. Ishii, M. & Maeda, N. Oversulfated chondroitin sulfate plays critical roles in the neuronal migration in the cerebral cortex. *J. Biol. Chem.* **283,** 32610–32620 (2008).

43. Kitagawa, H., Tsutsumi, K., Tone, Y. & Sugahara, K. Developmental Regulation of the Sulfation Profile of Chondroitin Sulfate Chains in the Chicken Embryo Brain. *J. Biol. Chem.* **272,** 31377–31381 (1997).

44. Mitsunaga, C., Mikami, T., Mizumoto, S., Fukuda, J. & Sugahara, K. Chondroitin sulfate/dermatan sulfate hybrid chains in the development of cerebellum. Spatiotemporal regulation of the expression of critical disulfated disaccharides by specific sulfotransferases. *J. Biol. Chem.* **281,** 18942–18952 (2006).

45. Sugahara, K. & Mikami, T. Chondroitin/dermatan sulfate in the central nervous system. *Curr. Opin. Struct. Biol.* **17,** 536–545 (2007).

46. Ishii, M. & Maeda, N. Spatiotemporal expression of chondroitin sulfate sulfotransferases in the postnatal developing mouse cerebellum. *Glycobiology* **18,**

602–614 (2008).

47. Maeda, N. Structural variation of chondroitin sulfate and its roles in the central nervous system. *Cent. Nerv. Sys. Agents Med. Chem.* **10,** 22–31 (2010).

48. Purushothaman, A. *et al.* Functions of chondroitin sulfate/dermatan sulfate chains in brain development. Critical roles of E and iE disaccharide units recognized by a single chain antibody GD3G7. *J. Biol. Chem.* **282,** 19442–19452 (2007).

49. Ly, M. *et al.* The proteoglycan bikunin has a defined sequence. *Nat. Chem. Biol.* **7,** 827–833 (2011).

50. Bicknese, A. R., Sheppard, A. M., O'Leary, D. D. M. & Pearlman, A. L. Thalamocortidal Axons Extend Along a Chondroitin Sulfate Proteoglycan-enriched Pathway Coincident with the Neocortical Subplate and Distinct from the Efferent Path. *J. Neurosci.* **14,** 3500–3510 (1994).

51. Sheppard, A. M., Hamilton, S. K. & Pearlman, A. L. Changes in the distribution of extracellular matrix components accompany early morphogenetic events of mammalian cortical development. *J. Neurosci.* **11,** 3928–3942 (1991).

52. Bao, X. *et al.* Heparin-binding growth factor, pleiotrophin, mediates neuritogenic activity of embryonic pig brain-derived chondroitin sulfate/dermatan sulfate hybrid chains. *J. Biol. Chem.* **280,** 9180–9191 (2005).

53. Clement, A. M., Nadanaka, S., Masayama, K., Mandl, C. & Sugahara, K. The DSD-1 Carbohydrate Epitope Depends on Sulfation, Correlates with Chondroitin Sulfate D Motifs, and Is Sufficient to Promote Neurite Outgrowth. *J. Biol. Chem.* **273,** 28444–28453 (1998).

54. Clement, A. M., Sugahara, K. & Faissner, A. Chondroitin sulfate E promotes neurite

outgrowth of rat embryonic day 18 hippocampal neurons. *Neurosci. Lett.* **269,** 125–128 (1999).

55. Faissner, A. *et al.* Isolation of a Neural Chondroitin Sulfate Proteoglycan with Neurite Outgrowth Promoting Properties. *J. Cell Biol.* **126,** 783–799 (1994).
56. Garwood, J. *et al.* DSD-1-proteoglycan is the mouse homolog of phosphacan and displays opposing effects on neurite outgrowth dependent on neuronal lineage. *J. Neurosci.* **19,** 3888–3899 (1999).
57. Hikino, M. *et al.* Oversulfated dermatan sulfate exhibits neurite outgrowth-promoting activity toward embryonic mouse hippocampal neurons: implications of dermatan sulfate in neuritogenesis in the brain. *J. Biol. Chem.* **278,** 43744–43754 (2003).
58. Nadanaka, S., Clement, A., Masayama, K., Faissner, A. & Sugahara, K. Characteristic hexasaccharide sequences in octasaccharides derived from shark cartilage chondroitin sulfate D with a neurite outgrowth promoting activity. *J. Biol. Chem.* **273,** 3296–3307 (1998).
59. Nandini, C. D. *et al.* Structural and functional characterization of oversulfated chondroitin sulfate/dermatan sulfate hybrid chains from the notochord of hagfish. Neuritogenic and binding activities for growth factors and neurotrophic factors. *J. Biol. Chem.* **279,** 50799–50809 (2004).
60. Ito, Y. *et al.* Structural characterization of the epitopes of the monoclonal antibodies 473HD, CS-56, and MO-225 specific for chondroitin sulfate D-type using the oligosaccharide library. *Glycobiology* **15,** 593–603 (2005).
61. Maeda, N. & Noda, M. Involvement of receptor-like protein tyrosine phosphatase

ζ/RPTPβ and its ligand pleiotrophin/heparin-binding growth-associated molecule (HB-GAM) in neuronal migration. *J. Cell Biol.* **142,** 203–216 (1998).

62. Ueoka, C. *et al.* Neuronal Cell Adhesion, Mediated by the Heparin-binding Neuroregulatory Factor Midkine, Is Specifically Inhibited by Chondroitin Sulfate E: STRUCTURAL AND FUNCTIONAL IMPLICATIONS OF THE OVER-SULFATED CHONDROITIN SULFATE. *J. Biol. Chem.* **275,** 37407–37413 (2000).

63. Häcker, U., Nybakken, K. & Perrimon, N. Heparan sulphate proteoglycans: the sweet side of development. *Nat. Rev. Mol. Cell Biol.* **6,** 530–541 (2005).

64. Nandini, C. D., Itoh, N. & Sugahara, K. Novel 70-kDa Chondroitin Sulfate/Dermatan Sulfate Hybrid Chains with a Unique Heterogenous Sulfation Pattern from Shark Skin, Which Exhibit Neuritogenic Activity and Binding Activities for Growth Factors and Neurotrophic Factors. *J. Biol. Chem.* **280,** 4058–4069 (2005).

65. Shipp, E. L. & Hsieh-Wilson, L. C. Profiling the sulfation specificities of glycosaminoglycan interactions with growth factors and chemotactic proteins using microarrays. *Chem. Biol.* **14,** 195–208 (2007).

66. Beller, J. A. & Snow, D. M. Proteoglycans: road signs for neurite outgrowth. *Neural Regen. Res.* **9,** 343 (2014).

67. Hantaz-Ambroise, D., Vigny, M. & Koenig, J. Heparan sulfate proteoglycan and laminin mediate two different types of neurite outgrowth. *J. Neurosci.* **7,** 2293–2304 (1987).

68. Jung Kim, M., Cotman, S. L., Halfter, W. & Cole, G. J. The heparan sulfate

proteoglycan agrin modulates neurite outgrowth mediated by FGF-2. *Dev. Neurobiol.* **55,** 261–277 (2003).

69. Lander, A. D., Fujii, D. K., Gospodarowicz, D. & Reichardt, L. F. Characterization of a factor that promotes neurite outgrowth: evidence linking activity to a heparan sulfate proteoglycan. *J. Cell Biol.* **94,** 574–585 (1982).

70. Li, F., Shetty, A. K. & Sugahara, K. Neuritogenic activity of chondroitin/dermatan sulfate hybrid chains of embryonic pig brain and their mimicry from shark liver INVOLVEMENT OF THE PLEIOTROPHIN AND HEPATOCYTE GROWTH FACTOR SIGNALING PATHWAYS. *J. Biol. Chem.* **282,** 2956–2966 (2007).

71. Tully, S. E. *et al.* A Chondroitin Sulfate Small Molecule that Stimulates Neuronal Growth. *J. Am. Chem. Soc.* **126,** 7736–7737 (2004).

72. Sotogaku, N. *et al.* Activation of phospholipase C pathways by a synthetic chondroitin sulfate-E tetrasaccharide promotes neurite outgrowth of dopaminergic neurons. *J. Neurochem.* **103,** 749–760 (2007).

73. Mikami, T., Yasunaga, D. & Kitagawa, H. Contactin-1 is a functional receptor for neuroregulatory chondroitin sulfate-E. *J. Biol. Chem.* **284,** 4494–4499 (2009).

74. Bernfield, M. *et al.* Functions of cell surface heparan sulfate proteoglycans. *Annu. Rev. Biochem.* **68,** 729–777 (1999).

75. Chan, J. A. *et al.* Proteoglycan interactions with Sonic Hedgehog specify mitogenic responses. *Nat Neurosci* **12,** 409–417 (2009).

76. Xu, D. & Esko, J. D. Demystifying heparan sulfate-protein interactions. *Annu. Rev. Biochem.* **83,** 129–157 (2014).

77. Pulsipher, A., Griffin, M. E., Stone, S. E., Brown, J. M. & Hsieh-Wilson, L. C.

Directing neuronal signaling through cell-surface glycan engineering. *J. Am. Chem. Soc.* **136,** 6794–6797 (2014).

78. Pulsipher, A., Griffin, M. E., Stone, S. E. & Hsieh-Wilson, L. C. Long-Lived Engineering of Glycans to Direct Stem Cell Fate. *Angew. Chemie, Int. Ed. English* **54,** 1466–1470 (2015).

79. Dou, C. L. & Levine, J. M. Inhibition of Neurite Growth by the NG2 Chondroitin Sulfate Proteoglycan. *J. Neurosci.* **14,** 7616–7628 (1994).

80. Koprivica, V. *et al.* EGFR activation mediates inhibition of axon regeneration by myelin and chondroitin sulfate proteoglycans. *Science (80-.).* **310,** 106–110 (2005).

81. Monnier, P. P., Sierra, A., Schwab, J. M., Henke-Fahle, S. & Mueller, B. K. The Rho/ROCK pathway mediates neurite growth-inhibitory activity associated with the chondroitin sulfate proteoglycans of the CNS glial scar. *Mol. Cell. Neurosci.* **22,** 319–330 (2003).

82. Snow, D. M. & Letourneau, P. C. Neurite Outgrowth on a Step Gradient of Chondroitin Sulfate Proteoglycan (CS-PG). *J. Neurobiol.* **23,** 322–336 (1992).

83. Ughrin, Y. M., Chen, Z. J. & Levine, J. M. Multiple regions of the NG2 proteoglycan inhibit neurite growth and induce growth cone collapse. *J. Neurosci.* **23,** 175–186 (2003).

84. Laabs, T. L. *et al.* Inhibiting glycosaminoglycan chain polymerization decreases the inhibitory activity of astrocyte-derived chondroitin sulfate proteoglycans. *J. Neurosci.* **27,** 14494–14501 (2007).

85. Borisoff, J. F. *et al.* Suppression of Rho-kinase activity promotes axonal growth on inhibitory CNS substrates. *Mol. Cell. Neurosci.* **22,** 405–416 (2003).

86. Maekawa, M. *et al.* Signaling from Rho to the Actin Cytoskeleton Through Protein Kinases ROCK and LIM-kinase. *Science (80-.).* **285,** 895–898 (1999).

87. Wu, K. Y. *et al.* Local translation of RhoA regulates growth cone collapse. *Nature* **436,** 1020–1024 (2005).

88. Kaneko, M., Kubo, T., Hata, K., Yamaguchi, A. & Yamashita, T. Repulsion of cerebellar granule neurons by chondroitin sulfate proteoglycans is mediated by MAPK pathway. *Neurosci. Lett.* **423,** 62–67 (2007).

89. Wang, H. *et al.* Chondroitin-4-sulfation negatively regulates axonal guidance and growth. *J. Cell Sci.* **121,** 3083–3091 (2008).

90. Smith-Thomas, L. C. *et al.* Increased axon regeneration in astrocytes grown in the presence of proteoglycan synthesis inhibitors. *J. Cell Sci.* **108,** 1307–1315 (1995).

91. Inatani, M. *et al.* Inhibitory effects of neurocan and phosphacan on neurite outgrowth from retinal ganglion cells in culture. *Invest. Ophthalmol. Vis. Sci.* **42,** 1930–1938 (2001).

92. Lemons, M. L., Sandy, J. D., Anderson, D. K. & Howland, D. R. Intact aggrecan and chondroitin sulfate-depleted aggrecan core glycoprotein inhibit axon growth in the adult rat spinal cord. *Exp. Neurol.* **184,** 981–990 (2003).

93. Schmalfeldt, M., Bandtlow, C. E., Dours-Zimmermann, M. T., Winterhalter, K. H. & Zimmermann, D. R. Brain derived versican V2 is a potent inhibitor of axonal growth. *J Cell Sci* **113,** 807–816 (2000).

94. Maeda, N. & Noda, M. 6B4 proteoglycan/phosphacan is a repulsive substratum but promotes morphological differentiation of cortical neurons. *Development* **122,** 647–658 (1996).

95. Milev, P. *et al.* Interactions of the chondroitin sulfate proteoglycan phosphacan, the extracellular domain of a receptor-type protein tyrosine phosphatase, with neurons, glia, and neural cell adhesion molecules. *J. Cell Biol.* **127,** 1703–1715 (1994).

96. Hensch, T. K. Critical period plasticity in local cortical circuits. *Nat. Rev. Neurosci.* **6,** 877–888 (2005).

97. Morishita, H. & Hensch, T. K. Critical period revisited: impact on vision. *Curr. Opin. Neurobiol.* **18,** 101–107 (2008).

98. Pizzorusso, T. *et al.* Reactivation of ocular dominance plasticity in the adult visual cortex. *Science (80-.).* **298,** 1248–1251 (2002).

99. Pizzorusso, T. *et al.* Structural and functional recovery from early monocular deprivation in adult rats. *Proc. Natl. Acad. Sci.* **103,** 8517–8522 (2006).

100. De Vivo, L. *et al.* Extracellular matrix inhibits structural and functional plasticity of dendritic spines in the adult visual cortex. *Nat. Commun.* **4,** 1484 (2013).

101. Orlando, C., Ster, J., Gerber, U., Fawcett, J. W. & Raineteau, O. Perisynaptic chondroitin sulfate proteoglycans restrict structural plasticity in an integrin-dependent manner. *J. Neurosci.* **32,** 18009–17, 18017a (2012).

102. Grumet, M. *et al.* Interactions with tenascin and differential effects on cell adhesion of neurocan and phosphacan, two major chondroitin sulfate proteoglycans of nervous tissue. *J. Biol. Chem.* **269,** 12142–12146 (1994).

103. Matsumoto, K. *et al.* Distinct interaction of versican/PG-M with hyaluronan and link protein. *J. Biol. Chem.* **278,** 41205–41212 (2003).

104. Carulli, D. *et al.* Animals lacking link protein have attenuated perineuronal nets and persistent plasticity. *Brain* **133,** 2331–2347 (2010).

105. Koppe, G., Bruckner, G., Hartig, W., Delpech, B. & Bigl, V. Characterization of proteoglycan-containing perineuronal nets by enzymatic treatments of rat brain sections. *Histochem. J.* **29,** 11–20 (1997).

106. Miyata, S., Komatsu, Y., Yoshimura, Y., Taya, C. & Kitagawa, H. Persistent cortical plasticity by upregulation of chondroitin 6-sulfation. *Nat. Neurosci.* **15,** 414–422 (2012).

107. Sugiyama, S., Prochiantz, A. & Hensch, T. K. From brain formation to plasticity: insights on Otx2 homeoprotein. *Dev. Growth Differ.* **51,** 369–377 (2009).

108. Spatazza, J. *et al.* Choroid-plexus-derived Otx2 homeoprotein constrains adult cortical plasticity. *Cell Rep.* **3,** 1815–1823 (2013).

109. Sugiyama, S. *et al.* Experience-dependent transfer of Otx2 homeoprotein into the visual cortex activates postnatal plasticity. *Cell* **134,** 508–520 (2008).

110. Beurdeley, M. *et al.* Otx2 binding to perineuronal nets persistently regulates plasticity in the mature visual cortex. *J. Neurosci.* **32,** 9429–9437 (2012).

111. Despras, G. *et al.* Toward libraries of biotinylated chondroitin sulfate analogues: from synthesis to in vivo studies. *Chem. A Eur. J.* **19,** 531–540 (2013).

112. Dick, G. *et al.* Semaphorin 3A binds to the perineuronal nets via chondroitin sulfate type E motifs in rodent brains. *J. Biol. Chem.* **288,** 27384–27395 (2013).

113. Vo, T. *et al.* The chemorepulsive axon guidance protein semaphorin3A is a constituent of perineuronal nets in the adult rodent brain. *Mol. Cell. Neurosci.* **56,** 186–200 (2013).

114. Carulli, D., Foscarin, S., Faralli, A., Pajaj, E. & Rossi, F. Modulation of semaphorin3A in perineuronal nets during structural plasticity in the adult

cerebellum. *Mol. Cell. Neurosci.* **57,** 10–22 (2013).

115. Cregg, J. M. *et al.* Functional regeneration beyond the glial scar. *Exp. Neurol.* **253,** 197–207 (2014).

116. Jones, L. L., Margolis, R. U. & Tuszynski, M. H. The chondroitin sulfate proteoglycans neurocan, brevican, phosphacan, and versican are differentially regulated following spinal cord injury. *Exp. Neurol.* **182,** 399–411 (2003).

117. McKeon, R. J., Jurynec, M. J. & Buck, C. R. The chondroitin sulfate proteoglycans neurocan and phosphacan are expressed by reactive astrocytes in the chronic CNS glial scar. *J. Neurosci.* **19,** 10778–10788 (1999).

118. Tang, X., Davies, J. E. & Davies, S. J. A. Changes in distribution, cell associations, and protein expression levels of NG2, neurocan, phosphacan, brevican, versican V2, and tenascin-C during acute to chronic maturation of spinal cord scar tissue. *J. Neurosci.* **71,** 427–444 (2003).

119. Bradbury, E. J. & Carter, L. M. Manipulating the glial scar: Chondroitinase ABC as a therapy for spinal cord injury. *Brain Res. Bull.* **84,** 306–316 (2011).

120. Fouad, K. *et al.* Combining Schwann cell bridges and olfactory-ensheathing glia grafts with chondroitinase promotes locomotor recovery after complete transection of the spinal cord. *J. Neurosci.* **25,** 1169–1178 (2005).

121. García-Alías, G. *et al.* Chondroitinase ABC combined with neurotrophin NT-3 secretion and NR2D expression promotes axonal plasticity and functional recovery in rats with lateral hemisection of the spinal cord. *J. Neurosci.* **31,** 17788–17799 (2011).

122. Moon, L. D. F., Asher, R. A., Rhodes, K. E. & Fawcett, J. W. Regeneration of CNS

axons back to their target following treatment of adult rat brain with chondroitinase ABC. *Nat. Neurosci.* **4,** 465–466 (2001).

123. Alilain, W. J., Horn, K. P., Hu, H., Dick, T. E. & Silver, J. Functional regeneration of respiratory pathways after spinal cord injury. *Nature* **475,** 196–200 (2011).

124. Barritt, A. W. *et al.* Chondroitinase ABC promotes sprouting of intact and injured spinal systems after spinal cord injury. *J. Neurosci.* **26,** 10856–10867 (2006).

125. Bartus, K. *et al.* Large-scale chondroitin sulfate proteoglycan digestion with chondroitinase gene therapy leads to reduced pathology and modulates macrophage phenotype following spinal cord contusion injury. *J. Neurosci.* **34,** 4822–4836 (2014).

126. Bradbury, E. J. *et al.* Chondroitinase ABC promotes functional recovery after spinal cord injury. *Nature* **416,** 636–640 (2002).

127. García-Alías, G., Barkhuysen, S., Buckle, M. & Fawcett, J. W. Chondroitinase ABC treatment opens a window of opportunity for task-specific rehabilitation. *Nat. Neurosci.* **12,** 1145–1151 (2009).

128. Hunanyan, A. S. *et al.* Role of chondroitin sulfate proteoglycans in axonal conduction in Mammalian spinal cord. *J. Neurosci.* **30,** 7761–7769 (2010).

129. Imagama, S. *et al.* Keratan sulfate restricts neural plasticity after spinal cord injury. *J. Neurosci.* **31,** 17091–17102 (2011).

130. Ishikawa, Y., Imagama, S., Ohgomori, T., Ishiguro, N. & Kadomatsu, K. A combination of keratan sulfate digestion and rehabilitation promotes anatomical plasticity after rat spinal cord injury. *Neurosci. Lett.* **593,** 13–18 (2015).

131. Funderburgh, J. L. Keratan sulfate: structure, biosynthesis, and function.

Glycobiology **10,** 951–958 (2000).

132. Kadomatsu, K. & Sakamoto, K. Sulfated glycans in network rewiring and plasticity after neuronal injuries. *Neurosci. Res.* **78,** 50–54 (2014).

133. Takeuchi, K. *et al.* Chondroitin sulphate N-acetylgalactosaminyl-transferase-1 inhibits recovery from neural injury. *Nat. Commun.* **4,** 2740 (2013).

134. Ito, Z. *et al.* N-acetylglucosamine 6-O-sulfotransferase-1-deficient mice show better functional recovery after spinal cord injury. *J. Neurosci.* **30,** 5937–5947 (2010).

135. Zhang, H. *et al.* N-Acetylglucosamine 6-O-sulfotransferase-1 is required for brain keratan sulfate biosynthesis and glial scar formation after brain injury. *Glycobiology* **16,** 702–710 (2006).

136. Karumbaiah, L. *et al.* Targeted downregulation of N-acetylgalactosamine 4-sulfate 6-O-sulfotransferase significantly mitigates chondroitin sulfate proteoglycan-mediated inhibition. *Glia* **59,** 981–996 (2011).

137. Lin, R., Rosahl, T. W., Whiting, P. J., Fawcett, J. W. & Kwok, J. C. 6-Sulphated chondroitins have a positive influence on axonal regeneration. *PLoS One* **6,** e21499 (2011).

138. Properzi, F. *et al.* Chondroitin 6-sulphate synthesis is up-regulated in injured CNS, induced by injury-related cytokines and enhanced in axon-growth inhibitory glia. *Eur. J. Neurosci.* **21,** 378–390 (2005).

139. Gilbert, R. J. *et al.* CS-4,6 is differentially upregulated in glial scar and is a potent inhibitor of neurite extension. *Mol. Cell. Neurosci.* **29,** 545–558 (2005).

140. Mckeon, R. J., Höke, A. & Silver, J. Injury-induced proteoglycans inhibit the potential for laminin-mediated axon growth on astrocytic scars. *Exp. Neurol.* **136,**

32–43 (1995).

141. Olson, L. Medicine: clearing a path for nerve growth. *Nature* **416,** 589–590 (2002).

142. Sharma, K., Selzer, M. E. & Li, S. Scar-mediated inhibition and CSPG receptors in the CNS. *Exp. Neurol.* **237,** 370–378 (2012).

143. Coles, C. H. *et al.* Proteoglycan-specific molecular switch for RPTPσ clustering and neuronal extension. *Science (80-.).* **332,** 484–488 (2011).

144. Lang, B. T. *et al.* Modulation of the proteoglycan receptor PTPsigma promotes recovery after spinal cord injury. *Nature* **518,** 404–408 (2015).

145. Shimbo, M., Ando, S., Sugiura, N., Kimata, K. & Ichijo, H. Moderate repulsive effects of E-unit-containing chondroitin sulfate (CSE) on behavior of retinal growth cones. *Brain Res.* **1491,** 34–43 (2013).

Chapter 2: Carbohydrate Induced Eph Receptor Clustering Inhibits Neurite Growth

Abstract

Chondroitin sulfate proteoglycans (CSPGs) are a major barrier to regenerating axons in the central nervous system (CNS), exerting their inhibitory effect through their polysaccharide side chains. Chondroitin sulfate (CS) potently inhibits axon regeneration through modulation of inhibitory signaling pathways induced by carbohydrate binding to protein ligands and receptors. Here, we identify a novel carbohydrate-protein interaction between CS and EphA4 that inhibits axon regrowth. We characterize the mechanism of activation and demonstrate carbohydrate binding induces phosphorylation of the intracellular kinase domain through clustering of cell surface EphA4. Collectively, our studies present a novel mechanism of EphA4 activation by CS independent of the canonical ephrin ligands and uncover the role of this interaction in inhibition of neurite regrowth after injury. Our results underscore a mechanism of action by which carbohydrates can function as direct, activating ligands for protein receptors and provide mechanistic insights into the inhibition of axon growth by CS following injury to the CNS.

Introduction

Central nervous system (CNS) injury has lasting emotional and economic effects on patients and their loved ones. These debilitating injuries are characterized by impaired motor and sensory function due the failure of axons to regenerate past the site of injury[1]. Inhibition of axon regrowth has been linked to inhibitory extracellular matrix molecules produced in response to CNS damage[2,3]. Chondroitin sulfate proteoglycans (CSPGs) prevent axon regeneration and impede functional recovery following injury to the CNS. The inhibitory activity of CSPGs is primarily associated with their chondroitin sulfate (CS) polysaccharide side chains. In fact, *in vivo* digestion of CS chains using chondroitinase ABC (ChABC) promotes axon growth, sprouting, and plasticity in the CNS[4,5]. Importantly, our lab has previously shown that the CS-E sulfation motif is a key structural determinant contributing to the inhibitory activity of CS and that blocking this motif with a CS-E specific antibody can promote axon regeneration[6]. Thus, deciphering the underlying molecular mechanisms by which CS exerts its inhibitory effects may provide novel ways to promote functional recovery after injury.

Recent work suggests CS actively inhibits axon regeneration through the direct engagement of soluble ligands and cell surface receptors via carbohydrate-protein interactions[7,8]. Moreover, targeting specific CS-receptors has emerged as a potential therapeutic avenue to promote axon regeneration following injury to the CNS[9]. However, residual inhibition is frequently observed after deletion of individual CS-binding proteins, suggesting functional redundancy within the system[10,11]. Together, these results suggest that additional, unknown CS receptors contribute to the prevention of axon regrowth,

whose discovery could allow for a more complete understanding of the multifaceted inhibitory effects of CS.

One class of receptors known to control proper development and maintenance of the nervous system are the Eph family of receptor tyrosine kinases[12]. Members of the Eph receptor family, including both EphA and EphB receptors, are upregulated after injury to the adult CNS, and these proteins have been implicated in the prevention of regeneration following injury[13–15]. Moreover, this family of receptors has been suggested as therapeutic targets for promoting regeneration following CNS injury[16,17]. In particular, the genetic deletion of the EphA4 receptors in mice led to an increase in neural regeneration and functional recovery after CNS injury[18]. In addition, pharmacological blocking of EphA4 receptor activity after spinal cord injury allowed axonal regrowth, improved grip strength, and motor function in injured mice[19–21].

Here, we identify and characterize the mechanism of activation of a novel CS receptor important for inhibiting axon regrowth after injury. We demonstrate that CS binding to the extracellular domain of EphA4 promotes receptor clustering and phosphorylation of the intracellular kinase domain. Importantly, we demonstrate that this carbohydrate-protein interaction is functionally relevant using a microfluidics based axotomy assay; neurons expressing CS binding deficient mutants of EphA4 show improved regeneration when cultured in a CS rich environment. The combined results suggest that CS acts as a ligand for EphA4 and elicits an inhibitory response towards neurite growth, highlighting a new mechanism of activation for the Eph family of receptors and providing new functional insights into the molecular mechanisms of neural regeneration.

Results

CS binds to EphA4 and inhibits neurite outgrowth

We previously performed a pull down of CS-E binding proteins from rat brain homogenate enriched for membrane proteins to identify putative carbohydrate receptors[6]. In addition to the receptor PTPσ, this screen identified members of the Eph family of receptor tyrosine kinases, specifically EphA4. We first examined the potential interaction between CSPGs and EphA4. The complete ectodomain of EphA4 (residues 20-547), fused to the human immunoglobulin Fc domain to generate the fusion protein EphA4-Fc, bound strongly to biotinylated-CSPGs immobilized on streptavidin-coated plates (Fig. 2.1a). Binding was not observed for CSPGs pre-digested with ChABC to remove their glycosaminoglycan side chains, showing this binding was carbohydrate dependent. We turned to carbohydrate microarrays to explore the sulfation patterns responsible for CS-EphA4 interactions. CS polysaccharides enriched in specific sulfation motifs were arrayed on poly-D-lysine coated glass slides and incubated with EphA4-Fc. Strong binding to CS-E enriched polysaccharides was observed (Fig. 2.1b). The weakest binding was observed CS-A and CS-C, followed by CS-D and CS, a preparation containing a mix of sulfation patterns. A similar trend was observed for EphA4-Fc binding to biotinylated CS polysaccharides immobilized on streptavidin-coated plates (Fig. 2.1c). Kinetic analysis using surface plasmon resonance revealed that EphA4-Fc binds to CS-E polysaccharides with high nanomolar affinity (K_D = 856 nM, Fig. 2.1d).

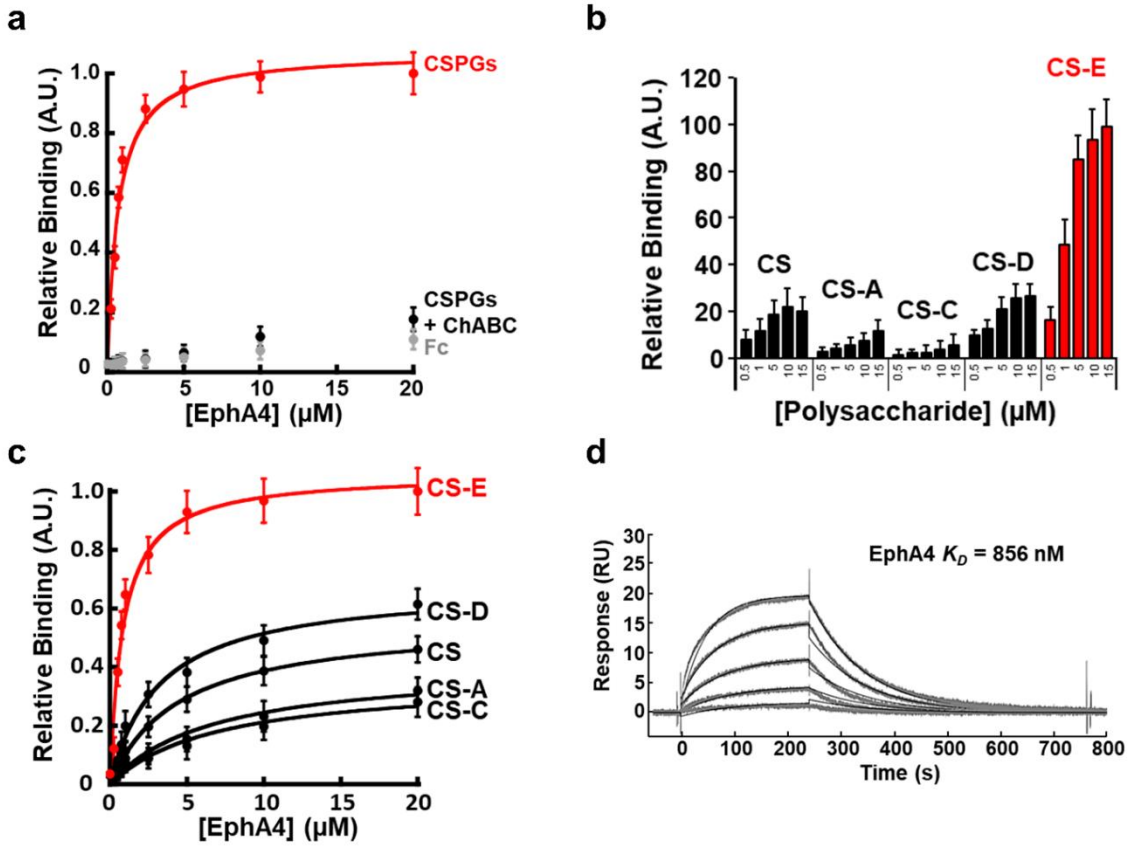

Figure 2.1: EphA4 binds the glycosaminoglycan side chains of CSPGs (**a**) EphA4-Fc binds to CSPGs and CSPGs pre-digested with ChABC to remove GAG side chains, immobilized on streptavidin coated plates. Fc alone shows no binding to CSPGs. Bound protein detected with anti-human IgG Fc antibody conjugated to HRP (n=3, mean ± SD, error bars). (**b**) EphA4-Fc binds to CS-E-enriched polysaccharides on glycosaminoglycan microarrays printed with CS polysaccharides enriched in CS-A, -C, -D, and -E motifs (n=10 per condition, mean ± SD, error bars). (**c**) EphA4-Fc binds to biotinylated CS immobilized on streptavidin coated plates. CS polysaccharides are enriched in CS-A, -C, -D, and -E sulfation motifs. The amount of bound EphA4-Fc was detected using anti-human IgG Fc antibody conjugated to HRP. The experiment was performed in triplicate, and mean values (± SD, error bars) are shown. (d) Kinetic analysis of the interaction between EphA4-Fc and CS-E polysaccharides by surface plasmon resonance. CS-E polysaccharides were covalently immobilized onto the surface via reductive amination chemistry.

To explore EphA4-CS interactions in a more biologically relevant context, we examined whether EphA4-Fc interacts with CSPGs that are produced endogenously by astrocytes, a cell type that produces inhibitory CSPGs at sites of neural injury preventing axon regeneration. Importantly, Neu7 astrocytes express significant amounts of the CS-E motif[22], a specific sulfation motif that potently inhibits axon regeneration and the motif identified to strongly interact with EphA4. EphA4-Fc, but not Fc alone, was found to bind astrocyte cultures, as shown by both enzymatic detection and immunofluorescence (Fig. 2.2a, b, c). The involvement of CS chains was confirmed by pretreatment of astrocytes with ChABC, which significantly reduced EphA4-Fc binding. Blocking the CS-E motif using a CS-E specific antibody significantly reduced the amount of surface bound EphA4-Fc (Fig. 2.2a, d)

We reasoned the observed interaction between EphA4 and CS may contribute to inhibition of neurite outgrowth. To determine the role of EphA4 in CS-mediated inhibition, we analyzed the neurite growth of dorsal root ganglion (DRG) neurons derived from EphA4$^{-/-}$ mice cultured on a substratum coated with CSPGs or CS-E-enriched polysaccharides (Fig. 2.3a, b). Deletion of EphA4 significantly attenuated CSPG- and CS-E-induced inhibition of neurite outgrowth in DRG neurons, and inhibition is not observed for CSPGs pre-treated with ChABC. These results indicate that the EphA4-CS interaction inhibits neurite growth and may contribute to the CS mediated inhibition of axon regeneration *in vivo*.

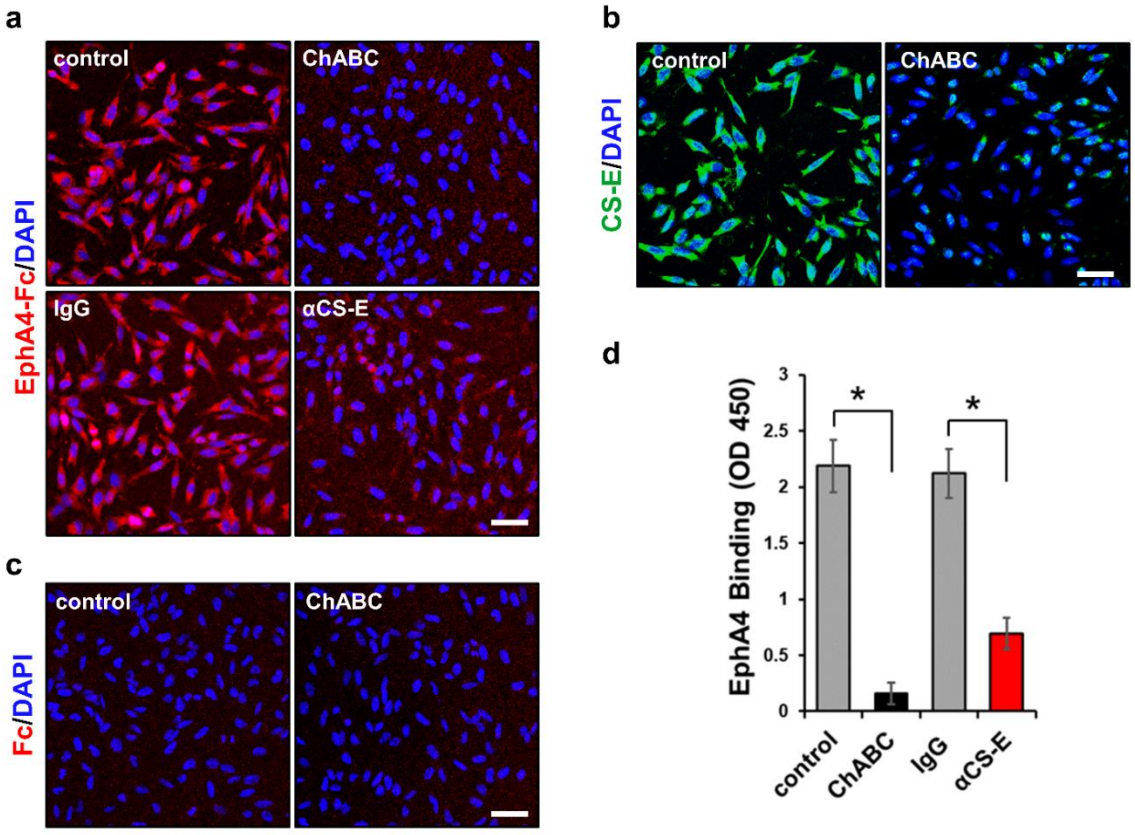

Figure 2.2: CS expression and EphA4 binding to Neu7 astrocytes. (**a**) Representative immunofluorescence images of EphA4-Fc bound to the surface of Neu7 astrocytes treated with ChABC to remove glycosaminoglycan side chains (top-right) and untreated control (top-left); EphA4-Fc binding is blocked by pre-treatment of Neu7 astrocytes with a CS-E antibody (bottom-right) but not by isotype matched IgG control antibody (bottom-left) (scale bar, 50 μm). (**b**) Chondroitin sulfate expression on Neu7 astrocytes. Representative immunofluorescence images of Neu7 astrocytes stained with anti-CS-E antibody. Control (left) and ChABC digested (right) to remove CS side chains (scale bar, 50 μm). (**c**) Fc does not bind to the surface of Neu7 astrocytes (scale bar, 50 μm). (d) Quantification of bound EphA4 to Neu7 cells treated with ChABC to remove glycosaminoglycan side chains, pre-blocked with isotype matched IgG control antibody, or αCS-E antibody; bound EphA4 detected using anti-human IgG Fc antibody conjugated to HRP (± SD, error bars, n = 3 per condition).

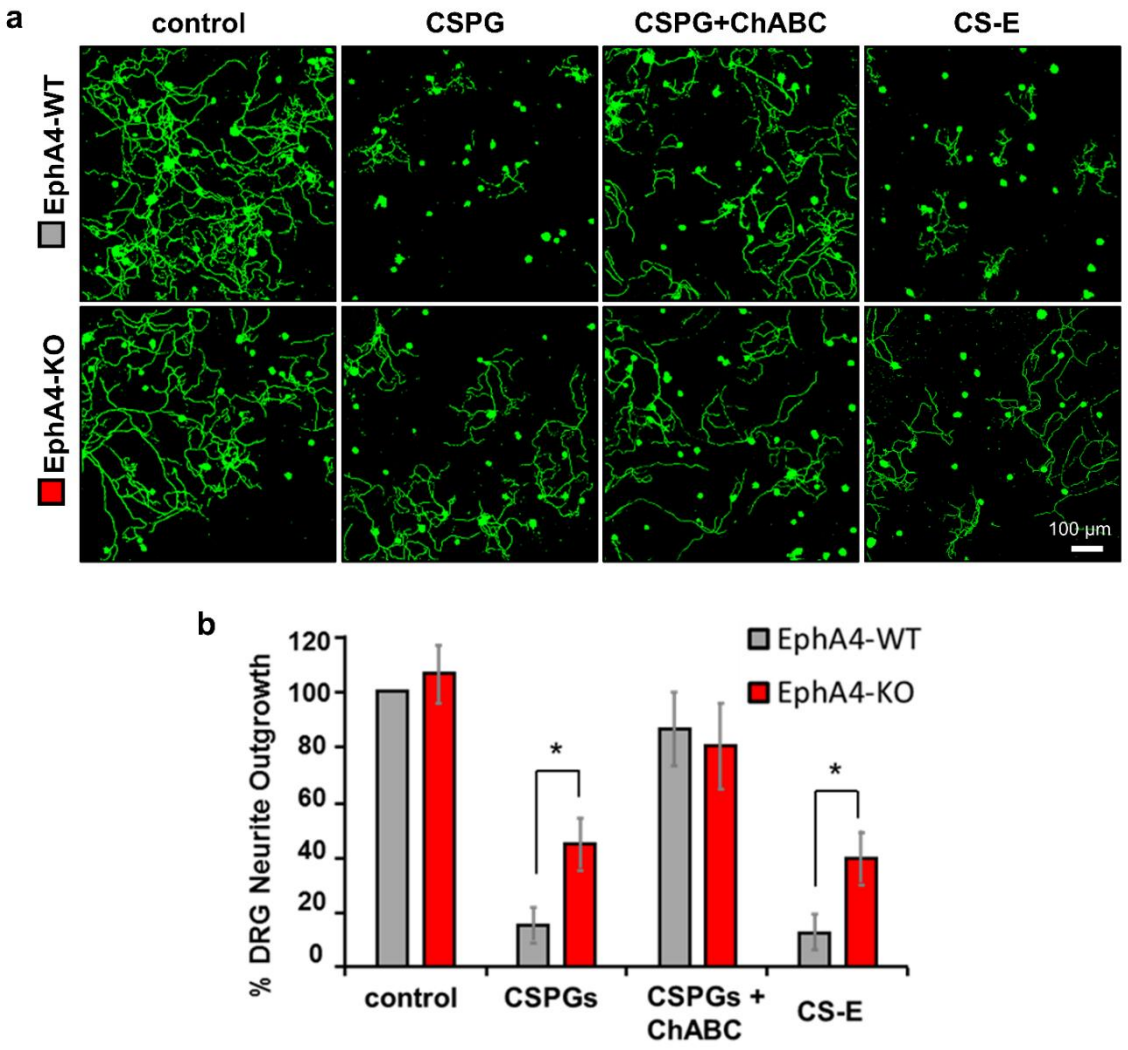

Figure 2.3: DRGs lacking EphA4 show improved neurite outgrowth when cultured on a substratum of inhibitory CS (**a**) Dissociated mouse P6 DRGs from EphA4-WT and EphA4-KO mice were cultured on a substratum of CSPGs or CSPGs pre-digested with ChABC to remove glycosaminoglycan side chains, or CS-E enriched polysaccharides. Neurons were cultured for 24 h and fixed and stained with anti-βIII-tubulin antibody. Representative images (scale bar, 100 µm) and (**b**) quantification of average neurite length (± SEM, error bars) from three experiments (n = 150-200 cells per condition). ANOVA analysis ($F = 101.26$, $P < 0.0001$) with post hoc Tukey's HSD shows a significant effect between these groups (* $P < 0.01$).

CS induces EphA4 clustering and phosphorylation

Eph receptor engagement with ephrin ligands results in clustering of the extracellular domain and phosphorylation of the intracellular kinase domain[23,24]. To investigate the ability of CS to activate EphA4, we first asked whether CS could cluster EphA4 in a similar manner to ephrin ligands. We developed a microscopy-based assay to visualize cell-surface EphA4 by inserting an *N*-terminal HA tag between the signal peptide and ligand binding domain, HA-EphA4. Immunofluorescence staining of unpermeabilized COS-7 cells that were transfected with this construct showed robust surface staining (Fig. 2.4a,b). Furthermore, HA-EphA4 is uniformly distributed across the cell surface. To confirm clustering of HA-EphA4, cells were stimulated with pre-clustered ephrinA5-Fc. Immunostaining revealed the formation of distinct HA-EphA4 puncta on the cell surface, suggesting the presence of concentrated receptor clusters (Fig. 2.4c). Treatment of EphA4-HA expressing cells with CS-E enriched polysaccharides revealed a similar punctate staining as ephrinA5-Fc treated cells. Importantly, receptor clustering is dependent on the glycosaminoglycan side chains. Distinct puncta are not present on cells stimulated with CSPGs pre-digested with ChABC. CS binding to EphA4 is sufficient to induce receptor clustering in a similar manner as its natural ligand, ephrinA5.

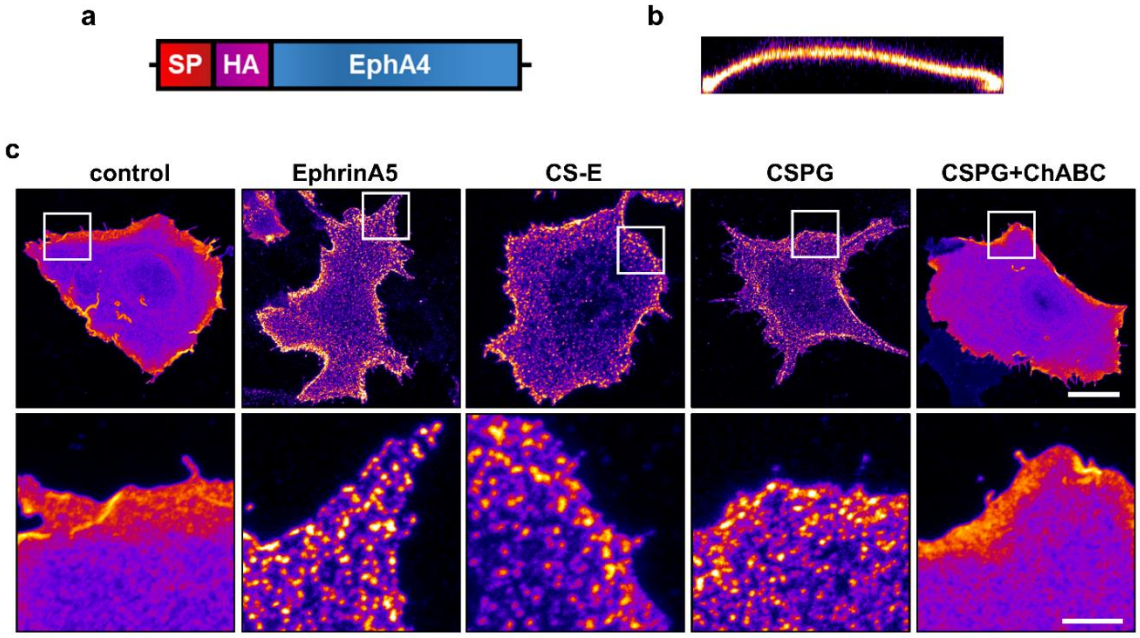

Figure 2.4: CS clusters cell surface EphA4 (**a**) Full length EphA4 construct used in clustering assay. An N-terminal HA-tag was inserted between the signal peptide (SP) and the ligand binding domain of EphA4. (**b**) Cross-section (X-Z plane) of COS7 cell expressing EphA4 containing an N-terminal HA-tag. Only cell-surface EphA4 is detected. (**c**) Cell surface EphA4 is clustered by stimulation with EphrinA5-Fc, CS-E polysaccharides, and CSPGs but not by CSPGs pre-digested with ChABC to remove glycosaminoglycan side chains. N-terminal HA-tagged EphA4 was visualized by immunostaining with an HA antibody. Representative images showing maximum intensity projections of z-stacks of single cells (63x): full cell (top; scale bar, 20 μm) and zoom-in of boxed area (bottom; scale bar, 5 μm).

We next examined whether EphA4 clustering via CS could lead to increased tyrosine phosphorylation. COS-7 cells were transfected with full-length EphA4 containing a *C*-terminal Myc tag. Cells were stimulated with pre-clustered ephrinA5-Fc or CSPGs, total EphA4 was immunoprecipiated with an anti-Myc antibody, and tyrosine phosphorylation was assayed by Western blot (Fig. 2.5a). As expected, stimulation with ephrinA5-Fc increased tyrosine phosphorylation of EphA4. Excitingly, cells treated with CSPGs revealed an induction of tyrosine phosphorylation of EphA4. We next examined the sulfation dependency of EphA4 tyrosine phosphorylation by CS. Stimulation with

polysaccharides enriched in specific sulfation motifs revealed an induction of tyrosine phosphorylation when cells were stimulated by CS-E (Fig. 2.5b). A modest degree of phosphorylation was observed for cells stimulated with CS-D, mirroring trends observed in binding to these sulfation pattern enriched CS preparations. These results suggest that CS polysaccharides are sufficient to cluster and elicit tyrosine phosphorylation of EphA4, indicative of functional Eph receptor signaling clusters.

Finally, we examined the role of CS-E in EphA4 phosphorylation *in vivo*. To test this, we used mice containing a targeted gene disruption of *N*-acetylgalactosamine 4-sulfate 6-*O* sulfotransferase 15 (Chst15), the enzyme that generates CS-E via addition of a sulfate group to the 6-O position of GalNAc on CS-A. Consistent with *in vitro* results, removal of CS-E motif resulted in a reduction in tyrosine phosphorylation of EphA4

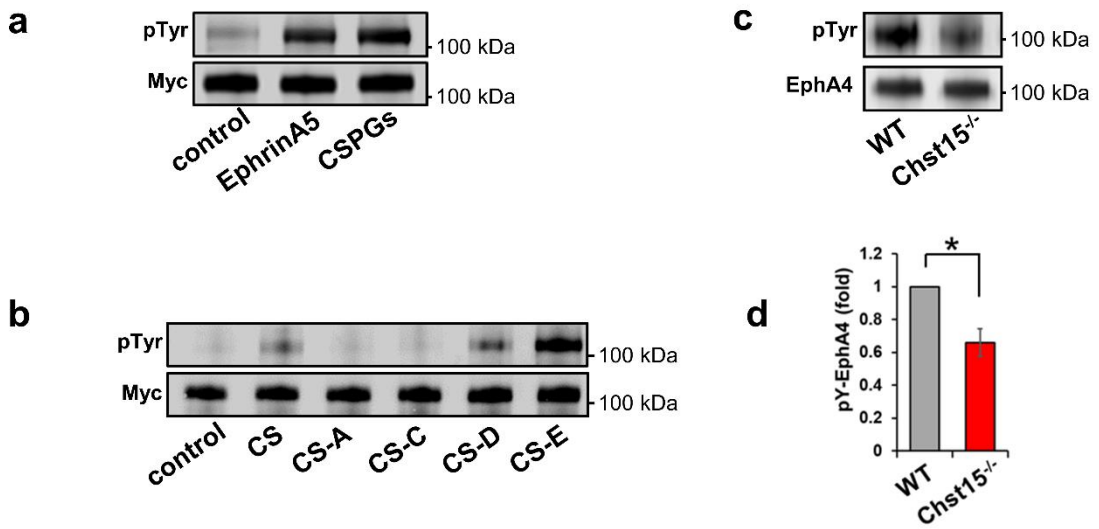

Figure 2.5: CS induces tyrosine phosphorylation of EphA4 (**a**) Western blot of phosphotyrosine EphA4 (pTyr) and total EphA4 (Myc) immunoprecipiated with a Myc antibody from COS7 cells stimulated with EphrinA5-Fc and CSPGs, and (**b**) CS polysaccharides and CS enriched in CS-A, -C, -D, and -E sulfation motifs. (**c**) Western blot of phosphotyrosine EphA4 (pTyr) and total EphA4 (EphA4) immunoprecipiated, with an EphA4 antibody, from hippocampal lysates of WT and Chst15$^{-/-}$ mice. (**d**) Quantification of phosphotyrosine EphA4 from WT and Chst15$^{-/-}$ mice (n=3, mean ± SD, error bars). * $P < 0.05$, Student's t-test.

immunoprecipiated from hippocampal lysates (Fig. 2.5c,d). Taken together, these studies demonstrate that the CS-E motif is sufficient to cluster and activate the receptor EphA4.

CS binds distal to the canonical ligand-binding domain

We next aimed to determine the site of CS-EphA4 interactions. We first generated electrostatic surface potential maps for EphA4 to provide insights into regions that may bind CS. Immediately evident is the localization of electropositive regions of EphA4 to the EGF and the two FN3 domains. In contrast, the ligand binding domain (LBD) and sushi domain are electronegative. We generated two different Fc fusion constructs of the ectodomain of EphA4, EphA4^{LBD}-Fc (residues 20-209) and EphA4^{FN3}-Fc (residues 210-547). We first tested binding of these EphA4 truncations to biotinylated CS-E immobilized on streptavidin-coated plates (Fig. 2.6a). EphA4^{FN3}-Fc bound strongly to CS-E enriched polysaccharides, comparable to the full ectodomain fusion protein, EphA4-Fc. The LBD, EphA4^{LBD}-Fc, showed a significant decrease in binding to CS-E.

We then examined if CS interactions with the fibronectin domains of EphA4 are sufficient to induce the clustering and phosphorylation of EphA4 in a cellular context. In the cell-surface clustering assay described above, COS-7 cells expressing EphA4$^{\Delta LBD}$ (residues 210-986) truncation containing an *N*-terminal HA tag, HA-EphA4$^{\Delta LBD}$, were stimulated with pre-clustered ephrinA5-Fc or CS-E enriched polysaccharides (Fig. 2.6c, d). Here, we observed the formation of distinct puncta on the surface of cells stimulated with CS-E polysaccharides. However, stimulation with ephrinA5-Fc did not induce clustering of HA-EphA4$^{\Delta LBD}$, showing instead uniform receptor expression on the cell surface. To test if clustering of LBD truncation by CS results in tyrosine phosphorylation of EphA4, COS-7 cells were transfected with a LBD truncation containing a *C*-terminal

Myc tag, EphA4$^{\Delta LBD}$ (residues 210-986), and stimulated with pre-clustered ephrinA5-Fc or CS-E enriched polysaccharides (Fig. 2.6b). Total EphA4 was immunoprecipiated using an anti-Myc antibody, and tyrosine phosphorylation was assayed by Western blot. As expected, this truncation was no longer phosphorylated in response to stimulation by ephrinA5-Fc. However, stimulation with CS-E polysaccharides still induces tyrosine phosphorylation of the intracellular kinase domain. These results suggest CS-E clusters and phosphorylates EphA4 independent of the ligand binding domain.

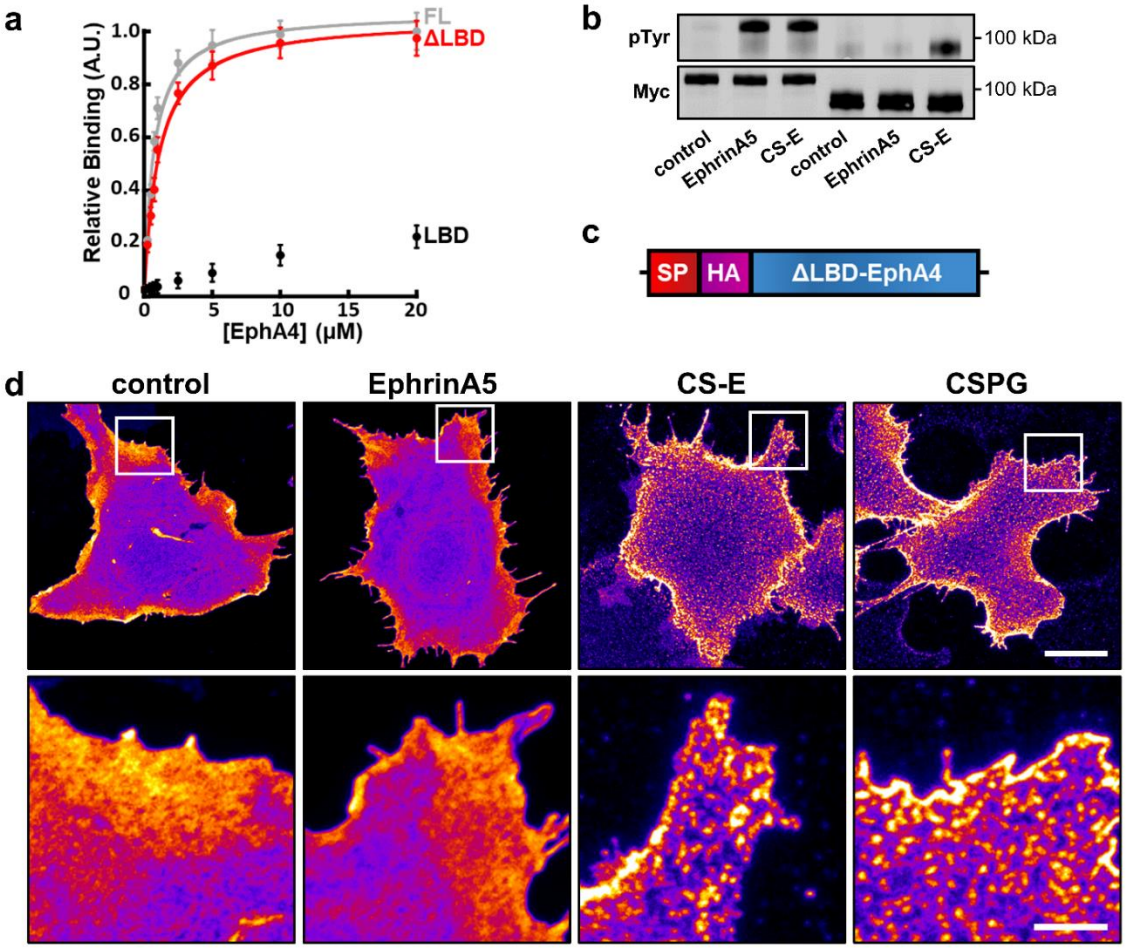

Figure 2.6: Receptor clustering and phosphorylation is independent of ligand binding domain (**a**) Ectodomain constructs EphA4-Fc and ΔLBD-Fc, but not LBD-Fc bind to biotinylated CS-E immobilized on streptavidin coated plates. Bound protein detected with anti-human IgG Fc antibody conjugated to HRP (n=3, mean ± SD, error bars). (b) Western blot analysis of full length EphA4 (left) and ΔLBD-EphA4 immunoprecipiated with a Myc antibody from COS7 cells stimulated with EphrinA5-Fc and CS-E polysaccharides. (**c**) Ligand binding domain truncation of EphA4 (ΔLBD-EphA4) used in clustering assay. An N-terminal HA-tag was inserted between the signal peptide (SP) and the sushi domain of EphA4. (**d**) Cell surface ΔLBD-EphA4, containing the intracellular kinase domain, is clustered by CS-E polysaccharides, and CSPGs but not EphrinA5-Fc. Representative images showing maximum intensity projections of z-stacks of single cells (63x): full cell (top; scale bar, 20 μm) and zoom-in of boxed area (bottom; scale bar, 5 μm).

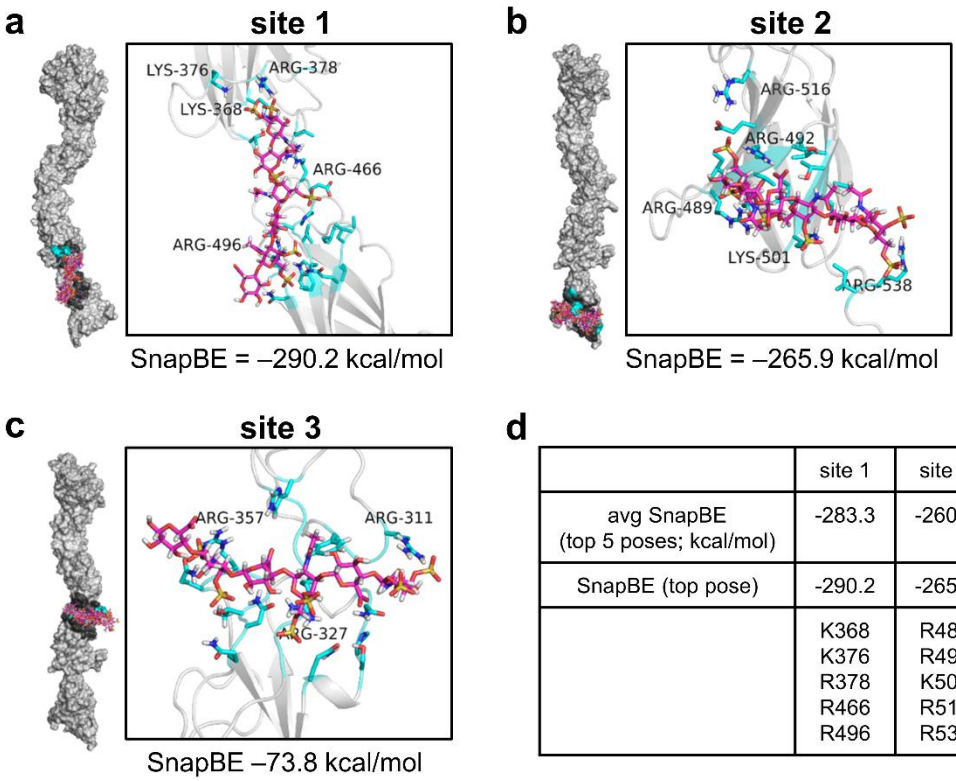

	site 1	site 2	site 3
avg SnapBE (top 5 poses; kcal/mol)	-283.3	-260.6	-65.7
SnapBE (top pose)	-290.2	-265.9	-73.8
	K368 K376 R378 R466 R496	R489 R492 K501 R516 R538	K292 R311 R327 R357 K394

Figure 2.7: Computational docking of CS-E hexasaccharide (**a**, **b**, **c**) Computational docking of a CS-E hexasaccharide identified three potential binding sites, top five poses are shown on surface representation of EphA4 ectodomain with residues within 5 Å of ligand colored black. Zoomed in structure shows the top pose for each site. The SnapBE (snap binding E = complex E – protein E – ligand E) for top pose for each site (**a**) site 1 = -290.2 kcal/mol, (**b**) site 2 = -265.9 kcal/mol, and (**c**) site 3 = -73.8 kcal/mol. (**d**) Summary for the three putative CS-E binding sites. The average SnapBE for the top 5 poses, SnapBE for the top pose, and Arginine and Lysine residues found in these potential binding sites are listed.

Loss of CS binding prevents EphA4 phosphorylation

To better understand CS interactions with EphA4, we utilized our recently developed GAG-DOCK methodology to identify glycosaminoglycan binding sites on proteins.[25] The top docked poses all clustered to three regions of EphA4 outlined by the following arginine and lysine residues: site 1, K368, K376, R378, R466, and R496; site 2, R489, R492, K501, R516, and R538; site 3, K292, R311, R327, R357, and K394 (Fig. 2.7). The average SnapBE (snap binding E = complex E – protein E – ligand E) for site 1 (-283.3

kcal/mol) and site 2 (-260.6 kcal/mol) were significantly better than site 3 (-60.4 kcal/mol). We generated ectodomain EphA4-Fc fusion proteins with key arginine and lysine residues mutated to alanine to assess mutant binding to biotinylated CS-E immobilized on streptavidin-coated plates (Fig. 2.8a). Binding was significantly reduced for site 1, EphA4$^{5A:1}$-Fc, and site 2, EphA4$^{5A:2}$-Fc. However, residual binding to CS-E was still observed, likely due to binding from the non-mutated site. The site 3 mutant, EphA4$^{5A:3}$-Fc, displayed similar affinity for CS-E as WT EphA4-Fc. The combined mutant of site 1 and site 2, EphA4^{10A}-Fc showed an ever further decrease of CS-E binding, suggesting both of these sites contribute to binding. In fact, these two sites form a contiguous surface that wraps around the two FN3 domains of EphA4 (Fig 2.8c). Electrostatic surface potential map of the ectodomain of the combined mutant, EphA4^{10A}, reveals a shift from electropositive to electronegative character of this region (Fig. 2.8b). Moreover, binding to CSPGs produced by Neu7 cells is significantly reduced for EphA4^{10A}-Fc (Fig 2.8d, e). These findings suggest the set of arginine and lysine residues found in site 1 and site 2 contribute to CS-E binding.

We next examined the ability of CS to induce the phosphorylation of these CS-E binding deficient mutant EphA4. We generated a full length EphA4 constructs of the site 1, site 2, and the combined site 1 and site 2 mutants to assess their ability to be phosphorylated by stimulation with CS-E polysaccharides (Fig. 2.8f, g). The individual site mutants of site 1 and site 2 show modest decrease in tyrosine phosphorylation but each are still activated by CS-E. Only the double site mutant showed a complete loss of tyrosine phosphorylation after CS-E stimulation. Importantly, these CS-E binding site mutants are still active and functional receptors. Ephrin-A5 induces comparable levels of tyrosine

phosphorylation of all EphA4 mutants used in this study. These results confirm that CS-E-mediated EphA4 activation occurs through binding sites 1 and 2 identified using our computational method.

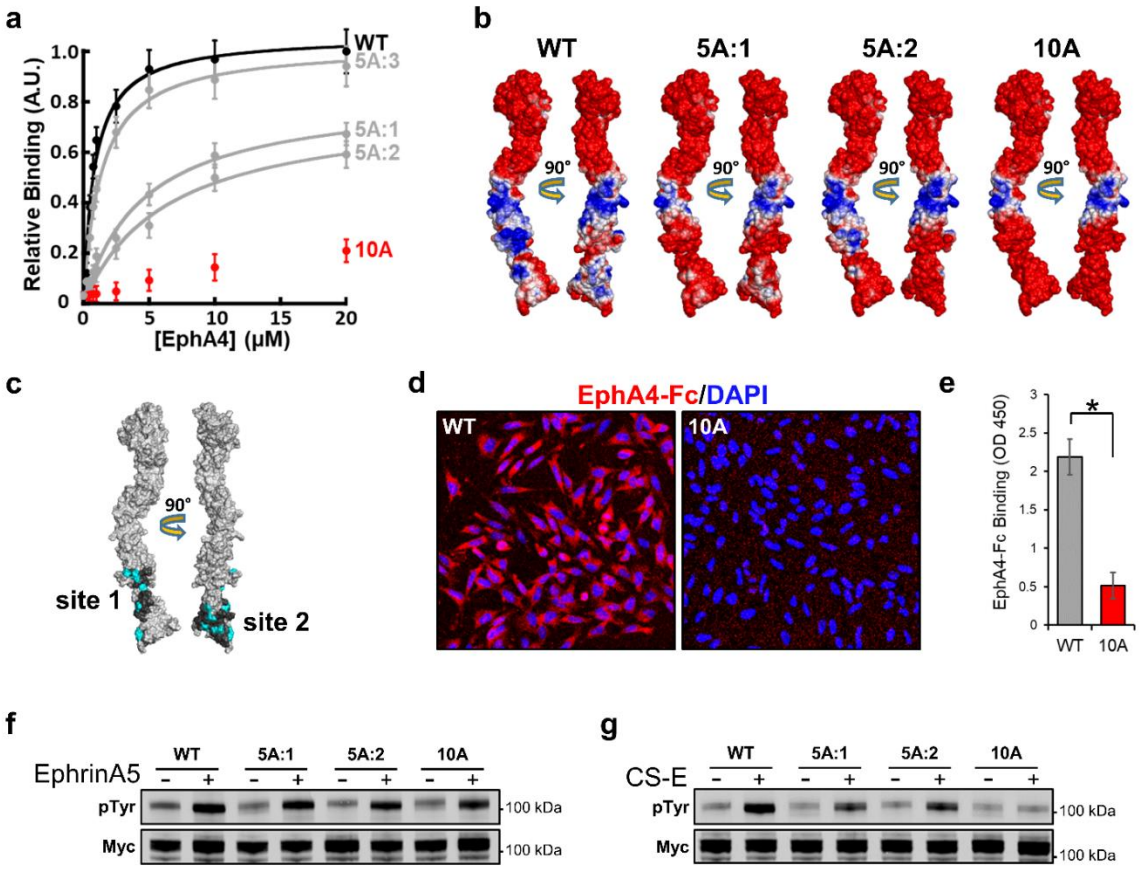

Figure 2.8: Loss of carbohydrate binding attenuates EphA4 phosphorylation (a) EphA4 mutant binding to biotinylated CS-E immobilized on streptavidin coated plates; site 1 mutant, EphA4$^{5A:1}$-Fc (K368A, K376A, R378A, R466A, R496A); site 2 mutant, EphA4$^{5A:2}$-Fc (R489A, R492A, K501A, R516A, R538A); site 3 mutant, EphA4$^{5A:3}$-Fc (K292A, R311A, R327A, R357A, K394A); EphA4^{10A}-Fc (5A:1 + 5A:2) (n=3, mean ± SD, error bars). (**b**) Electrostatic potential map of the ectodomain for WT, 5A:1, 5A:2, and 10A mutants. (**c**) Site 1 and site 2 form a contiguous region in the fibronectin domains. Residues within 5 Å of ligand colored black and arginine and lysine residues colored cyan. (**d**) EphA4^{WT}-Fc and EphA4^{10A}-Fc (5A:1 + 5A:2) bound to the surface of Neu7 astrocytes (scale bar, 50 μm). (**e**) Quantification of (**d**), bound EphA4-Fc detected by anti-human IgG Fc antibody conjugated to HRP (± SD, error bars, n = 3 per condition). * $P < 0.01$, Student's t-test. Western blot analysis of full length EphA4 mutants (WT, 5A:1, 5A:2, and 10A) expressed in COS7 cells and immunoprecipiated with a Myc antibody after being stimulated with (**f**) EphrinA5 and (**g**) CS-E polysaccharides.

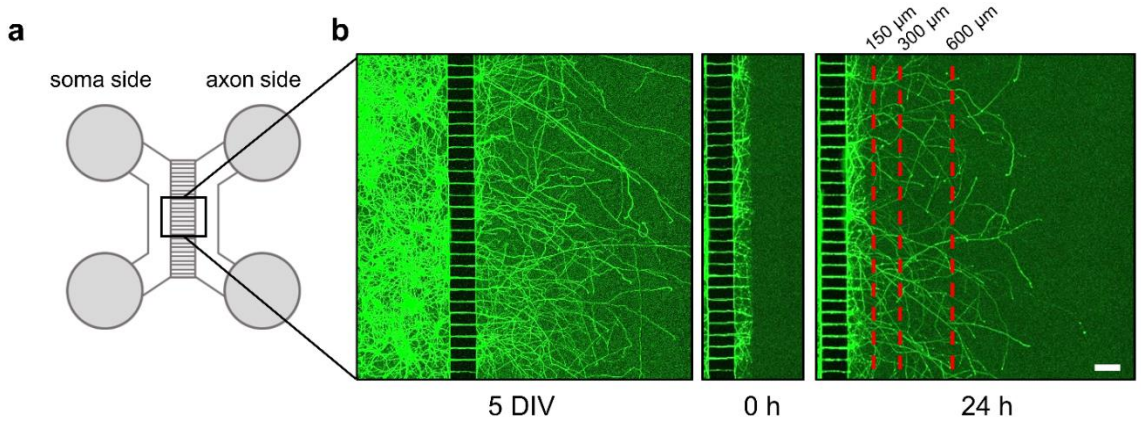

Figure 2.9: Microfluidic Axotomy Assay (**a)** Microfluidic cell culture device for isolation of neuron soma from axons. Microgroove barriers prevent soma from entering channels (axon channels are 150 µm long). (**b**) *In vitro* axotomy assay. E16 cortical neurons from EphA4$^{-/-}$ mice transduced with lentivirus construct expressing EphA4^{WT} or EphA4^{10A} under EF-1α promoter and GFP under CMV promoter. Neurons were cultured for 5 days in vitro (DIV) and axotomy pe2.rformed by aspirating media from the axon side. Neurons were cultured for 24 h post-axotomy and imaged (scale bar, 150 µm). The number of axons that grew 150 µm, 300 µm, and 600 µm from the end of the microgroove barriers (represented by dashed red lines) were counted.

CS binding deficient mutants show improved axon regrowth

We ultimately wanted to examine the functional importance of the CS-EphA4 interaction towards the growth of severed axons. To this end, we utilized an *in vitro* axotomy assay using a microfluidic cell culture platform[26]. These microfluidic devices contain separate compartments connected by microgroove channels that allow the growth of neuronal processes but not cell bodies (Fig. 2.9a). Neurons were cultured for five days, and allowed to extend their processes through the microgroove channels to the neurite compartment. Neurites were severed by aspirating media from the neurite compartment of the device without affecting the cell bodies. Media containing CS-E was added to the neurite compartment, and neurons were cultured for 24 h post-axotomy (Fig. 2.9b). We generated lentiviruses to expresses EphA4^{WT} or EphA4^{10A} under the elongation factor-1

alpha (EF-1α) promoter and GFP under the cytomegalovirus (CMV) promoter (Fig. 2.10a,b,c). We confirmed expression of EphA4^{WT}, EphA4^{10A}, and GFP in transduced cortical neurons derived from EphA4$^{-/-}$ mice by Western blot and immunofluorescence.

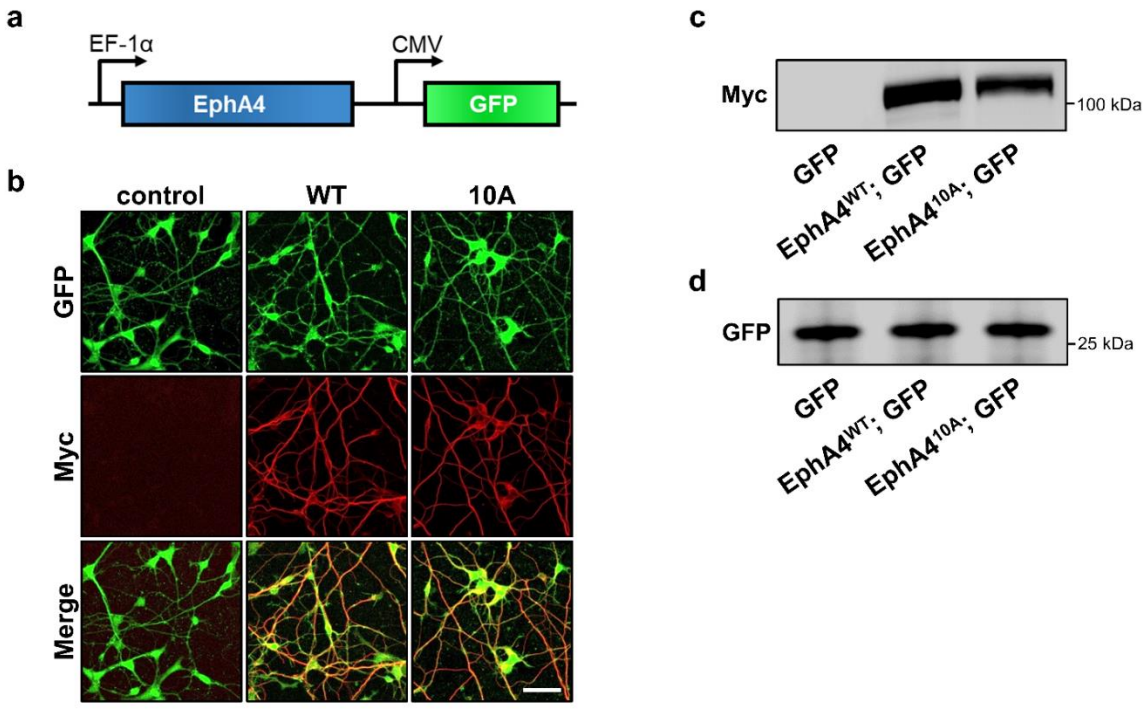

Figure 2.10: Lentivirus expression of mutant EphA4 receptor. (**a**) Lentivirus construct expressing full length EphA4^{WT} and EphA4^{10A} under Elongation Factor 1 alpha (EF-1α) promoter and GFP under CMV promoter. (**b)** E16 cortical neurons from EphA4-KO mice transduced with lentivirus construct expressing full length EphA4^{WT}, EphA4^{10A} (with a C-terminal Myc-tag) under Elongation Factor 1 alpha (EF-1α) promoter and GFP under CMV promoter. Neurons were cultured for three days then fixed and stained with anti-GFP antibody and anti-Myc antibody (scale bar, 50 µm). (**c)** Immunoprecipitation using an anti-Myc antibody from neuronal lysates and analyzed by Western blot using an anti-Myc antibody. (**d**) Western blot of lysates using anti-GFP antibody.

We quantified the regrowth of neurons expressing WT and CS-binding deficient mutant EphA4 receptors following axotomy by counting the number of neurites that extend 150 μm, 300 μm, and 600 μm from the edge of the microgroove channels. Importantly, no change in neurite regrowth was observed from unstimulated neurons expressing either $EphA4^{WT}$ or $EphA4^{10A}$ (Fig. 2.11a,b). When media containing CS-E was added to the neurite compartment post-axotomy, we observed a significant decrease in regeneration of neurons expressing $EphA4^{WT}$ compared to those expressing $EphA4^{10A}$ (Fig. 2.11c,d). At each measured distance from the microgroove channels, 150 μm, 300 μm, and 600 μm, neurons expressing $EphA4^{WT}$ exhibited impaired regenerative abilities. Most strikingly, neurons expressing $EphA4^{WT}$ showed no neurites that grew past 600 μm as seen with $EphA4^{10A}$-expressing cells. Together, these results show that preventing CS-E binding to EphA4 increases both the number and length of regenerating axons when cultured in a CS-E rich environment, such as the glial scar.

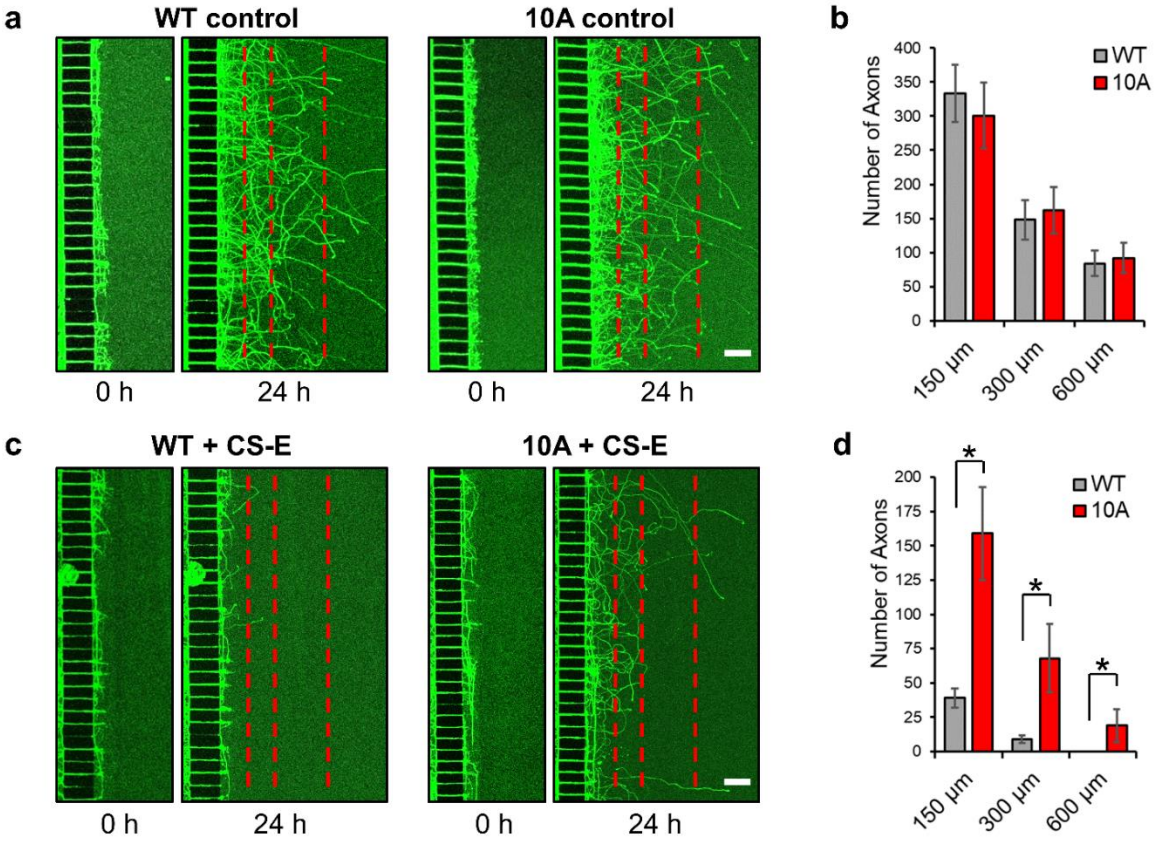

Figure 2.11: Loss of CS-E binding promotes axon regeneration *In vitro* axotomy assay. E16 cortical neurons from EphA4$^{-/-}$ mice transduced with lentivirus construct expressing EphA4^{WT} or EphA4^{10A} under EF-1α promoter and GFP under CMV promoter. Neurons were cultured for 5 days in vitro (DIV) and axotomy performed by aspirating media from the axon side. Neurons were cultured for 24 h post-axotomy and imaged (scale bar, 150 µm). The number of axons that grew 150 µm, 300 µm, and 600 µm from the end of the microgroove barriers (represented by dashed red lines) were counted. (**a**) Neurons expressing EphA4^{WT} and EphA4^{10A} show similar axon regrowth following axotomy, in the absence of CS-E polysaccharides. E16 cortical neurons from EphA4-KO mice transduced with lentivirus construct EphA4^{WT} and EphA4^{10A} and GFP. (**b**) Quantification of (**a**), axon regeneration of in the absence of CS-E. (**c**) *In vitro* regeneration of EphA4-KO cortical neurons expressing EphA4^{WT} and EphA4^{10A}. Following axotomy, media containing CS-E polysaccharides was placed in the axon side and cultured for 24 h. (**d**) Quantification of (**c**), axon regeneration in the presence of CS-E polysaccharides. The average number of axons growing 150 µm, 300 µm, and 600 µm from the end of the microgroove barriers from five independent experiments (± SD, error bars) are shown. * $P < 0.01$, Student's t-test.

Discussion

Chondroitin sulfate inhibits axon regeneration through its ability to engage cell surface receptors and soluble ligands found in the extracellular matrix[8]. This diverse set of interactions allows CS to activate intracellular signaling pathways both by immobilizing ligands at the cell surface and by directly activating receptor complexes. Here, we set out to identify and characterize novel CS-binding receptors that inhibit axon regrowth. Our work identified the EphA4 receptor as a novel pathway by which CS actively inhibits outgrowth. Upregulation and activation of EphA4 has previously been linked with the inhibition of axon regeneration, and our work highlights a new molecular mechanism that utilizes injury-induced extracellular carbohydrates.

In particular, we demonstrate how the injury-induced CS-E sulfation motif binds electropositive residues in the extracellular domain of EphA4, induces the formation pf receptor clusters on the cell surface and stimulates phosphorylation of the intracellular kinase domain. Ultimately, this carbohydrate-protein interaction inhibits the regrowth of severed axons. Moreover, the inhibitory growth effect of CS-E on neurite outgrowth is strongly attenuated after genetic deletion of EphA4, illustrating the importance of this newly discovered carbohydrate-protein interaction. These studies elucidate the mechanisms of CS-mediated inhibition by identifying a novel CS receptor, EphA4, and characterizing a new mechanism of Eph receptor activation by carbohydrates found in the extracellular matrix post injury.

The identification of a novel protein that mediates the inhibitory effect of CS advances our understanding of inhibition of axon regeneration and provide new therapeutic targets to promote recovery of axon growth after injury to the nervous system as observed

for other CS-activated pathways. In addition, we demonstrate how the identification of the molecular determinants of these carbohydrate-protein interactions afford additional ways to alleviate CS-mediated inhibition by targeting alternative mechanisms of EphA4 activation. Blocking specific CS-protein interactions can promote regrowth in a manner that does not drastically alter the extracellular matrix like ChABC treatment, providing a more fine-tuned approach to modulating neurite growth.

Together, our experiments detail the functional outcome of CS-E binding to EphA4 within the adult CNS and provide a new mechanism for axonal inhibition after spinal cord injury. EphA4 has also been implicated in other biological contexts such as CST development[27,28] and dendritic spine morphology[29], highlighting possible further roles for this newly discovered carbohydrate-protein interaction. Moreover, the Eph family of receptors is the largest group within the receptor tyrosine kinase superfamily, and CS binding may not be relegated only to EphA4. Lastly, our work highlights how GAGs may more broadly act as active signaling molecules within the ECM through direct receptor engagement rather than simply structural elements or recruiters of soluble ligands. Our results open up exciting possibilities both to target novel, underlying mechanisms that prevent recovery after spinal cord injury and to better understand the broader roles of these near ubiquitous components of the ECM.

References:

1. Ahuja CS, Wilson JR, Nori S, et al. Traumatic spinal cord injury. *Nat Rev Dis Prim*. 2017;3:17018. doi:10.1038/nrdp.2017.18.
2. Bartus K, James ND, Bosch KD, Bradbury EJ. Chondroitin sulphate proteoglycans: key modulators of spinal cord and brain plasticity. *Exp Neurol*. 2012;235(1):5-17. doi:10.1016/j.expneurol.2011.08.008.
3. Silver J, Miller JH. Regeneration beyond the glial scar. *Nat Rev Neurosci*. 2004;5(2):146-156. http://dx.doi.org/10.1038/nrn1326.
4. Alilain WJ, Horn KP, Hu H, Dick TE, Silver J. Functional regeneration of respiratory pathways after spinal cord injury. *Nature*. 2011;475(7355):196-200. doi:10.1038/nature10199.
5. Bradbury EJ, Moon LDF, Popat RJ, et al. Chondroitinase ABC promotes functional recovery after spinal cord injury. *Nature*. 2002;416:636-640.
6. Brown JM, Xia J, Zhuang B, et al. A sulfated carbohydrate epitope inhibits axon regeneration after injury. *Proc Natl Acad Sci*. 2012;109(13):4768-4773.
7. Miller GM, Hsieh-Wilson LC. Sugar-dependent modulation of neuronal development, regeneration, and plasticity by chondroitin sulfate proteoglycans. *Exp Neurol*. 2015;274:115-125.
8. Sharma K, Selzer ME, Li S. Scar-mediated inhibition and CSPG receptors in the CNS. *Exp Neurol*. 2012;237(2):370-378. doi:10.1016/j.expneurol.2012.07.009.
9. Lang BT, Cregg JM, DePaul MA, et al. Modulation of the proteoglycan receptor PTPsigma promotes recovery after spinal cord injury. *Nature*. 2015;518(7539):404-408. doi:10.1038/nature13974.

10. Shen Y, Tenney AP, Busch SA, et al. PTPσ is a receptor for chondroitin sulfate proteoglycan, an inhibitor of neural regeneration. *Science (80-).* 2009;326(5952):592-596.

11. Dickendesher TL, Baldwin KT, Mironova YA, et al. NgR1 and NgR3 are receptors for chondroitin sulfate proteoglycans. *Nat Neurosci*. 2012;15(5):703-712.

12. Lisabeth EM, Falivelli G, Pasquale EB. Eph receptor signaling and ephrins. *Cold Spring Harb Perspect Biol*. 2013;5(9).

13. Goldshmit Y, McLenachan S, Turnley A. Roles of Eph receptors and ephrins in the normal and damaged adult CNS. *Brain Res Rev*. 2006;52(2):327-345.

14. Coulthard MG, Morgan M, Woodruff TM, et al. Eph/Ephrin signaling in injury and inflammation. *Am J Pathol*. 2012;181(5):1493-1503.

15. Giger RJ, Hollis ER, Tuszynski MH. Guidance molecules in axon regeneration. *Cold Spring Harb Perspect Biol*. 2010;2(7):a001867.

16. Barquilla A, Pasquale EB. Eph receptors and ephrins: therapeutic opportunities. *Annu Rev Pharmacol Toxicol*. 2015;55:465-487.

17. Du J, Fu C, Sretavan DW. Eph/ephrin signaling as a potential therapeutic target after central nervous system injury. *Curr Pharm Des*. 2007;13(24):2507-2518.

18. Goldshmit Y, Galea MP, Wise G, Bartlett PF, Turnley AM. Axonal regeneration and lack of astrocytic gliosis in EphA4-deficient mice. *J Neurosci*. 2004;24(45):10064-10073.

19. Goldshmit Y, Spanevello MD, Tajouri S, et al. EphA4 blockers promote axonal regeneration and functional recovery following spinal cord injury in mice. *PLoS One*. 2011;6(9):1-12. doi:10.1371/journal.pone.0024636.

20. Spanevello MD, Tajouri SI, Mirciov C, et al. Acute delivery of EphA4-Fc improves functional recovery after contusive spinal cord injury in rats. *J Neurotrauma*. 2013;30(12):1023-1034.

21. Fabes J, Anderson P, Brennan C, Bolsover S. Regeneration-enhancing effects of EphA4 blocking peptide following corticospinal tract injury in adult rat spinal cord. *Eur J Neurosci*. 2007;26(9):2496-2505.

22. Properzi F, Carulli D, Asher RA, et al. Chondroitin 6-sulphate synthesis is up-regulated in injured CNS, induced by injury-related cytokines and enhanced in axon-growth inhibitory glia. *Eur J Neurosci*. 2005;21(2):378-390.

23. Nikolov DB, Xu K, Himanen JP. Eph/ephrin recognition and the role of Eph/ephrin clusters in signaling initiation. *Biochim Biophys Acta (BBA)-Proteins Proteomics*. 2013;1834(10):2160-2165.

24. Janes PW, Nievergall E, Lackmann M. Concepts and consequences of Eph receptor clustering. In: *Seminars in Cell & Developmental Biology*. Vol 23. Elsevier; 2012:43-50.

25. Adam R. Griffith, Claude J. Rogers, Gregory M. Miller, b Ravinder Abrol, Linda C. Hsieh-Wilson WAGI. Predicting glycosaminoglycan-surface protein interactions: Implications for studying axonal growth. *Proc Natl Acad Sci USA*. 2017.

26. Taylor AM, Blurton-Jones M, Rhee SW, Cribbs DH, Cotman CW, Jeon NL. A microfluidic culture platform for CNS axonal injury, regeneration and transport. *Nat Methods*. 2005;2(8):599-605.

27. Dottori M, Hartley L, Galea M, et al. EphA4 (Sek1) receptor tyrosine kinase is required for the development of the corticospinal tract. *Proc Natl Acad Sci*.

1998;95(22):13248-13253.

28. Canty AJ, Greferath U, Turnley AM, Murphy M. Eph tyrosine kinase receptor EphA4 is required for the topographic mapping of the corticospinal tract. *Proc Natl Acad Sci*. 2006;103(42):15629-15634.

29. Murai KK, Nguyen LN, Irie F, Yamaguchi Y, Pasquale EB. Control of hippocampal dendritic spine morphology through ephrin-A3/EphA4 signaling. *Nat Neurosci*. 2003;6(2):153.

30. Volpi N, Galeotti F, Yang B, Linhardt RJ. Analysis of glycosaminoglycan-derived, precolumn, 2-aminoacridone–labeled disaccharides with LC-fluorescence and LC-MS detection. *Nat Protoc*. 2014;9(3):541-558.

31. Campeau E, Ruhl VE, Rodier F, et al. A versatile viral system for expression and depletion of proteins in mammalian cells. *PLoS One*. 2009;4(8):e6529.

32. Kutner RH, Zhang X-Y, Reiser J. Production, concentration and titration of pseudotyped HIV-1-based lentiviral vectors. *Nat Protoc*. 2009;4(4):495-505.

33. Rogers CJ, Clark PM, Tully SE, et al. Elucidating glycosaminoglycan–protein–protein interactions using carbohydrate microarray and computational approaches. *Proc Natl Acad Sci*. 2011;108(24):9747-9752.

34. Baker NA, Sept D, Joseph S, Holst MJ, McCammon JA. Electrostatics of nanosystems: application to microtubules and the ribosome. *Proc Natl Acad Sci*. 2001;98(18):10037-10041.

35. Hilgenberg LGW, Smith MA. Preparation of Dissociated Mouse Cortical Neuron Cultures. *J Vis Exp*. 2007;(10):562. doi:10.3791/562.

36. Park JW, Vahidi B, Taylor AM, Rhee SW, Jeon NL. Microfluidic culture platform

for neuroscience research. *Nat Protoc*. 2006;1(4):2128-2136.

Materials and Methods

Molecular Cloning: Mouse EphA4 (Accession: BC052164, IMAGE:6512978) was used in this study. EphA4 inserts were PCR amplified and cloned into pcDNA3.1/myc-His A vector (ThermoFisher) using NEBuilder HiFi DNA assembly cloning kit (New England BioLabs).

Fc fusion protein constructs and production: pcDNA3.1 vector was digested with HindIII and AgeI, leaving the 6x-his tag but removing the myc epitope. The murine Ig kappa chain leader sequence followed by the human IgG1 Fc region, containing a HindIII between the leader sequence and the Fc portion, was cloned into pcDNA3.1 vector. For generation of EphA4-Fc fusion proteins, the ectodomain of EphA4, lacking the EphA4 signal peptide (Residues 1-18) was PCR amplified and inserted between the Ig kappa chain leader sequence and the IgG1 Fc. This generates an EphA4-Fc fusion protein containing an C-terminal 6x-his tag. The following EphA4-Fc constructs were used in this study:

	EphA4 Residues	Mutations
$EphA4^{WT}$-Fc	19-547	None
$EphA4^{LBD}$-Fc	19-209	None
$EphA4^{\Delta BD}$-Fc	210-547	None
$EphA4^{5A:1}$-Fc	19-547	K368A, K376A, R378A, R466A, R496A
$EphA4^{5A:2}$-Fc	19-547	R489A, R492A, K501A, R516A, R538A
$EphA4^{5A:3}$-Fc	19-547	K292A, R311A, R327A, R357A, K394A
$EphA4^{10:A}$-Fc	19-547	K368A, K376A, R378A, R466A, R496A, R489A, R492A, K501A, R516A, R538A

Fusion proteins were produced by transiently transfecting DNA constructs into HEK293T cells using lipofectamine 3000 (ThermoFisher) following manufacturers protocol.

HEK293T cells were cultured in DMEM (high glucose, GlutaMAX; ThermoFisher) supplemented with Pen Strep (ThermoFisher) and 2% heat inactivated fetal bovine serum (FBS; ThermoFisher). Cells were cultured a total of 5 days post transfection and media containing secreted proteins was collected, and Fc fusion proteins were purified using Ni-NTA agarose (Qiagen). The concentration of Fc fusion proteins was normalized based on Fc content.

ELISA Binding Assays: CSPGs (Millipore Sigma: CC117) and CS polysaccharides (CS, CS-A, CS-C, CS-D, CS-E; Seikagaku) were biotinylated using EZ-Link™ Sulfo-NHS-LC-Biotin (ThermoFisher) following manufactures protocol. Following biotinylation, excess reagent was removed using Amicon Ultra centrifugal filters with a 3K molecular weight cut off. For chondroitinase ABC digested CSPGs, CSPGs were first biotinylated and then digested with chondroitinase ABC (4 mU per μg CSPG; Millipore Sigma). Disaccharide units produced from chondroitinase digestion were removed by filtration through Amicon Ultra centrifugal filters with a 3K molecular weight cut off. Biotinylated CS preparations were normalized for uronic acid content using the carbazole assay[30]. For binding assays, biotinylated CSPGs and CS preparations were immobilized on streptavidin coated plates (20 μg/mL in PBS/0.05% tween for 2 h at RT; ThermoFisher). Plates were washed three times with PBS/0.05% tween before binding EphA4-Fc (1-20 μM in 0.1% BSA/PBS/0.05% tween for 2 h at RT) and then blocked (3% BSA/PBS/0.05% tween for 1 h at RT). Bound EphA4-Fc was detected using goat anti-human IgG Fc-HRP conjugate (1:5,000 dilution in 0.1% BSA/PBS/0.05% tween, 1 h at RT; ThermoFisher) and visualized using TMB substrate and stop solution (R&D Systems) and the absorbance was read at 450 nm was.

Neu7 Astrocyte Binding Assays: Neu7 cells were cultured in 96-well plates in DMEM (ThermoFisher) supplemented with 10% FBS (ThermoFisher). Prior to EphA4-Fc binding, Neu7 cells were washed with PBS, then fixed with 4% paraformaldehyde in PBS for 15 min at room temperature, and washed with PBS. Cells were blocked with 5% BSA/PBS, and then incubated with EphA4-Fc at 4 uM for 3 h at room temperature. Cells were washed with PBS and bound EphA4-Fc was detected in two ways. For immunofluorescence, cells were incubated with Alexa Fluor 647-conjugated goat anti-human IgG secondary antibody (1:2000; ThermoFisher) for 2h at room temperature, washed with PBS and imaged at 20x magnification. For detection with HRP, cells were incubated with IgG Fc-HRP conjugate (1:2,000 dilution in 0.1% BSA/PBS, 1 h at RT; ThermoFisher) and visualized using with TMB substrate and stop solution (R&D Systems), and the absorbance was read at 450 nm was. For ChABC treatment prior to EphA4-Fc binding, Neu7 cells were incubated for 2 h at 37°C (100 mU ChABC per well). For antibody blocking experiments prior to EphA4-Fc binding, Neu7 cells were incubated with CS-E antibody or IgG isotype matched control (Jackson ImmunoResearch) for 2 h at 37 °C (50 μg/mL in PBS).

Lentivirus Cloning and Production: Lentivirus DNA constructs were generated using the system developed by Campeau et al[31]. This system is based on the Gateway cloning technology (ThermoFisher). Full length EphA4 constructs (residues 1-986), $EphA4^{WT}$ and $EphA4^{10A}$ (containing the alanine mutations listed above), were cloned into pEF-ENTR A (addgene Plasmid #17427) entry vector digested with XbaI and BamHI. Entry vectors were recombined into the destination vector, pLenti CMV GFP DEST (addgene Plasmid #19732) using Gateway LR Clonase II Enzyme mix (ThermoFisher). For lentivirus production, confluent HEK293T cells were transfected with pLP1, pLP2, PLP/VSVG

(ThermoFisher), and pLenti using Lipofectamine 3000 according to manufacturer's protocol. Media was collected and replaced at 36 h, 48 h, and 72 h post transfection. After collection, media was centrifuged at 500 g for 10 min a 4°C, and supernatants combined and filtered through a 0.45 μm cellulose acetate filter. Lentivirus was concentrated by PEG precipitation[32]. Briefly, 6 mL 50% PEG 6000, 2.55 mL 4M NaCl, and 2.74 mL PBS is added to 24 mL of filtered supernatant and mixed end-over-end for 1.5 h at 4°C. This is centrifuged for 15 min, 7,000g, at 4°C forming a white pellet which is then resuspended in 1 mL of 50 mM Tris pH 7.4. Concentrated lentivirus was titrated by counting GFP positive cells 48 h after transducing COS7 cells.

Microarray assays: Microarrays were generated as described previously[33]. Arrays were blocked with 10% FBS in PBS with gentle rocking at 37 °C for 1 h, followed by a brief rinse with PBS. EphA4-Fc was prepared in a solution of 1% BSA, PBS, added to the slides in a total volume of 100 μl at a concentration of 2 μM, and incubated at room temperature for 3 h. The slides were washed with PBS, and then incubated with a Cy3 conjugated goat anti-human IgG antibody (Jackson ImmunoResearch; 1:5000 in 1% BSA, PBS) for 1 h in the dark with gentle rocking. Array was washed with PBS and scanned at 532 nm using a GenePix 5000a scanner. Fluorescence quantification was performed using GenePix 6.0 software (Molecular Devices). Experiments were performed in triplicate, and the data represent the average of 10 spots per concentration averaged from the three experiments (± SEM, error bars).

Surface plasmon resonance: All experiments were performed on a Biacore T100 at 25 ºC using a Sensor Chip CM5 with a running buffer composed of 0.01 M HEPES, pH 7.4, 0.15 M NaCl, 3 mM EDTA, 0.05% Surfactant P20 (HBS-EP+). For the EphA4 and EfnA3

interaction with CS-E-enriched polysaccharides, all flow cells were activated with NHS and EDC following the manufacturer's amine coupling protocol. Streptavidin (1 μM, 0.01 M NaOAc, pH 5.0) was conjugated to the activated surfaces until saturation, followed by ethanolamine blocking. Biotinylated CS-E, composed of ~61.5% of the CS-E disaccharide motif, the remainder of which is a mixture of CS-A, CS-C, and unsulfated disaccharides, was immobilized to flow cell 2 to give an RL of 25 response units (RU); biotinylated CS-C was immobilized to flow cell 4 to give a similar RL. Flow cells 1 and 3 were used as controls to subtract bulk response. EphA4-Fc or EfnA3-Fc was passed over the surface at 25 ºC with a flow rate of 80 μL·min–1 for 240 s, and the dissociation monitored for 600 s. The resulting sensorgrams were analyzed using Biacore T100 evaluation software V2.0 and fit to the heterogeneous ligand model with the value of bulk refractive index (RI) set to zero.

DRG neurite outgrowth: For CSPG and CS-E inhibition studies using DRG neurons from EphA4 +/+ and -/-, glass-bottom 96-well plates (Cellvis) pre-coated with Poly-D-lysine (0.1 mg/mL; SigmaAldrich), were coated with 50 uL mixture of laminin (10 μg/ml in PBS; company) and CSPGs (5 ug/mL; company) or a mixture of laminin and CS-E (10ug/mL; company) for 2 h at 37 °C and washed with PBS. DRGs were dissected from P6 mice as previously described[6]. Briefly, dissected DRGs were incubated in 0.125% trypsin w/ EDTA (ThermoFisher) for 15 min at 37 °C, followed by collagenase (Worthington; 4 mg/ml) for 15 min at 37 °C, triturated to dissociate to single cell suspensions, and seeded at 2000 cells per well. Cells were cultured for 24 h in Neurobasal (ThermoFisher) medium supplemented with GS21 (MTI GlobalStem) and GlutaMAX™ (ThermoFisher). Cultured DRG neurons were fixed with 4% paraformaldehyde in PBS for

20 min at room temperature, washed with PBS and incubated for 1 h in blocking buffer (1% BSA, 0.1% Triton X-100, PBS) at room temperature, and then incubated with anti-βIII tubulin (1:1000 in blocking buffer; Cell Signaling Technologies) overnight at 4°C, followed by Alexa Fluor 488-conjugated goat anti-mouse IgG secondary antibody (1:2000; ThermoFisher) for 2h at room temperature. Full wells were imaged using a Zeiss LSM 700 microscope and the total length of neurites and total neuron number for each well was measured using MetaMorph Neurite Outgrowth software, and used to calculate average outgrowth length per neuron. For all neurite outgrowth experiments, we performed statistical analysis using the one-way ANOVA; n = >200 cells per experiment, and results from at least three independent experiments were reported.

Activation Assays: COS-7 cells were transfected with full length EphA4 using Lipofectamine (ThermoFisher) and cultured for 2 days in DMEM (ThermoFisher) supplemented with 10% FBS (ThermoFisher). Prior to stimulation, cells were serum starved for 8 h by replacing media with DMEM supplemented with 1% FBS. Cells were stimulated medium to fresh medium containing CS-E (Seikagaku; 10 µg/ml) or Efn-Fc proteins (R&D systems; 1 µg/ml) and incubating for the time described at 37 °C. Cells were lysed with cold lysis buffer consisting of PBS with 1% Triton X-100 with protease inhibitor cocktail (Roche) and phosphatase inhibitor mixture. Lysates were clarified via centrifugation. For each sample, 50µl of protein A/G agarose (ThermoFisher) was added to an Eppendorf along with 1 µg of myc antibody (Cell Signaling Technology). Clarified lysate was added, and incubated at 4 °C with rotation for 2 h. Agarose was washed 3 times with lysis buffer, boiled with 2X loading dye (30 µl of 100 mM Tris, 200 mM DTT, 4% SDS, 0.10% bromophenol blue, 20% glycerol), and the eluate was resolved by SDS-PAGE

and transferred to PVDF membrane. Phosphorylated EphA4 was detected by immunoblotting with an anti-phosphotyrosine antibody, PY20 (1:1,000; BD Biosciences) following the manufacturer's protocol. After scanning, membranes were stripped (NewBlot 5X PVDF stripping buffer; LI-COR) and re-blotted with anti-EphA4 antibody (ThermoFisher).

Computational Docking: Crystal structure of the EphA4 ectodomain was used for docking studies (PDBID: 4M4R, chain A). This structure was prepared for docking by first performing sidechain optimizing on all residues using the SCREAM methodology and then subjecting these structures to brief minimization to relax unfavorable contacts. The detailed docking methodology is outlined elsewhere(GAGDock-REF). Briefly, a CS-E hexasaccharide was docked to the entire ectodomain surface of EphA4 to identify putative binding regions. Next, putative regions are subjected to an additional round of docking to more completely sample ligand conformations. Top poses were briefly minimized post docking to further optimize ligand-protein interactions. The interacting residues for each putative binding site were determined by analyzing the top five poses for each region to identify residues found within 5Å of the ligand. Images were created using PyMOL (Schrodinger, LLC), and the electrostatic maps were derived using Adaptive Poisson-Boltzmann Solver (APBS) software[34].

Microfluidic Axotomy Assay: Commercially available microfluidic devices containing a 150μm barrier were used for these studies (Xona Microfludics). Microfluidic devices were mounted in individual wells of a 6-well glass-bottom plate (Cellvis) that were pre-coated with Poly-D-lysine. Devices were prepared following manufactures protocol. Briefly, devices were conditioned by adding media to the soma side and incubating for 60 minutes

at 37°C, followed by the addition of media to the axon side and incubation at 37°C until use. Cortical neurons were dissected from EphA4$^{-/-}$ mice as previously described[35] and cultured in Neurobasal medium supplemented with GS21 and GlutaMAX™. Following dissection and dissociation of cortical neurons, cells (4 million/mL concentration) were transduced with lentivirus at a multiplicity of infection (MOI) of 10 and incubated at RT for 20 minutes. Prior to plating transduced neurons in microfluidic devices, excess media in the device was removed from both the soma and axon sides. Neurons were plated in the top chamber of the soma side (20 μL, 80,000 neurons/well) and incubated for 20 minutes at 37°C. Following plating, 150 μL of media was added to the soma and axon side. Neurons were cultured for 5 DIV before performing axotomy experiments. Axotomy was performed by aspirating media from the bottom chamber of the axon side of the device, this process removes all media from both chambers of the axon side[26,36]. This was repeated a total of three times by replacing media in the top chamber and aspirating media form the bottom chamber. Finally, media containing CS-E (10 μg/mL) was added to the axon side, devices were returned to the incubator, and neurons were cultured for an additional 24 hrs. Devices were imaged prior to axotomy, immediately post-axotomy, and 24 hrs post-axotomy and neurons visualized by their expression of GFP. The degree of regrworth was quantified by counting the number of processes that extend 150 μm, 300 μm, and 600 μm from the edge of the axon barrier.

Chapter 3: Computational Characterization of Eph Receptor Interactions with Chondroitin Sulfate

Abstract

Chondroitin sulfate proteoglycans (CSPGs) regulate neuronal plasticity, axon regeneration and guidance through their ability to bind protein ligands and cell surface receptors. In this way, extracellular CSPGs can modulate the activity of intracellular signaling pathways. The receptor tyrosine kinase EphA4 was identified as a CS receptor. CS interaction with EphA4 induces receptor clustering and phosphorylation of the intracellular kinase domain. Importantly, this CS-EphA4 interaction leads to the inhibition of axon regeneration. Here, a computational analysis of EphA4-CS interactions is performed to characterize the importance of key arginine and lysine residues towards CS binding, and to identify structural differences in CS-A, CS-C, CS-D, and CS-E docking to EphA4. Carbohydrate induced Eph receptor clustering could be a general mechanism of Eph receptor activation. Here, CS-E was docked to all EphA and EphB family members to predict those that may bind to CS. The relative strengths of the predicted binding energies are EphB4 > EphA8 > EphA1 > EphA3 > EphB1 > EphB3 > EphA7 > EphA5 > EphA4 > EphA6 > EphB2 > EphB6 > EphA2. In addition, the arginine and lysine residues that mediate CS binding are identified for each Eph receptor. These computational predictions provide mechanistic insights into Eph receptor activation by chondroitin sulfate and have implications for inhibition of axon regeneration following injury to the nervous system and axon guidance during development.

Introduction

Chondroitin sulfate proteoglycans (CSPGs) play diverse roles in the developing and mature nervous system.[1,2] CSPGs affect biological processes through their interactions with a diverse set of protein-binding proteins. In this manner, CSPGs can modulate intracellular signaling through binding cell surface receptors and soluble protein ligands found in the extracellular matrix.[3] To date, over 400 glycosaminoglycan (GAG) binding proteins have been identified including numerous chemokines and cytokines, growth factors and morphogens, extracellular structural proteins, and single-transmembrane signaling receptors.[4] The ability to characterize GAG-protein interactions is central to understanding the mechanisms of action of this important class of biomolecules.

Eph receptors make up the largest family of receptor tyrosine kinases.[5] Eph receptors are involved in many different physiological processes involved in the development of the nervous system, including cell patterning guidance attraction, and repulsion.[6] In addition to their roles in development, the Eph receptors are involved in the maintenance of the mature nervous system, through regulation of synaptic connections.[7,8] Importantly, members of the Eph family have been implicated in inhibiting axon regeneration following injury to the nervous system and have been identified as potential therapeutic targets for promoting regrowth and functional recovery.[9–11] EphA and EphB receptors are upregulated following injury in numerous animal models including optic nerve injury, spinal cord injury, and traumatic brain injury.[12] Of the Eph receptors, the role of EphA4 in inhibiting axon regeneration is the most thoroughly studied. Genetic deletion of EphA4 promotes axon regeneration following spinal cord injury in mice.[13] Importantly,

knockout of EphA4 leads to recovery of motor function. As outlined in Chapter 2, CS clusters and activates EphA4 and inhibits axon regeneration.

GAG-protein interactions are difficult to characterize using traditional biochemical techniques because these carbohydrates have high degree of structural complexity due varied stereochemistry, chain lengths, and patterns of sulfation. We recently developed a computational approach to identify and characterize GAG binding sites on a target protein.[14] This approach, GAG-Dock, was validated against known GAG-protein crystals structures and accurately reproduces (< 1 Å RMSD) the crystal structure. GAG-Dock successfully identified the heparin and chondroitin sulfate binding sites of the axon guidance proteins, protein tyrosine phosphatase σ (RPTPσ), and Nogo receptors 1-3 (NgR1-3). The accurate identification of CS binding sites will aid the understanding of CS mediated processes and in the development of therapeutics that specifically disrupt target CS-protein binding sites.

Here, a computational analysis is performed to characterize Eph receptor interactions with chondroitin sulfate. First, CS-A, CS-C, CS-D, and CS-E hexasaccharides will be docked to EphA4 to characterize differences in CS-EphA4 interactions due to specific sulfation patterns. Next, CS-E hexasaccharides were docked to all members of the broader Eph family to identify those likely to bind CS-E, and putative CS-E binding sites are predicted for each.

Results and Discussion

CS-A, CS-C, CS-D, and CS-E Docking to EphA4

As noted in Chapter 2, docking of a CS-E hexasaccharide identified two binding sites for EphA4. The two binding sites are outlined by the following arginine and lysine residues: site 1, K368, K376, R378, R466, and R496; site 2, R489, R492, K501, R516, and R538. To understand how specific sulfation motifs affect CS-EphA4 interactions, hexasaccharides of CS-A, CS-C, and CS-D were docked to site 1 and site 2 of EphA4. The top pose for each ligand docked to EphA4, ranked by snapbe (snap binding E = complex E – protein E – ligand E), are shown for site 1 (Fig. 3.1) and site 2 (Fig. 3.2); this data is further summarized in Fig. 3.3. For site 1, monosulfated disaccharide motifs CS-A (-150.0 kcal/mol; Fig. 3.1a) and CS-C (-157.6 kcal/mol; Fig. 3.1b) have similar docked energies. Of the disulfated disaccharide motifs CS-D (-259.3 kcal/mol; Fig. 3.1c) and CS-E (-290.3 kcal/mol; Fig. 3.1d), CS-E has stronger predicted docked energy. For site 2, CS-A (-169.7 kcal/mol; Fig. 3.2a) has a stronger predicted energy than CS-C (-139.4 kcal/mol; Fig. 3.2b). The disulfated disaccharide motifs CS-D (-242.2 kcal/mol; Fig. 3.2c) and CS-E (-265.9 kcal/mol; Fig. 3.2d). Predicted binding energies were stronger for CS-C, CS-D, and CS-E hexasaccharides docked to site 1 than site 2 (Fig. 3.3a,b). However, CS-A has a stronger binding energy for site 2 than site 1.

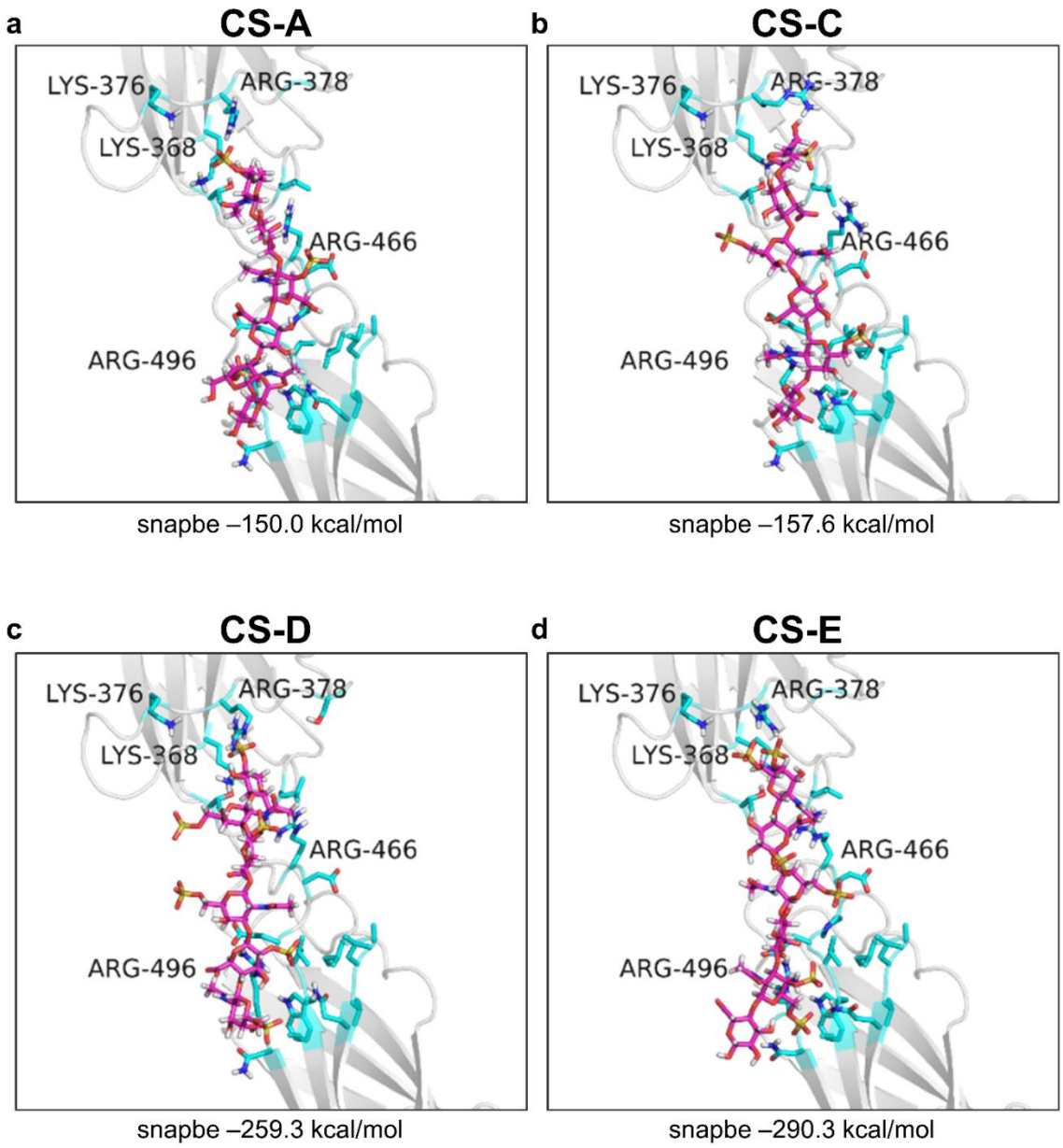

Figure 3.1: CS-A, CS-C, CS-D, and CS-E hexasaccharide docking to site 1 of EphA4 The top docked pose is shown for each hexasaccharide docked to site 1 of EphA4. Site 1 is located in the first Fibronectin type-III domain of EphA4 and contains the following Arginine and Lysine residues important for CS binding: Lys368, Lys376, Arg378, Arg466, and Arg496. The predicted snapbe (snap binding E = complex E – protein E – ligand E) for top pose for each site: (**a**) CS-A: -150.0 kcal/mol, (**b**) CS-C: -157.6 kcal/mol, (**c**) CS-D: -259.3 kcal/mol, and (**d**) CS-E: -290.3 kcal/mol.

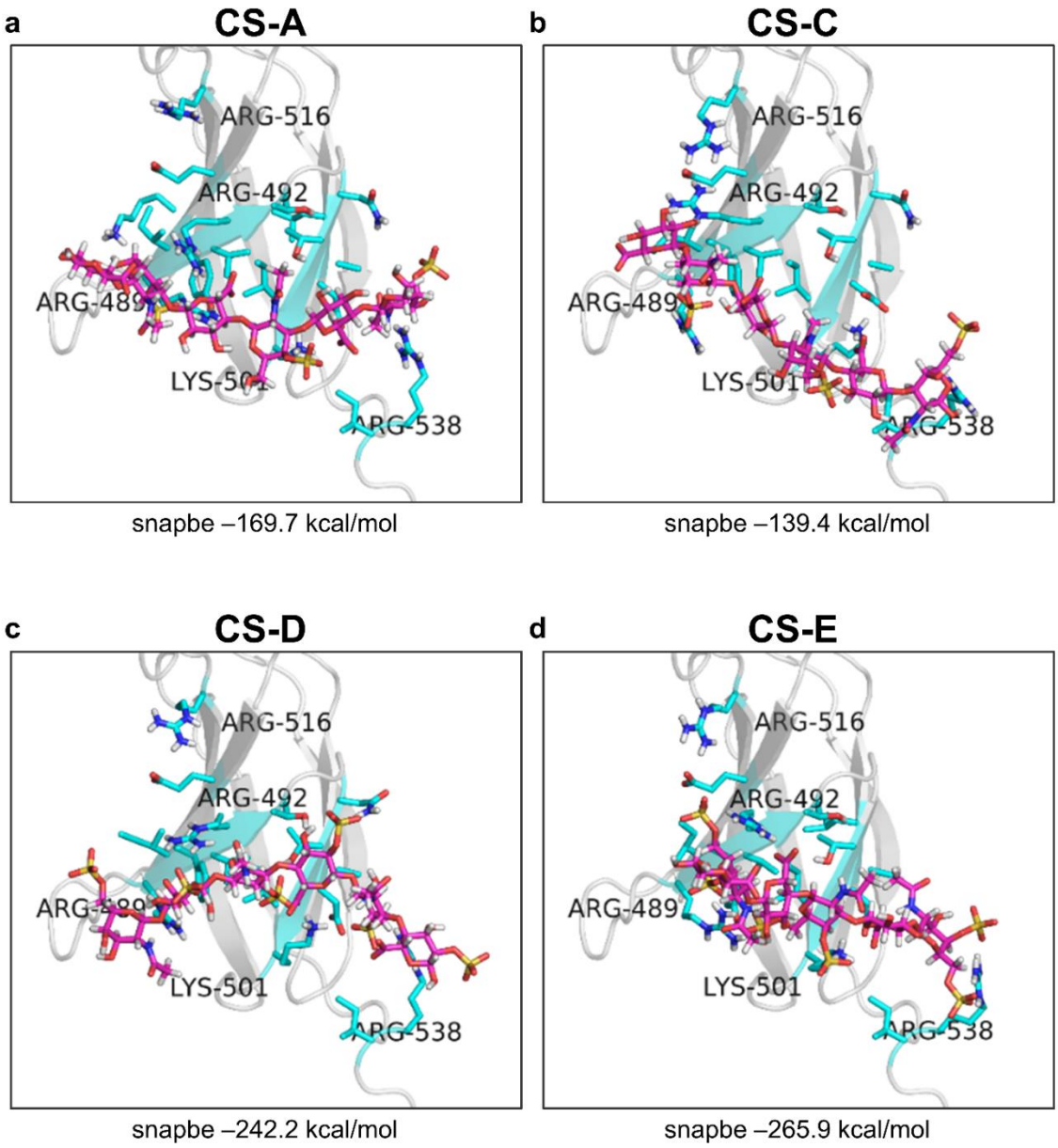

Figure 3.2: CS-A, CS-C, CS-D, and CS-E hexasaccharide docking to site 2 of EphA4 The top docked pose is shown for each hexasaccharide docked to site 2 of EphA4. Site 2 is located in the first Fibronectin type-III domain of EphA4 and contains the following Arginine and Lysine residues important for CS binding: Arg489, Arg492, Lys501, Arg516, and Arg538. The predicted snapbe (snap binding E = complex E – protein E – ligand E) for top pose for each site: (**a**) CS-A: -169.7 kcal/mol, (**b**) CS-C: -139.4 kcal/mol, (**c**) CS-D: -242.2 kcal/mol, and (**d**) CS-E: -265.9 kcal/mol.

Interesting differences in the protein-ligand interactions arise due to the structural placement of the sulfate groups of CS. For site 1, the top docked pose for CS-D (Fig. 3.1c) has two sulfate groups, from the internal disaccharide unit, pointing away from the protein into the solvent. While the top docked pose for CS-E (Fig. 3.1d) has all sulfate groups engaging the protein, resulting in a stronger binding energy than CS-D. For site 2, the top docked pose for CS-D (Fig. 3.2c) has the sulfate groups on the terminal disaccharide units, of both ends, directed away from the protein. CS-E (Fig. 3.2d) is able to adopt a conformation where all sulfate groups are able to engage with the protein, again resulting in a stronger predicted binding energy. The interaction energy between CS-E and arginine and lysine residues found in the binding site is lower than that of CS-D (Fig. 3.3c). Likewise, CS-E has stronger coulombic and hydrogen-bonding interactions with the protein than CS-D. Structural differences in the placement of sulfate groups constrain ligand-protein interactions and are attributed to the stronger predicted energy for CS-E than CS-D even though they are equally charged hexasaccharides.

a

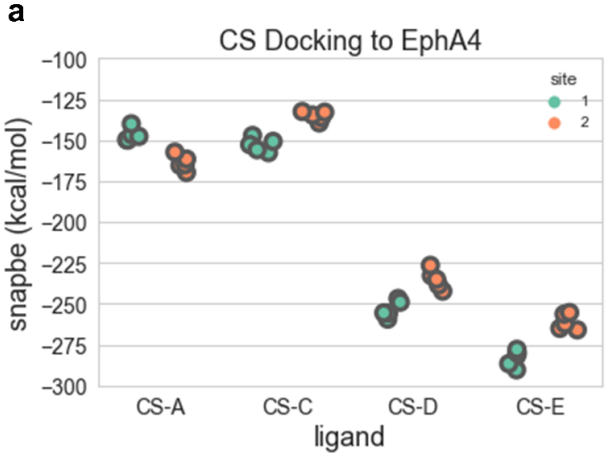

b

site	ligand	snapbe (avg top 5)	snapbe (top pose)
1	**CS-A**	-146.8	-150.0
	CS-C	-152.8	-157.6
	CS-D	-253.2	-259.3
	CS-E	-283.3	-290.3
2	**CS-A**	-163.8	-169.7
	CS-C	-135.1	-139.4
	CS-D	-235.0	-242.2
	CS-E	-260.9	-265.9

c

site	ligand	vdW	coulomb	hb	total
1	**CS-A**	0.47	-84.38	-3.60	-87.51
	CS-C	1.19	-77.98	-1.86	-78.65
	CS-D	1.14	-102.02	-3.41	-104.29
	CS-E	2.62	-113.92	-9.10	-120.41
2	**CS-A**	0.83	-77.41	-1.59	-78.17
	CS-C	0.66	-81.94	-2.75	-84.03
	CS-D	0.91	-103.63	-4.24	-106.96
	CS-E	1.76	-117.80	-6.12	-122.15

Figure 3.3: Summarized docking data for CS-A, CS-C, CS-D, and CS-E hexasaccharide docking to EphA4 (**a**) The snapbe for the top five poses for each ligand docked to site 1 and site 2 of EphA4. (**b**) The average snapbe for the top five poses and the snapbe for the top pose for each ligand docked to site 1 and site 2 of EphA4. (**c**) Energy decomposition for ligand interactions with arginine and lysine residues: site 1 (Lys368, Lys376, Arg378, Arg466, and Arg496) and site 2 (Arg489, Arg492, Lys501, Arg516, and Arg538). The average van der Waals (vdW), coulombic (coulomb), hydrogen-bond (hb), and total for each ligand-residue interaction are shown.

CS-E docking to EphA4 Mutants

The experimental binding of EphA4 mutants is highlighted in Chapter 2. These studies confirmed the importance of arginine and lysine residues found in site 1 and site 2. Binding was significantly for site 1 mutant (K368A, K376A, R378A, R466A, and R496A) and site 2 mutant (R489A, R492A, K501A, R516A, and R538A), but residual CS-E binding was observed for each mutant. Importantly, the site 1 and site 2 combined mutant showed a further decrease in CS-E binding. *In silico* mutations were performed to understand the contributions of key arginine and lysine residues towards predicted CS-E docking energies (Fig. 3.4a,b). CS-E was docked to three EphA4 mutants 5A:1 (site 1 mutant: K368A, K376A, R378A, R466A, and R496A), 5A:2 (site 2 mutant: R489A, R492A, K501A, R516A, and R538A), and 10A (combined site 1 and site 2 mutant). The individual mutants, 5A:1 and 5A:2, show decrease in predicted binding energy compared to WT. While the site 1 and site 2 combined mutant, 10A, shows an even further decrease in predicted CS-E binding energy. These computational findings mirror the experimental binding affinities, where individual site mutants show residual CS-E binding but the combined mutant shows a complete loss of CS-E binding. The combined results confirm the importance of these key arginine and lysine residues towards CS-E binding.

a

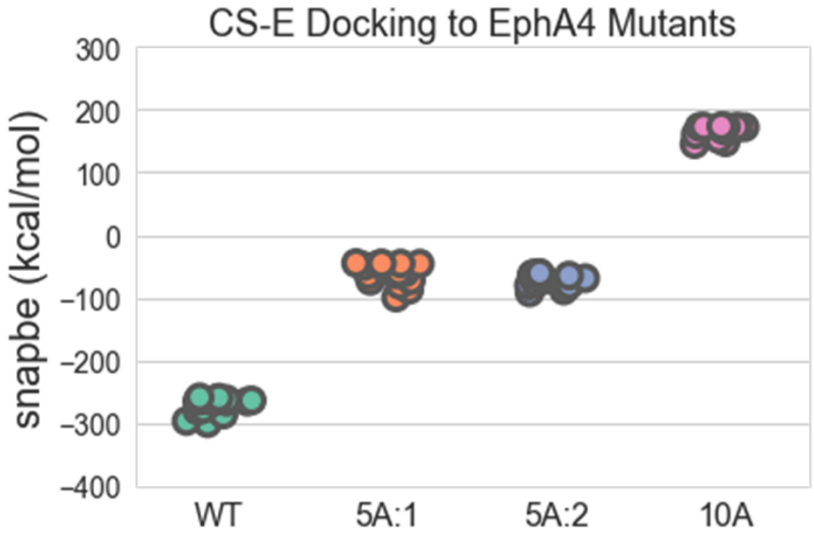

b

	WT	5A:1	5A:2	10A
avg snapbe (top 15 poses)	-265.39	-51.68	-65.39	170.32
Mutations		K368A K376A R378A R466A R496A	R489A R492A K501A R516A R538A	K368A K376A R378A R466A R496A R489A R492A K501A R516A R538A

Figure 3.4: CS-E docking to EphA4 mutants (**a**) Snapbe plotted for the top fifteen poses for CS-E docking to WT, 5A:1 (site 1 mutant: K368A, K376A, R378A, R466A, and R496A), 5A:2 (site 2 mutant: R489A, R492A, K501A, R516A, and R538A), and 10A (combined site 1 and site 2 mutant). (**b**) Average snapbe of the top fifteen poses for CS-E docking to EphA4 mutants.

Per-Residue Energy Decomposition of EphA4

Computational approaches can be used to characterize the relative importance of specific residues towards CS binding. Residue specific contributions towards CS binding are difficult to measure experimentally. To better understand CS-EphA4 interactions, per-residue energy decomposition was performed on arginine and lysine residues found in site 1 (K368, K376, R378, R466, and R496) and site 2 (R489, R492, K501, R516, and R538). These methods calculate the individual contributions towards ligand binding from coulombic, hydrogen bonding, and van der Waals forces for each residue. Per-residue energy decomposition was performed for the top five poses of CS-A, CS-C, CS-D, and CS-E docked to site 1 and site 2 of EphA4, Fig. 3.5, 3.6, 3.7).

The dominant contribution towards CS-E binding comes from coulombic interactions (Fig. 3.5b, 3.6b). For site 1, the relative importance of each residue towards CS-E binding is: R378 > K368 > R496 > R466 > K376 (Fig 3.5a). For site 2, the relative importance towards CS-E binding is: R489 > R538 > R492 > R501 > R516 (Fig. 3.6a). Per-residue decomposition provides insight into differences in predicted binding energies for the equally charged hexasaccharides CS-D and CS-E. For site 1, the residues K368, R376, and R378 have slightly stronger interactions with CS-E than CS-D. While R466 has similar interactions with CS-D and CS-E. However, residue R496 has significantly stronger interactions with CS-E than CS-D. For site 2, the residues R489 has slightly stronger interactions with CS-E than CS-D and R492 and R501 have slightly stronger interactions with CS-D then CS-E. The major differences occur with residue R516 and R538, these residues have significantly stronger interactions with CS-E than CS-D, and likely account for stronger predicted binding energy for CS-E than CS-D. Per-residue energy

decomposition provides a framework for understanding how CS-protein interactions are affected by sulfate placement.

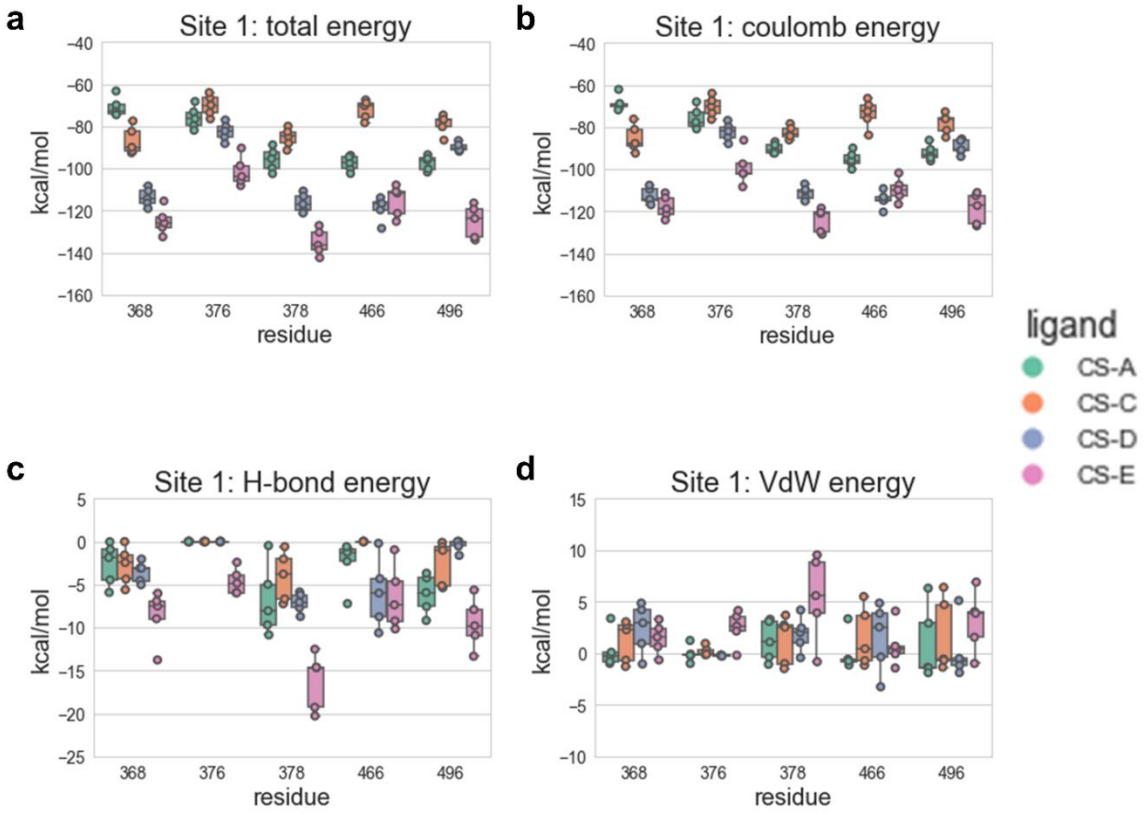

Figure 3.5: Per-Residue Energy Decomposition for site 1 The ligand interaction energy for each arginine and lysine residue found in the CS binding site for the top five poses of CS-A, CS-C, CS-D, and CS-E hexasaccharide docked to EphA4. Energetic contributions for (**a**) total, (**b**) coulombic, (**c**) hydrogen-bond, and (**d**) Van der Waals towards CS-EphA4 interactions with Lys368, Lys376, Arg378, Arg466, and Arg496.

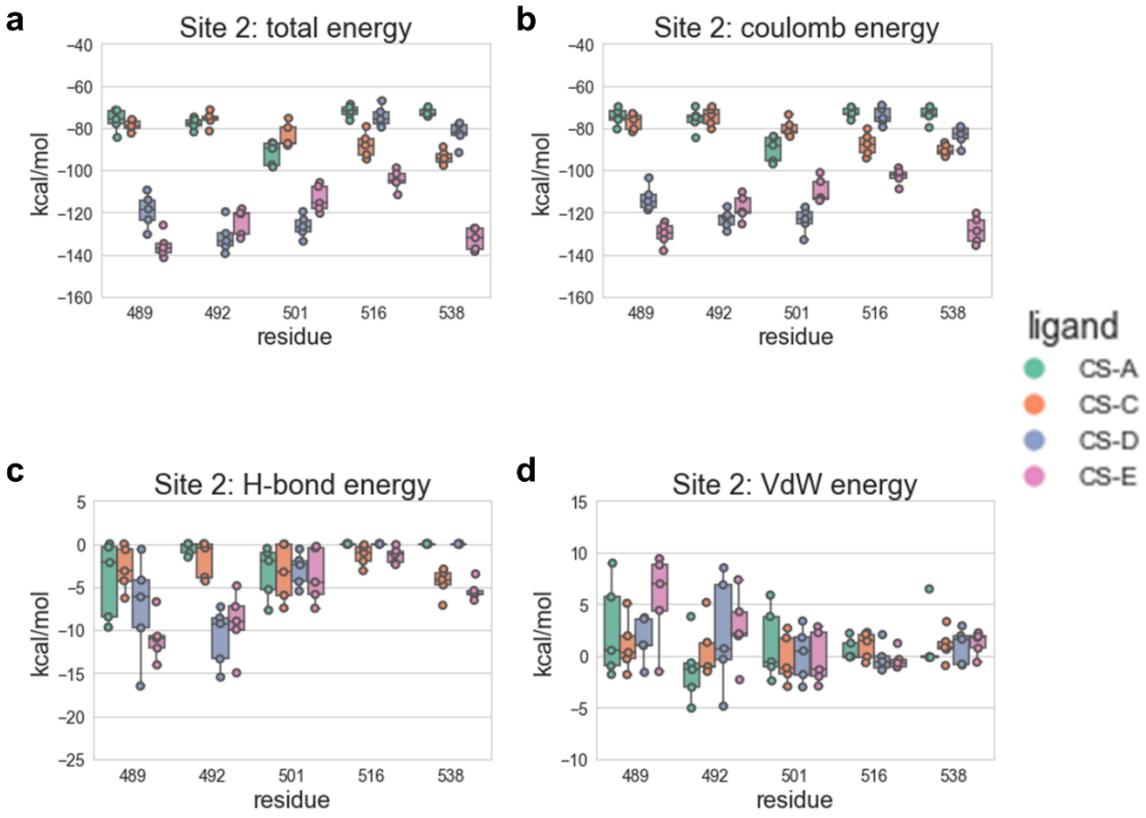

Figure 3.6: Per-Residue Energy Decomposition for site 2 The ligand interaction energy for each arginine and lysine residue found in the CS binding site for the top five poses of CS-A, CS-C, CS-D, and CS-E hexasaccharide docked to EphA4. Energetic contributions for (**a**) total, (**b**) coulombic, (**c**) hydrogen-bond, and (**d**) Van der Waals towards CS-EphA4 interactions with Arg489, Arg492, Lys501, Arg516, and Arg538.

site	ligand	residue	vdw	coulomb	hb	total
1	CS-A	368	0.28	-68.53	-2.64	-70.88
		376	-0.04	-75.81	0.00	-75.86
		378	1.20	-90.19	-6.81	-95.80
		466	0.01	-95.23	-2.45	-97.67
		496	0.91	-92.14	-6.12	-97.35
	CS-C	368	1.22	-85.26	-2.79	-86.84
		376	0.20	-70.27	0.00	-70.07
		378	1.29	-82.55	-4.06	-85.33
		466	1.54	-73.63	0.00	-72.08
		496	1.70	-78.20	-2.44	-78.94
	CS-D	368	2.38	-112.63	-3.55	-113.79
		376	-0.22	-82.26	0.00	-82.49
		378	1.85	-111.16	-7.11	-116.41
		466	1.53	-114.45	-5.98	-118.91
		496	0.17	-89.62	-0.42	-89.87
	CS-E	368	1.44	-117.81	-8.64	-125.01
		376	2.46	-99.22	-4.62	-101.38
		378	5.41	-124.14	-16.28	-135.01
		466	0.73	-109.66	-6.48	-115.40
		496	3.07	-118.80	-9.52	-125.24
2	CS-A	489	2.48	-74.64	-4.14	-76.30
		492	-1.26	-76.09	-0.52	-77.87
		501	1.12	-89.82	-3.30	-92.01
		516	0.63	-72.80	0.00	-72.17
		538	1.19	-73.69	0.00	-72.50
	CS-C	489	1.04	-77.00	-2.88	-78.84
		492	0.56	-74.57	-1.73	-75.75
		501	-0.29	-79.99	-3.34	-83.64
		516	1.00	-87.65	-1.32	-87.97
		538	1.03	-90.49	-4.47	-93.93
	CS-D	489	1.54	-113.28	-7.45	-119.19
		492	2.17	-123.12	-10.80	-131.75
		501	0.15	-123.73	-2.96	-126.54
		516	-0.23	-74.37	0.00	-74.60
		538	0.94	-83.64	0.00	-82.70
	CS-E	489	5.60	-130.29	-10.91	-135.60
		492	2.67	-117.88	-9.21	-124.42
		501	-0.24	-109.57	-3.71	-113.53
		516	-0.39	-102.88	-1.33	-104.62
		538	1.20	-128.37	-5.42	-132.60

Figure 3.7: Per-Residue Energy Decomposition for site 1 and site 2 The ligand interaction energy for each arginine and lysine residue found in the CS binding site for the top five poses of CS-A, CS-C, CS-D, and CS-E hexasaccharide docked to EphA4. Energetic contributions for total, coulombic, hydrogen-bond, and Van der Waals towards CS-EphA4 interactions for site 1 (Lys368, Lys376, Arg378, Arg466, and Arg496) and site 2 (Arg489, Arg492, Lys501, Arg516, and Arg538).

CS-E Docking to EphA and EphB Family

Members of the EphA and EphB family of receptor tyrosine kinases are essential for the proper development and function of the nervous system. In response to injury, EphA and EphB receptors are broadly upregulated in the injured tissue. Here, a CS-E hexasaccharide was docked to the ectodomain of all EphA and EphB family members. The relative strengths of the predicted binding energies are: EphB4 > EphA8 > EphA1 > EphA3 > EphB1 > EphB3 > EphA7 > EphA5 > EphA4 > EphA6 > EphB2 > EphB6 > EphA2 (Fig. 3.8a,b). As noted, EphA4 and EphB3 are CS-E binding proteins with predicted snapbe of -270.3 kcal/mol and -319.0 kcal/mol, respectively. This data suggests all Eph receptors with lower snapbe than EphA4 (EphB4, EphA8, EphA1, EphA3, EphB1, EphB3, EphA7, and EphA5) are predicted to be CS-E binding proteins. Likewise, EphA6 (-237.4 kcal/mol) has a similar snapbe to EphA4 and potentially binds CS-E. The Eph receptors EphB2 (-91.5 kcal/mol), EphB6 (-12.8 kcal/mol), and EphA2 (2.1 kcal/mol) are predicted to not bind CS-E. Indeed, experimental evidence shows EphB2 does not bind CS-E.

In addition to predicting which Eph receptors bind to CS-E, docking also identified the likely CS-E binding sites. The putative binding site for each receptor was characterized by identifying arginine and lysine residues found within 5Å of CS-E ligand form the top 15 poses (Fig. 3.8b). For three receptors, EphA3, EphA4, and EphB1, two potential binding sites were identified.

a

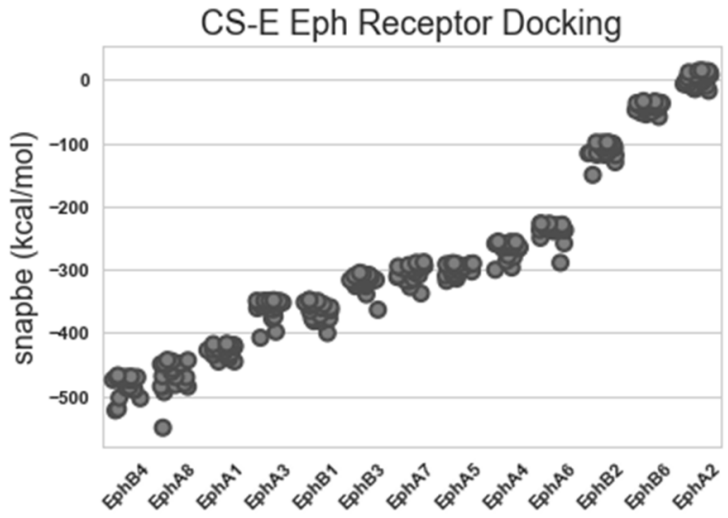

b

	Site 1		Site 2	
EphA1	-427.8	R375, K389, K455, K458, K459, R472, R474, R501, R542		
EphA2	2.1	R475, K477, K521		
EphA3	-280.2	R265, R273, K285, K288, K314, K354, R353	-361.5	K472, K476, R487, R509, R511, R521, K522
EphA4	-283.3	K368, K376, R378, R466, R496	-260.9	R489, R492, K501, R516, R538
EphA5	-299.9	K478, K479, K481, K511, R555, R556		
EphA6	-237.4	R279, K291, K294, K320, R329, R359, K360		
EphA7	-304.6	K479, K483, R486, R488, R516, R529		
EphA8	-468.1	K479, K481, K475, K490, R512, R514, R521		
EphB1	-354.2	K362, R364, R367, R368, R372	-363.3	R470, R485, R507, R509, K516, K520
EphB2	-91.5	K476, K487, R509, R511, R518, K522		
EphB3	-319.0	R336, K370, K371, R373, R386, R415, R435, R473 R355, K429		
EphB4	-483.1	R444, R491, R495, R483, K486 R510, K498, R499		
EphB6	-12.8	R492, R542		

Figure 3.8: Summarized docking data CS-E hexasaccharide docking to EphA and EphB family members (**a**) The snapbe for the top fifteen poses for each ligand docked to EphA1, EphA2, EphA3, EphA4, EphA5, EphA6, EphA7, EphA8, EphB1, EphB2, EphB3, EphB4, and EphB6. Receptors are graphed in order of average snapbe, lowest to highest. (**b**) The average snapbe for the top fifteen poses. Arginine and lysine residues found within 5Å of ligand are listed for each Eph receptor.

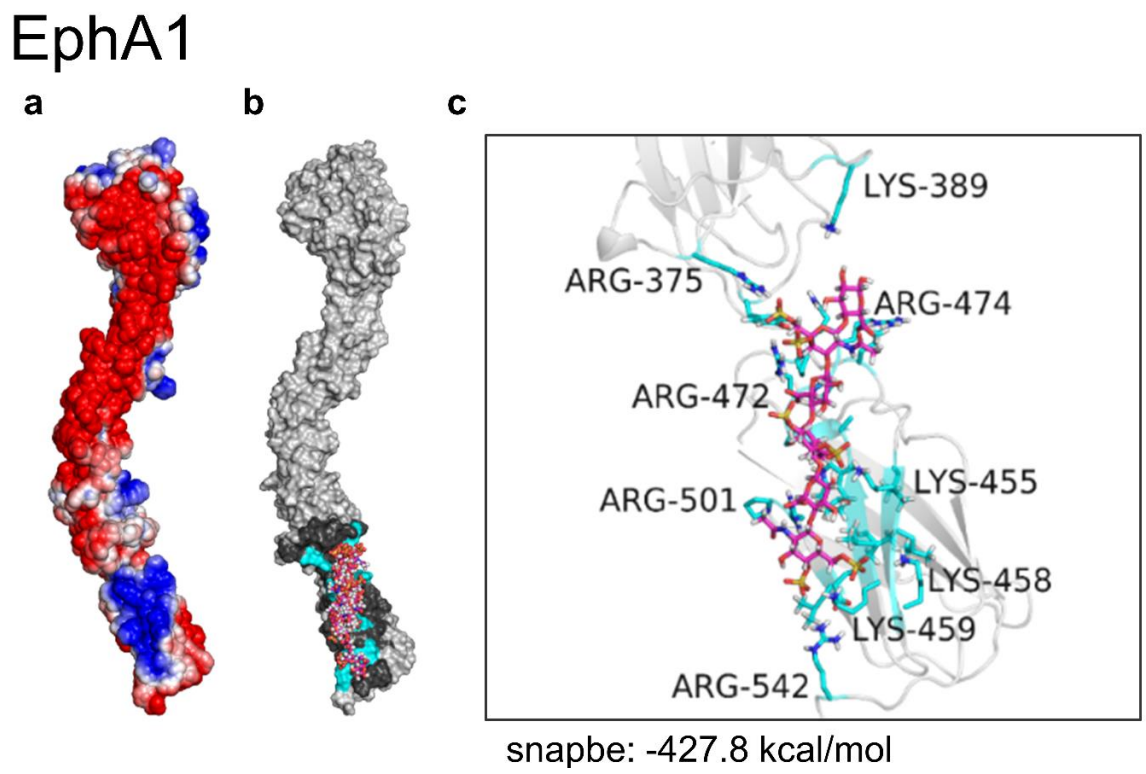

Figure 3.9: CS-E hexasaccharide docking to EphA1 (**a**) Electrostatic surface potential of EphA1. (**b**) The top five poses clustered to the second fibronectin domain of EphA1. Residues within 5Å of ligand (dark grey) and arginine and lysine residues within 5Å (cyan). (**c**) Zoom-in of binding site showing top pose. The predicted binding site contains the arginine and lysine residues R375, K389, K455, K458, K459, R472, R474, R501, and R542, with a predicted snapbe of -427.8 kcal/mol.

EphA1

EphA1 is not currently known to be upregulated following injury to the nervous, but is involved in central nervous system disorders including multiple sclerosis and glioblastoma.[15,16] EphA1 is predicted to be the third strongest CS-E binding protein with an average snapbe of -427.8 kcal/mol (Fig. 3.8b). The likely CS-E binding site is found in the second fibronectin domain and is outlined by the following arginine and lysine residues: R375, K389, K455, K458, K459, R472, R474, R501, and R542 (Fig. 3.9).

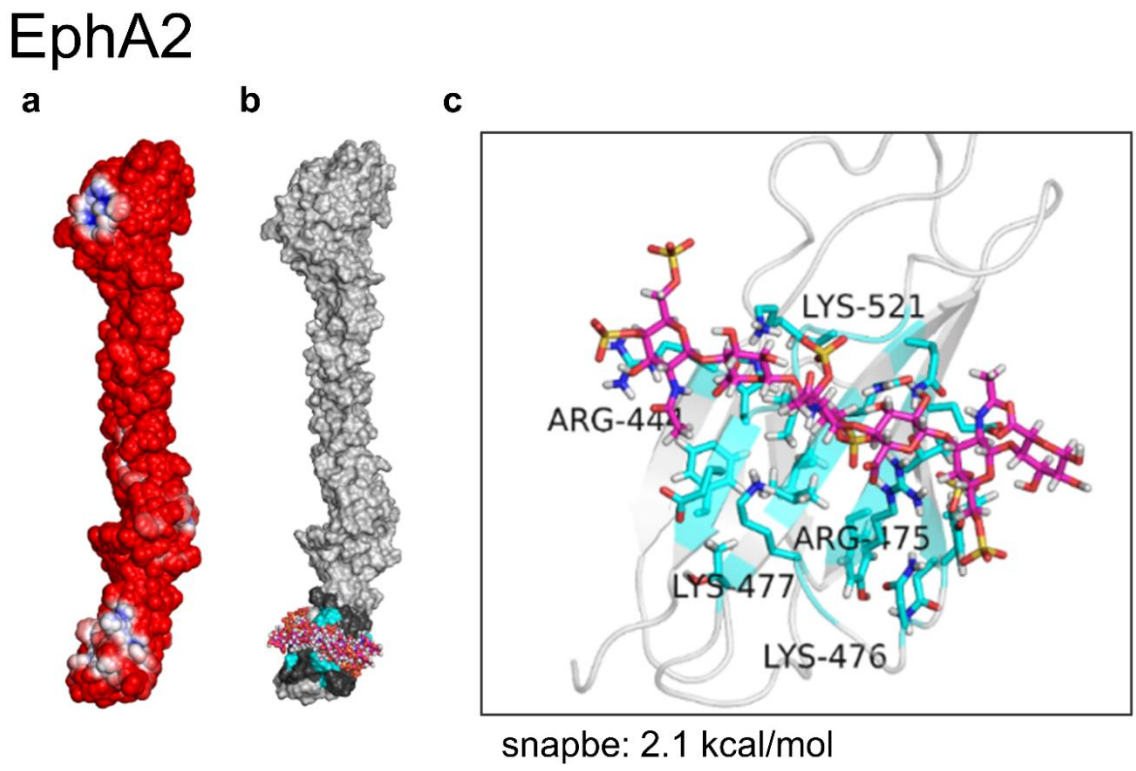

Figure 3.10: CS-E hexasaccharide docking to EphA2 (**a**) Electrostatic surface potential of EphA2. (**b**) The top five poses clustered to the second fibronectin domain of EphA2. Residues within 5Å of ligand (dark grey) and arginine and lysine residues within 5Å (cyan). (**c**) Zoom-in of binding site showing top pose. The predicted binding site contains the arginine and lysine residues R375, K389, K455, K458, K459, R472, R474, R501, and R542, with a predicted snapbe of -427.8 kcal/mol.

EphA2

EphA2 is upregulated in the cortex following subdural hematoma in rats.[17] EphA2 is predicted to be the thirteenth strongest CS-E binding protein with an average snapbe of 2.1 kcal/mol (Fig. 3.8b). EphA2 is very electronegative and predicted to not bind CS-E. The top docked poses clustered to a region in the fibronectin domain and weakly interacts with the following arginine and lysine residues: R475, K477, and K521 (Fig. 3.10).

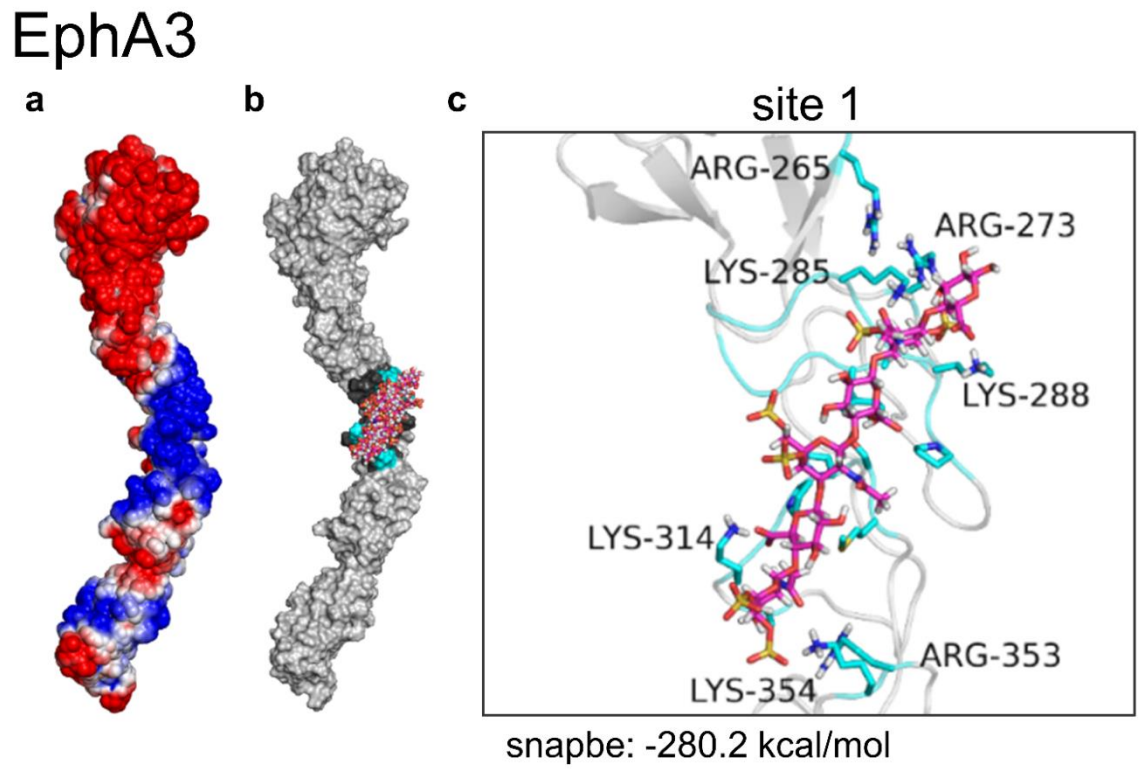

Figure 3.11: CS-E hexasaccharide docking to EphA3: site1 (**a**) Electrostatic surface potential of EphA3. (**b**) The top five poses clustered to the EGF/sushi domain of EphA3. Residues within 5Å of ligand (dark grey) and arginine and lysine residues within 5Å (cyan). (**c**) Zoom-in of binding site showing top pose. The predicted binding site contains the arginine and lysine residues R265, R273, K285, K288, K314, K354, and R353, with a predicted snapbe of -280.2 kcal/mol.

EphA3

EphA3 is upregulated in numerous injury models of the CNS. Following spinal cord injury, EphA3 is upregulated in astrocytes, oligodendrocytes, and motor neurons.[18,19] EphA3 is upregulated in retinal ganglion cells following optic nerve injury, and upregulated in hippocampal and cortical neurons following brain injury.[17,20,21] EphA3 is predicted to be the fourth strongest CS-E binding protein. EphA3 has two potential binding sites each with an average snapbe of -280.2 kcal/mol and -361.5 kcal/mol (Fig. 3.8b). The first CS-E binding site is located in the EGF/sushi domain of EphA3 and contains the following

arginine and lysine residues: R265, R273, K285, K288, K314, K354, and R353, with an average snapbe of -280.2 kcal/mol (Fig. 3.11). The second CS-E binding site is located in the second fibronectin domain of EphA3 and is outlined by the following arginine and lysine residues: K472, K476, R487, R509, R511, R521, and K522 with an average snapbe of -361.5 kcal/mol (Fig. 3.12).

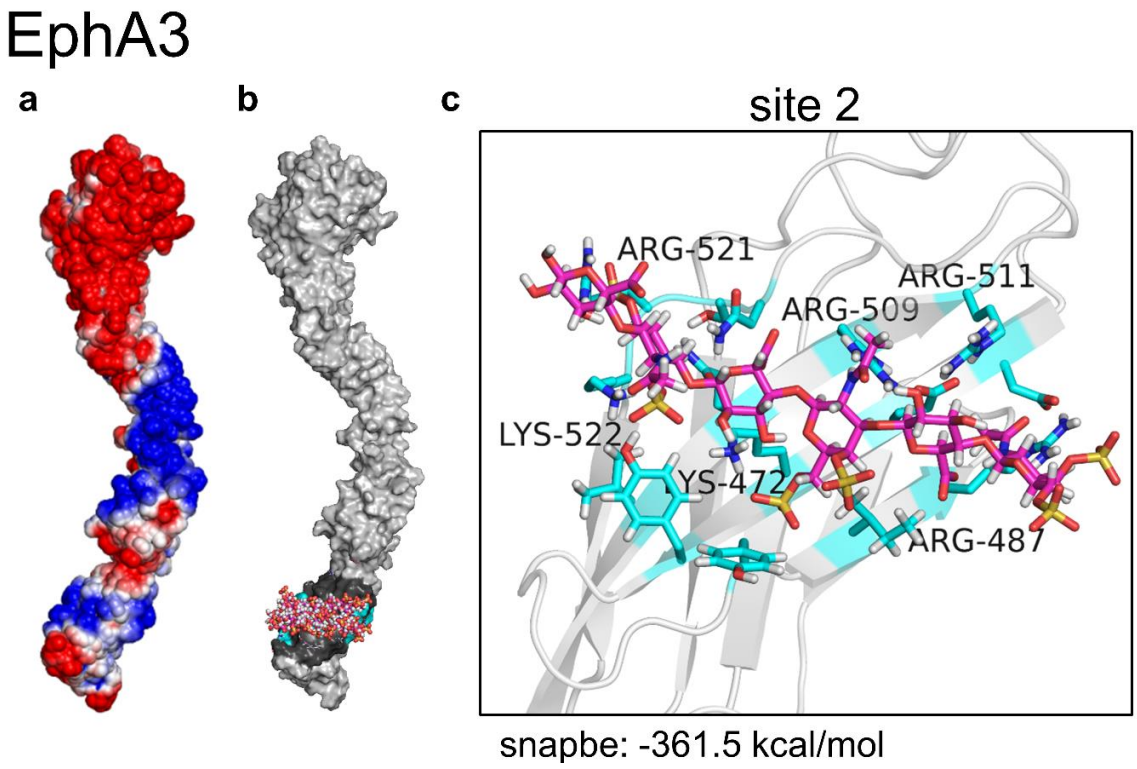

Figure 3.12: CS-E hexasaccharide docking to EphA3: site 2 (**a**) Electrostatic surface potential of EphA3. (**b**) The top five poses clustered to the second fibronectin domain of EphA3. Residues within 5Å of ligand (dark grey) and arginine and lysine residues within 5Å (cyan). (**c**) Zoom-in of binding site showing top pose. The predicted binding site contains the arginine and lysine residues K472, K476, R487, R509, R511, R521, and K522 with a predicted snapbe of -361.5 kcal/mol.

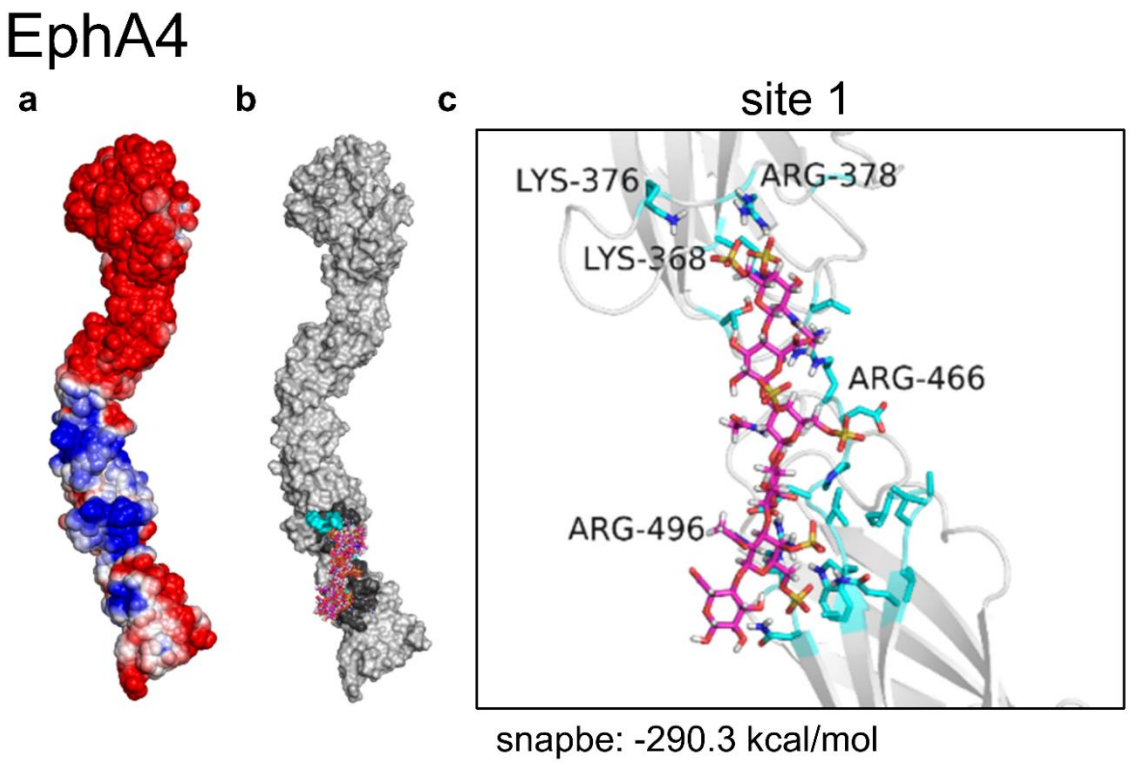

Figure 3.13: CS-E hexasaccharide docking to EphA4: site 1 (**a**) Electrostatic surface potential of EphA4. (**b**) The top five poses clustered to the first fibronectin domain of EphA4. Residues within 5Å of ligand (dark grey) and arginine and lysine residues within 5Å (cyan). (**c**) Zoom-in of binding site showing top pose. The predicted binding site contains the arginine and lysine residues K368, K376, R378, R466, and R496, with a predicted snapbe of -290.3 kcal/mol.

EphA4

EphA4 is upregulated in both astrocytes and motor neurons following injury to the spinal cord, and in hippocampal neurons after brain injury.[18,21] In addition, genetic deletion of EphA4 promotes axon regeneration and recovery of motor function following injury to the spinal cord.[13] Importantly, EphA4 mediated inhibition of axon regeneration can be reversed through therapeutic intervention.[22,23] EphA4 is predicted to be the ninth strongest CS-E binding protein. CS docking to EphA4 is more thoroughly analyzed in the preceding sections. Briefly, top poses docked to EphA4 clustered to two, each with an average snapbe

of -270.3 kcal/mol and -251.8 kcal/mol (Fig. 3.8b). The first CS-E binding site is located in first fibronectin domain of EphA4 and contains the following arginine and lysine residues: K368, K376, R378, R466, and R496, with an average snapbe of -260.9 kcal/mol (Fig. 3.13). The second CS-E binding site is located in the second fibronectin domain of EphA4 and is outlined by the following arginine and lysine residues: R489, R492, K501, R516, R538 (Fig. 3.14).

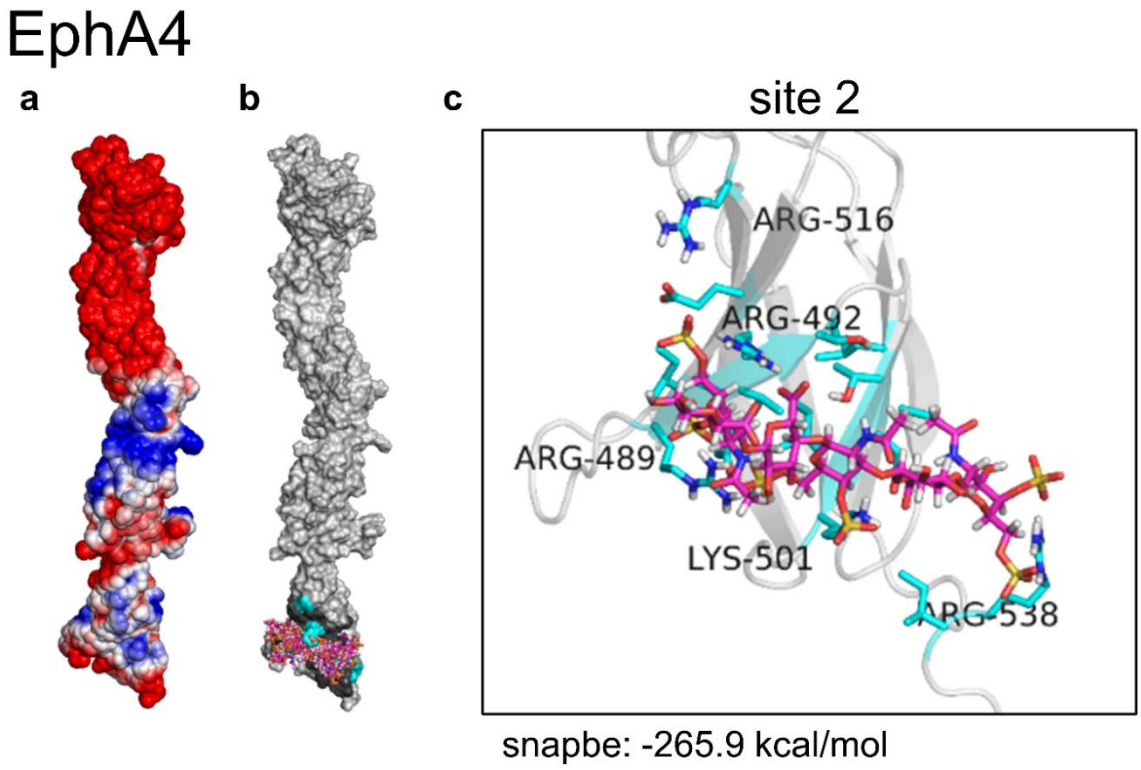

Figure 3.14: CS-E hexasaccharide docking to EphA4: site 2 (**a**) Electrostatic surface potential of EphA4. (**b**) The top five poses clustered to the second fibronectin domain of EphA4. Residues within 5Å of ligand (dark grey) and arginine and lysine residues within 5Å (cyan). (**c**) Zoom-in of binding site showing top pose. The predicted binding site contains the arginine and lysine residues R489, R492, K501, R516, and R538, with a predicted snapbe of -265.9 kcal/mol.

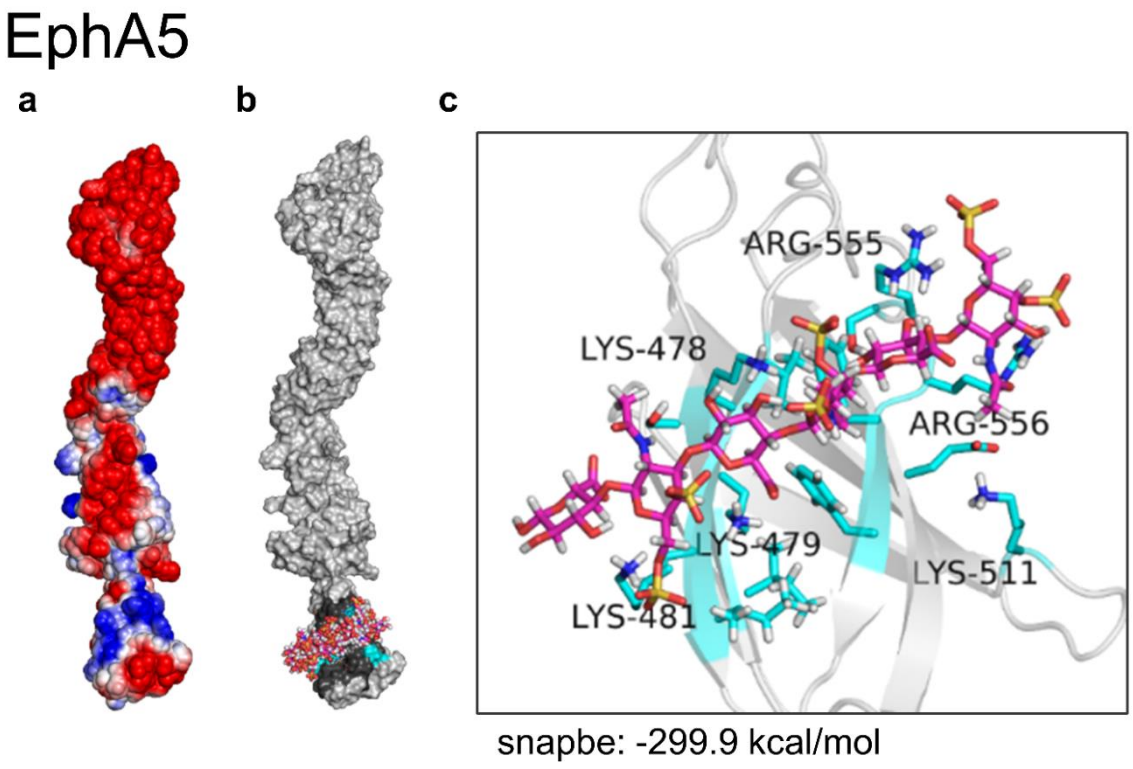

Figure 3.15: CS-E hexasaccharide docking to EphA5 (**a**) Electrostatic surface potential of EphA5. (**b**) The top five poses clustered to the second fibronectin domain of EphA5. Residues within 5Å of ligand (dark grey) and arginine and lysine residues within 5Å (cyan). (**c**) Zoom-in of binding site showing top pose. The predicted binding site contains the arginine and lysine residues K478, K479, K481, K511, R555, and R556, with a predicted snapbe of -299.9 kcal/mol.

EphA5

EphA5 is upregulated following spinal cord injury and brain injury in astrocytes and hippocampal neurons, respectively.[18,21] However, EphA5 is downregulated in optic nerve injury models.[24,25] EphA5 is predicted to be the eighth strongest CS-E binding protein with an average snapbe of -299.9 kcal/mol (Fig. 3.8b). The likely CS-E binding site is found in the second fibronectin domain and is outlined by the following arginine and lysine residues: K478, K479, K481, K511, R555, and R556 (Fig. 3.15).

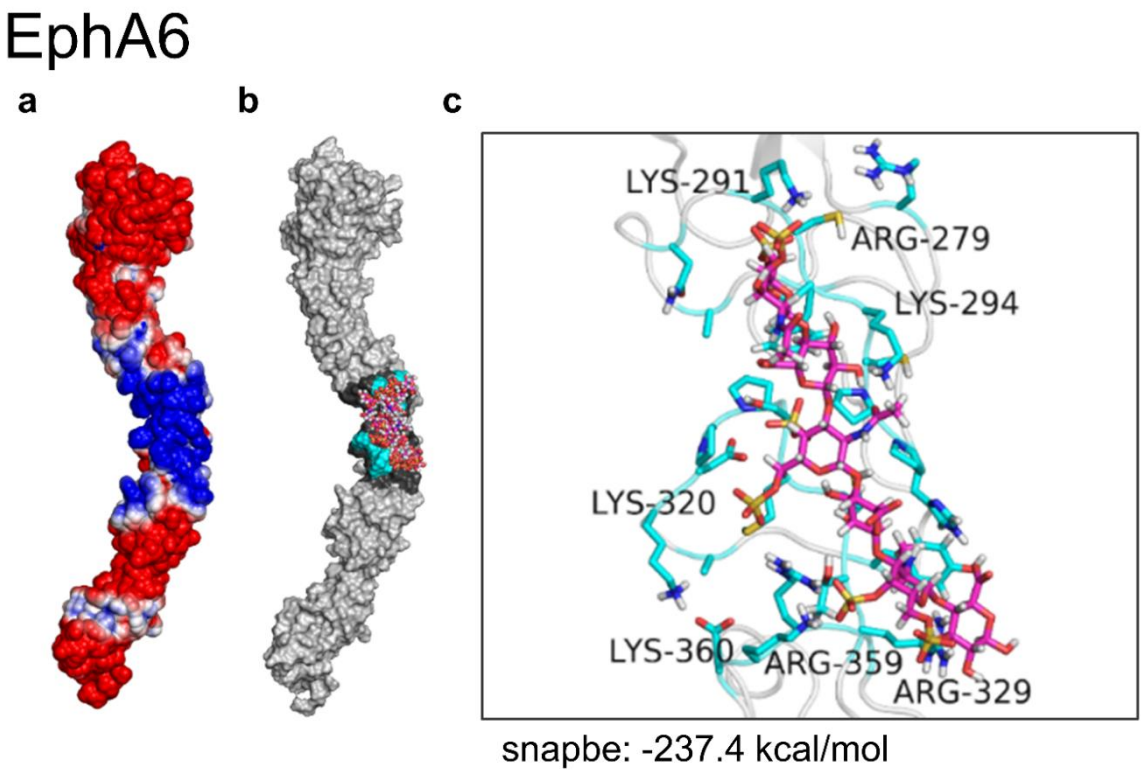

Figure 3.16: CS-E hexasaccharide docking to EphA6 (**a**) Electrostatic surface potential of EphA6. (**b**) The top five poses clustered to the EGF/sushi domain of EphA6. Residues within 5Å of ligand (dark grey) and arginine and lysine residues within 5Å (cyan). (**c**) Zoom-in of binding site showing top pose. The predicted binding site contains the arginine and lysine residues R279, K291, K294, K320, R329, R359, and K360, with a predicted snapbe of -237.4 kcal/mol.

EphA6

EphA6 is upregulated in astrocytes, oligodendrocytes, and motor neurons following injury to the spinal cord, and upregulated in hippocampal neurons post-brain injury.[18,21] EphA6 is predicted to be the tenth strongest CS-E binding protein with an average snapbe of -237.4 kcal/mol (Fig. 3.8b). The likely CS-E binding site is found in the EGF/sushi domain of EphA6. This region is outlined by the following arginine and lysine residues: R279, K291, K294, K320, R329, R359, and K360 (Fig. 3.16).

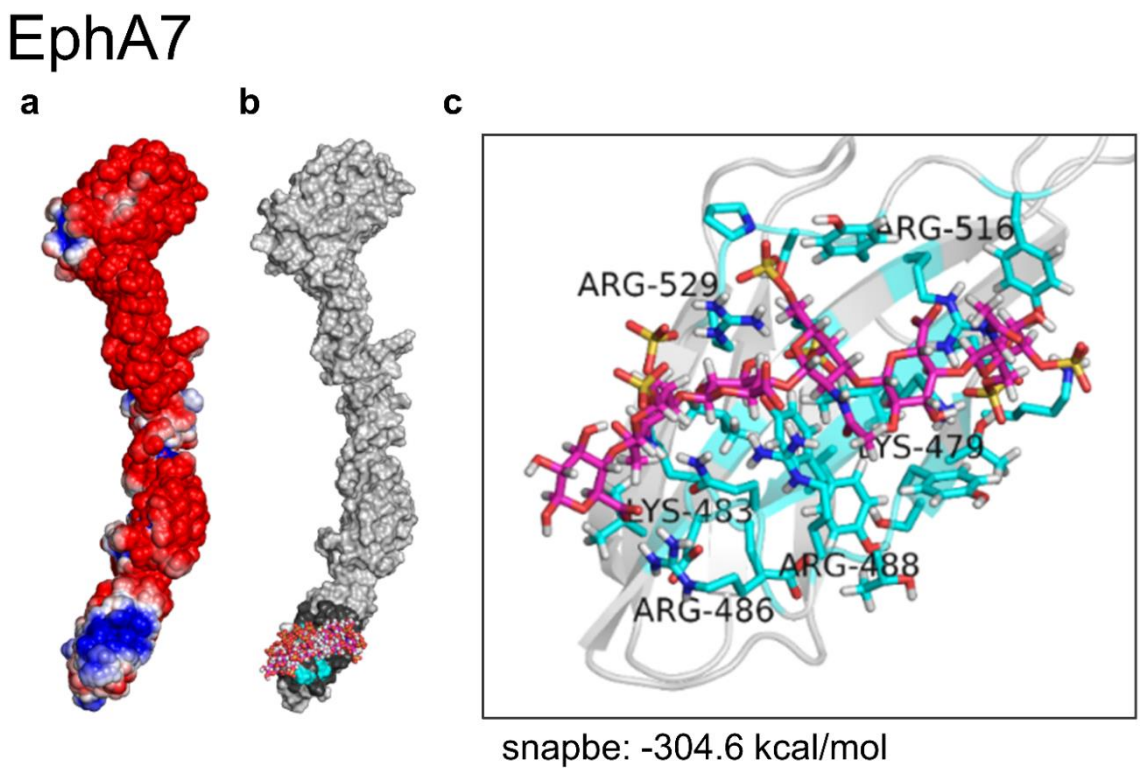

Figure 3.17: CS-E hexasaccharide docking to EphA7 (**a**) Electrostatic surface potential of EphA7. (**b**) The top five poses clustered to the second fibronectin domain of EphA7. Residues within 5Å of ligand (dark grey) and arginine and lysine residues within 5Å (cyan). (**c**) Zoom-in of binding site showing top pose. The predicted binding site contains the arginine and lysine residues K479, K483, R486, R488, R516, and R529, with a predicted snapbe of -304.6 kcal/mol.

EphA7

EphA6 is upregulated in astrocytes, oligodendrocytes, and motor neurons following injury to the spinal cord.[18] Importantly, blocking activation of EphA7 spinal cord injury results in significant recovery of hindlimb function in injured rats.[26] EphA7 is predicted to be the seventh strongest CS-E binding protein with an average snapbe of -304.6 kcal/mol (Fig. 3.8b). The likely CS-E binding site is found in the second fibronectin domain and is outlined by the following arginine and lysine residues: K479, K483, R486, R488, R516, and R529 (Fig. 3.17).

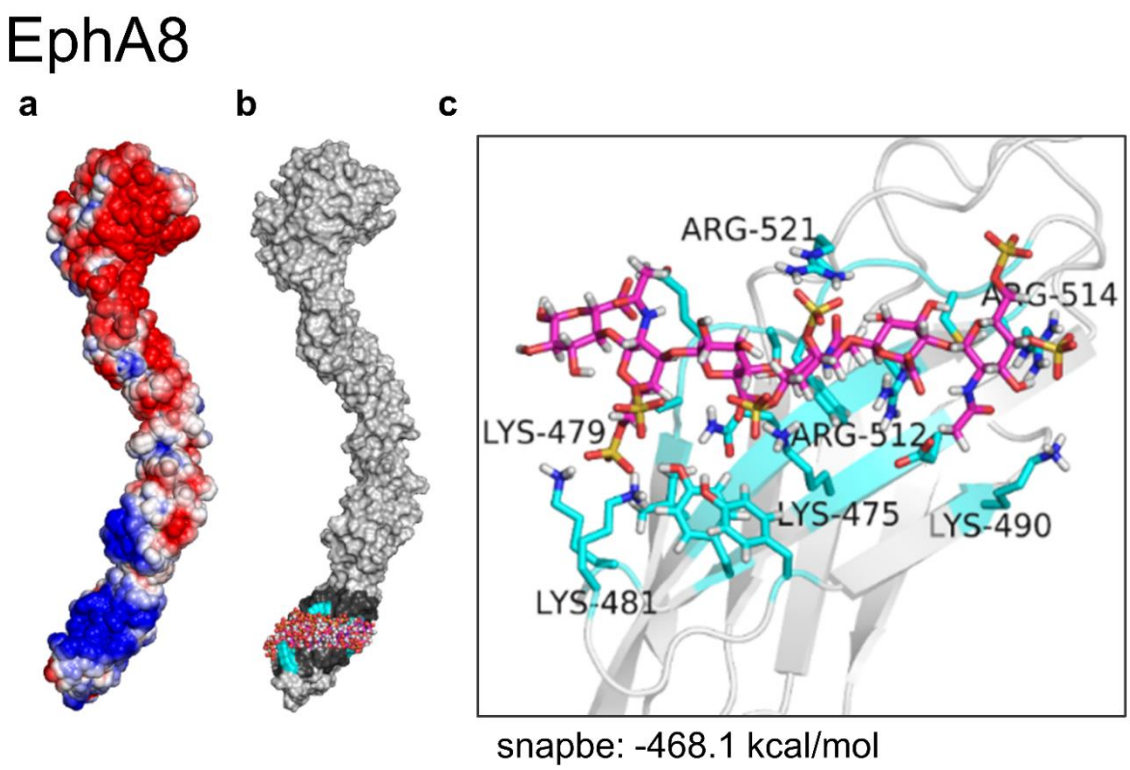

Figure 3.18: CS-E hexasaccharide docking to EphA8 (**a**) Electrostatic surface potential of EphA8. (**b**) The top five poses clustered to the second fibronectin domain of EphA8. Residues within 5Å of ligand (dark grey) and arginine and lysine residues within 5Å (cyan). (**c**) Zoom-in of binding site showing top pose. The predicted binding site contains the arginine and lysine residues K479, K481, K475, K490, R512, R514, and R521, with a predicted snapbe of -468.1 kcal/mol.

EphA8

In spinal cord injury models, EphA8 is upregulated in astrocytes, oligodendrocytes, axons in ventrolateral intermediate cells, and motor neurons.[18] EphA8 is predicted to be the second strongest CS-E binding protein with an average snapbe of -468.1 kcal/mol (Fig. 3.8b). The likely CS-E binding site is found in the second fibronectin domain and is outlined by the following arginine and lysine residues: K479, K481, K475, K490, R512, R514, and R521 (Fig. 3.18).

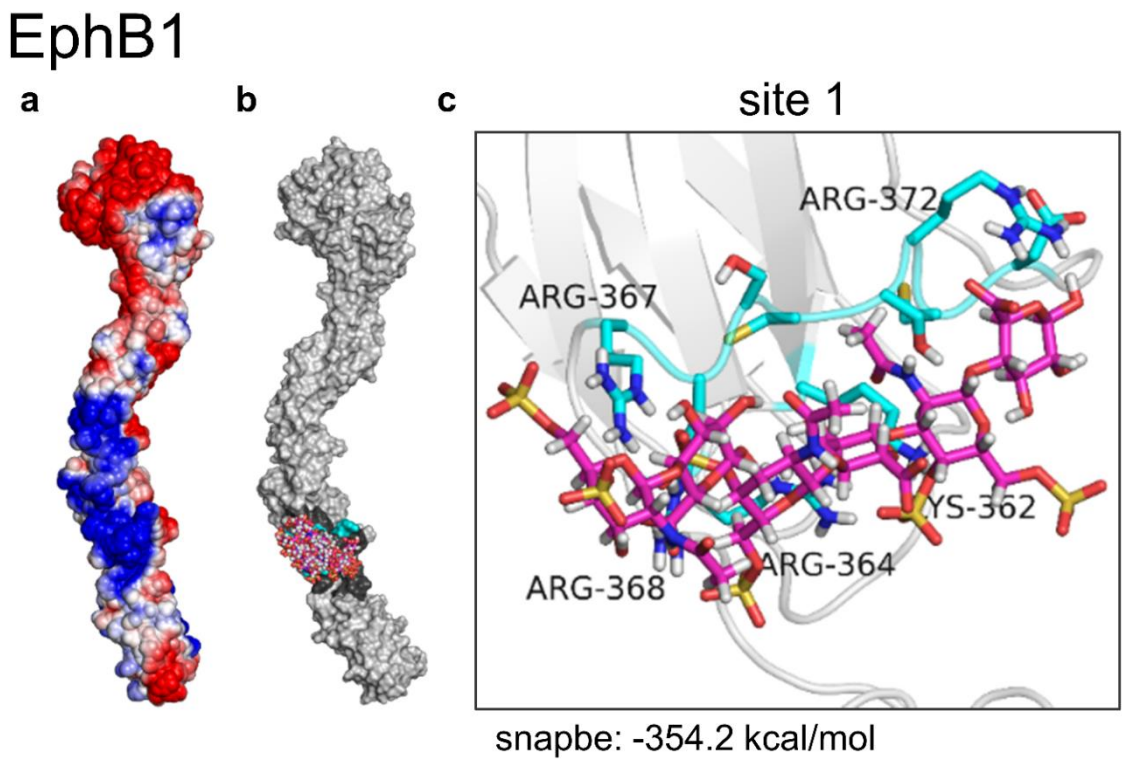

Figure 3.19: CS-E hexasaccharide docking to EphB1: site 1 (**a**) Electrostatic surface potential of EphB1. (**b**) The top five poses clustered to the first fibronectin domain of EphB1. Residues within 5Å of ligand (dark grey) and arginine and lysine residues within 5Å (cyan). (**c**) Zoom-in of binding site showing top pose. The predicted binding site contains the arginine and lysine residues K362, R364, R367, R368, and R372, with a predicted snapbe of -354.2 kcal/mol.

EphB1

EphB1 EphB1 is predicted to be the fifth strongest CS-E binding protein. EphB1 has two potential binding sites each with an average snapbe of -354.2 kcal/mol and -363.3 kcal/mol (Fig. 3.8b). The first CS-E binding site is located in the first fibronectin domain of EphB1 and contains the following arginine and lysine residues: K362, R364, R367, R368, and R372, with an average snapbe of -354.2 kcal/mol (Fig. 19). The second CS-E binding site is located in the second fibronectin domain of EphB1 and is outlined by the following

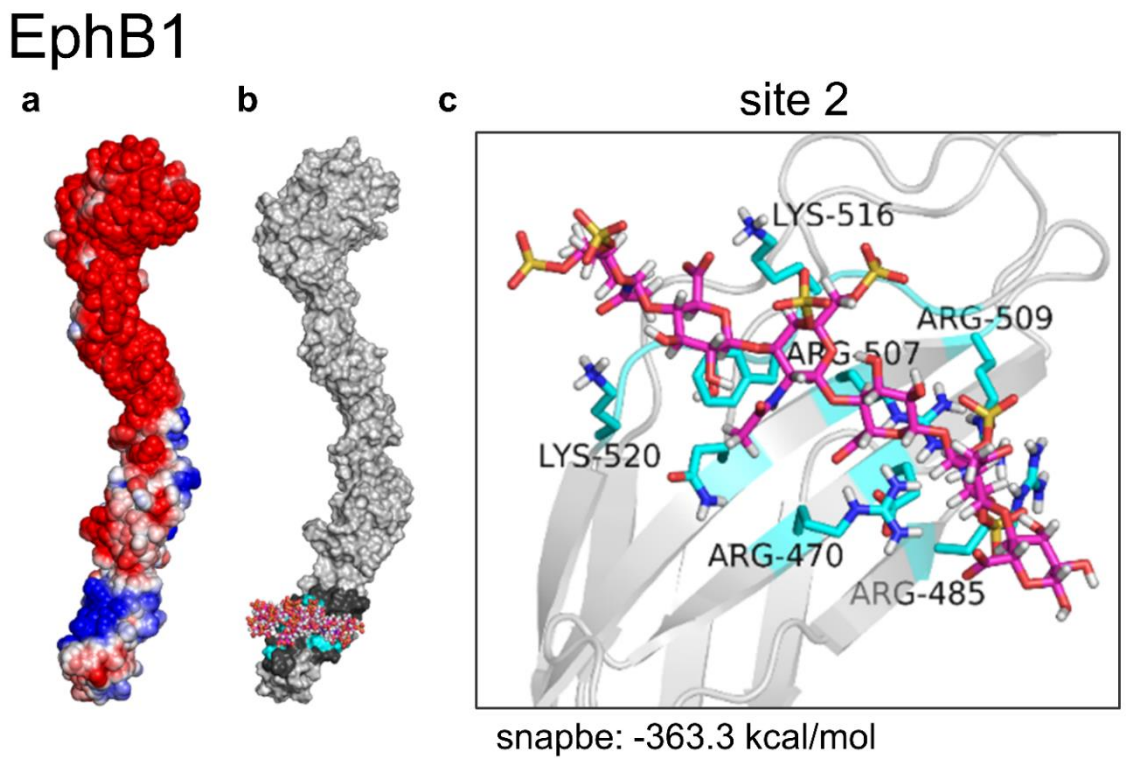

Figure 3.20: CS-E hexasaccharide docking to EphB1: site 2 (**a**) Electrostatic surface potential of EphB1. (**b**) The top five poses clustered to the second fibronectin domain of EphB1. Residues within 5Å of ligand (dark grey) and arginine and lysine residues within 5Å (cyan). (**c**) Zoom-in of binding site showing top pose. The predicted binding site contains the arginine and lysine residues R470, R485, R507, R509, K516, and K520, with a predicted snapbe of -363.3 kcal/mol.

arginine and lysine residues: R470, R485, R507, R509, K516, and K520, with an average snapbe of -363.3 kcal/mol (Fig. 3.20).

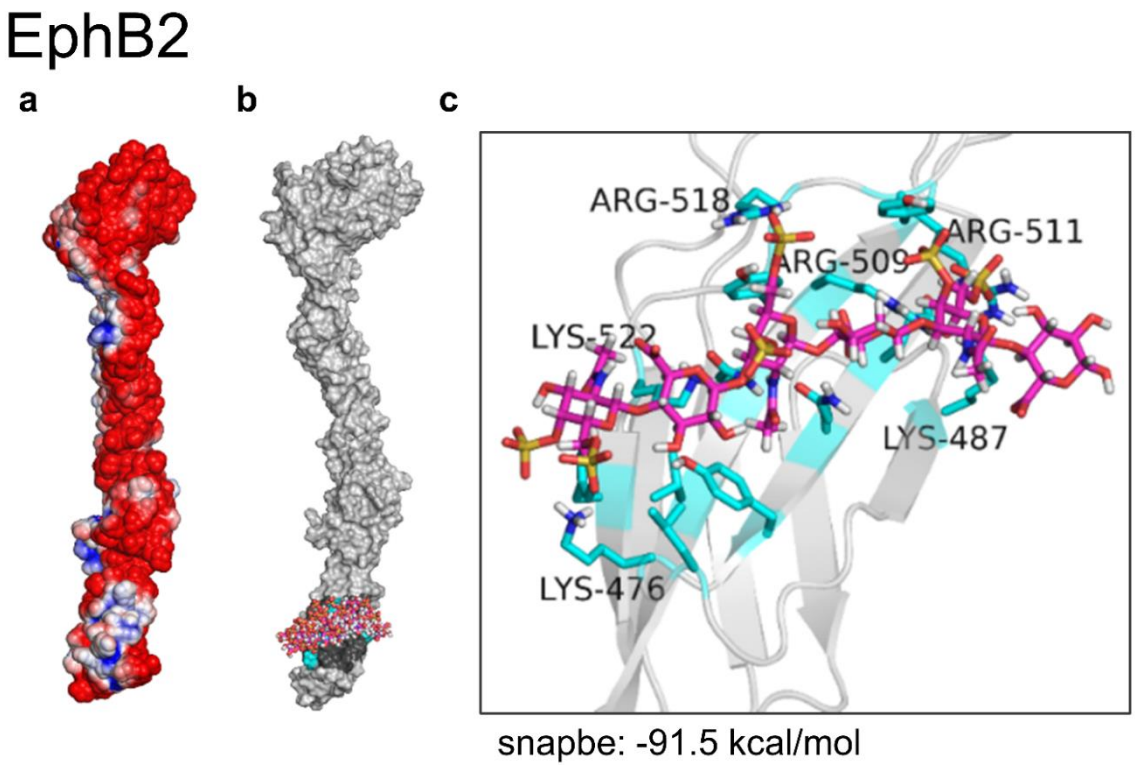

Figure 3.21: CS-E hexasaccharide docking to EphB2 (**a**) Electrostatic surface potential of EphA1. (**b**) The top five poses clustered to the second fibronectin domain of EphB2. Residues within 5Å of ligand (dark grey) and arginine and lysine residues within 5Å (cyan). (**c**) Zoom-in of binding site showing top pose. The predicted binding site contains the arginine and lysine residues K476, K487, R509, R511, R518, and K522, with a predicted snapbe of -91.5 kcal/mol.

EphB2

EphB2 is predicted to be the eleventh strongest CS-E binding protein with an average snapbe of -91.5 kcal/mol (Fig. 3.8b). Indeed, EphB2 has been experimentally confirmed to not bind CS-E.[27] The top docked poses all clustered in the second fibronectin domain and is outlined by the following arginine and lysine residues: K476, K487, R509, R511, R518, and K522 (Fig. 3.21).

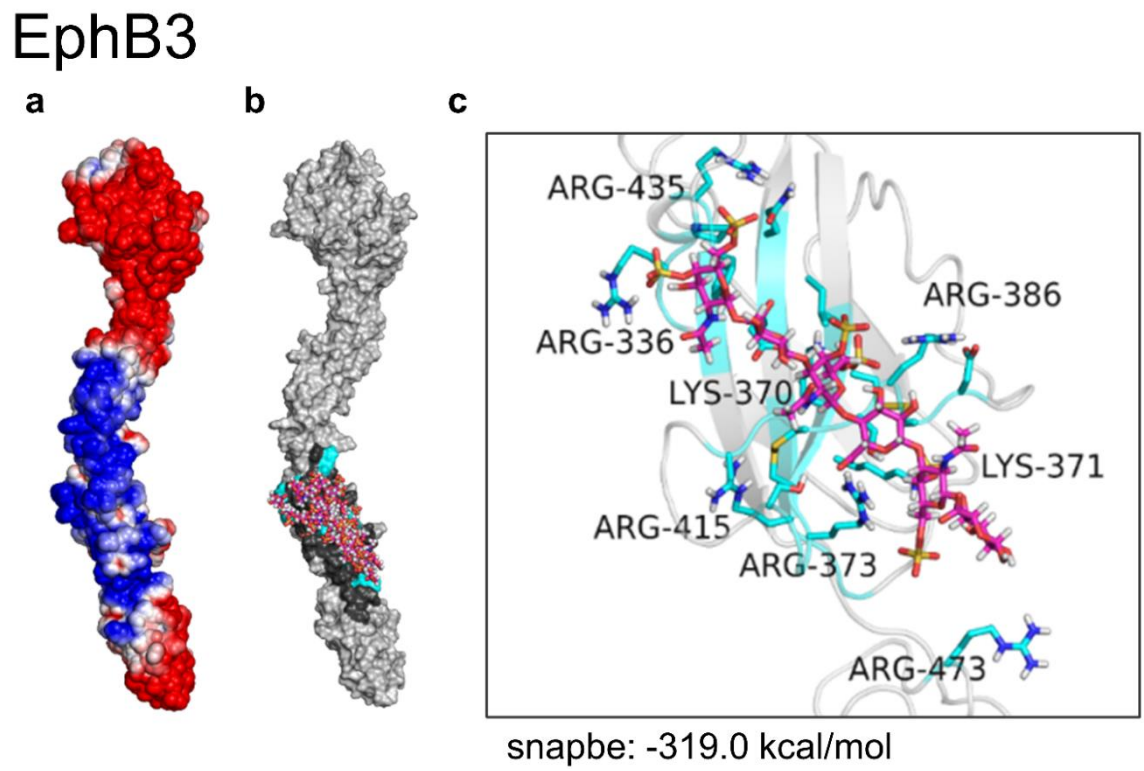

Figure 3.22: CS-E hexasaccharide docking to EphB3 (**a**) Electrostatic surface potential of EphB3. (**b**) The top five poses clustered to the first and second fibronectin domain of EphB3. Residues within 5Å of ligand (dark grey) and arginine and lysine residues within 5Å (cyan). (**c**) Zoom-in of binding site showing top pose. The predicted binding site contains the arginine and lysine residues R336, R355, K370, K371, R373, R386, R415, K429, R435, and R473, with a predicted snapbe of -319.0 kcal/mol.

EphB3

Following injury to the spinal cord, EphB3 is upregulated in astrocytes and ventral root axon, and is upregulated in the cortex following subdural hematoma, a traumatic brain injury model.[17,18,28,29] EphB3 is predicted to be the sixth strongest CS-E binding protein with an average snapbe of -319.0 kcal/mol (Fig. 3.8b). EphB3 has been confirmed as a CS-E binding protein.[27] The likely CS-E binding site is found in the first fibronectin domain and is outlined by the following arginine and lysine residues: R336, R355, K370, K371, R373, R386, R415, K429, R435, and R473 (Fig. 3.22).

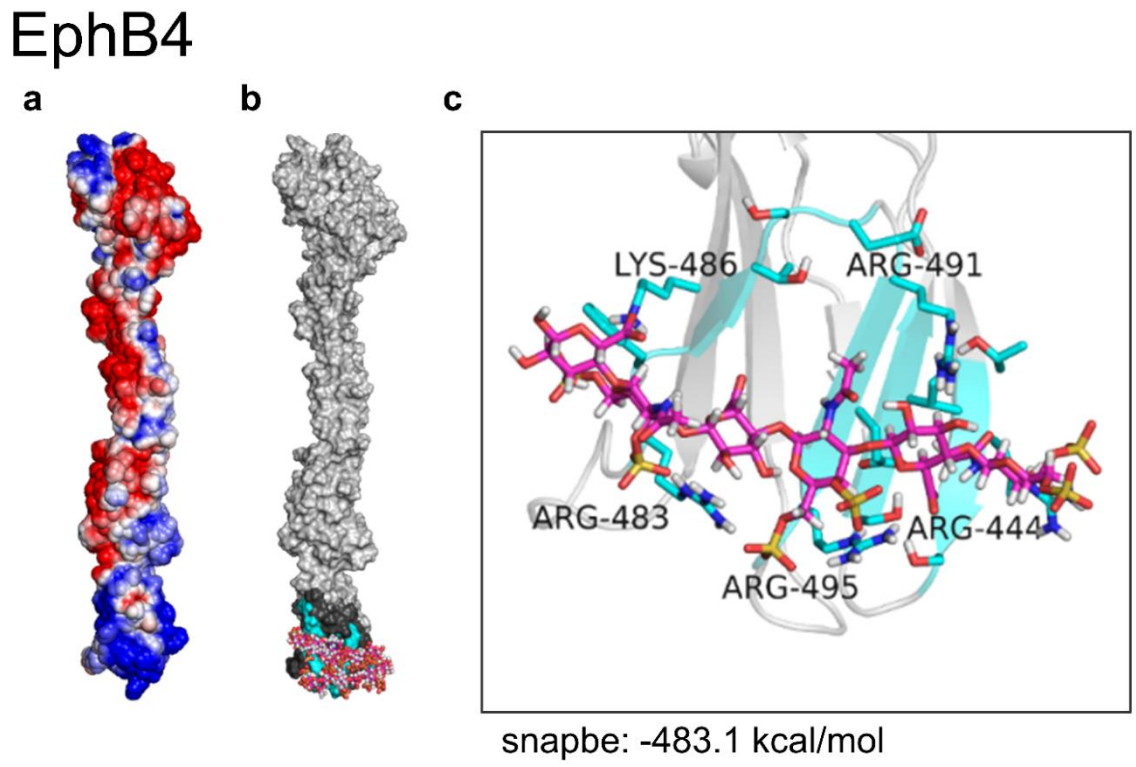

Figure 3.23: CS-E hexasaccharide docking to EphB4 (**a**) Electrostatic surface potential of EphB4. (**b**) The top five poses clustered to the second fibronectin domain of EphB4. Residues within 5Å of ligand (dark grey) and arginine and lysine residues within 5Å (cyan). (**c**) Zoom-in of binding site showing top pose. The predicted binding site contains the arginine and lysine residues R444, R491, R495, R483, K486, K498, R499, and R510, with a predicted snapbe of -483.1 kcal/mol.

EphB4

EphB4 is predicted to be the strongest CS-E binding protein with an average snapbe of -483.1 kcal/mol (Fig. 3.8b). The likely CS-E binding site is found in the second fibronectin domain and is outlined by the following arginine and lysine residues: R444, R491, R495, R483, K486, K498, R499, and R510 (Fig. 3.23). A role for EphB4 in nervous system injury has not been thoroughly explored, but its strong predicted interaction may be important for other systems during development and cancer progression.[5,7]

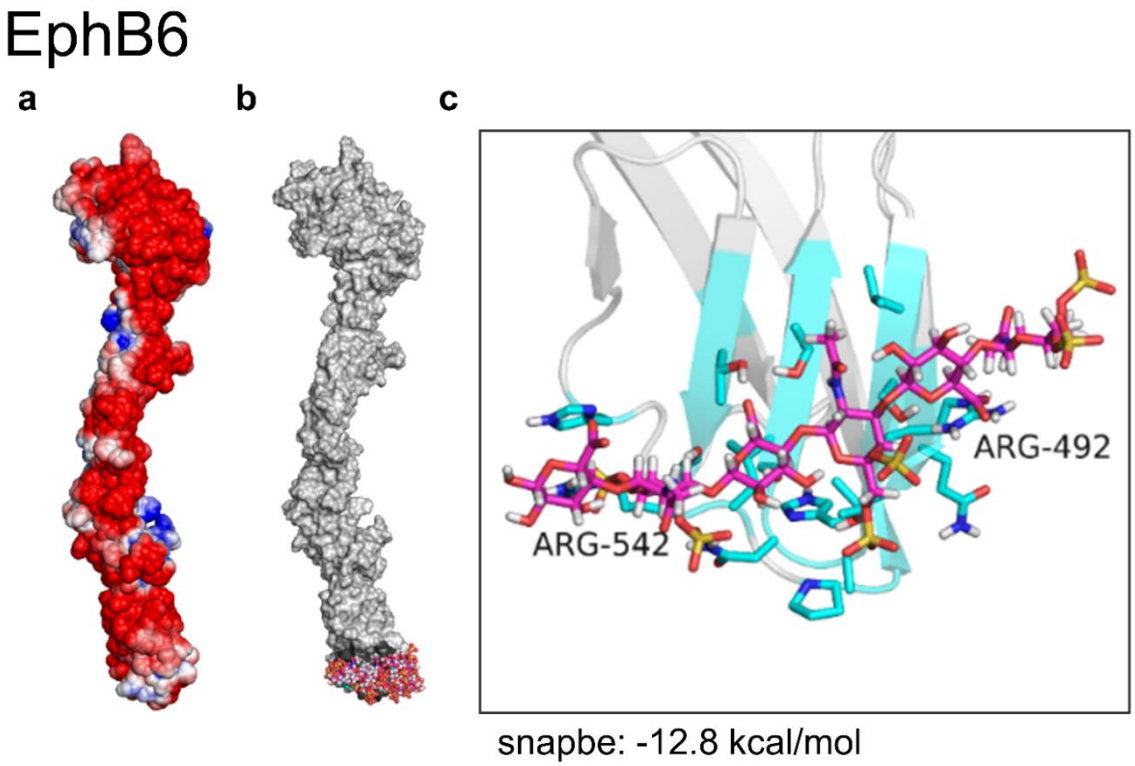

Figure 3.24: CS-E hexasaccharide docking to EphB6 (**a**) Electrostatic surface potential of EphB6. (**b**) The top five poses clustered to the second fibronectin domain of EphB6. Residues within 5Å of ligand (dark grey) and arginine and lysine residues within 5Å (cyan). (**c**) Zoom-in of binding site showing top pose. The predicted binding site contains the arginine and lysine residues R492 and R542, with a predicted snapbe of -12.8 kcal/mol.

EphB6

EphB6 is predicted to be the twelfth strongest CS-E binding protein with an average snapbe of -12.8 kcal/mol (Fig. 3.8b). EphB6 is predicted to not bind CS-E. The top poses were found to cluster in the second fibronectin domain and are outlined by the following arginine and lysine residues: R492 and R542 (Fig. 3.24).

Conclusions

CSPGs inhibit axon regeneration, in part, through their ability to engage cell surface receptors and soluble ligands found in the extracellular matrix.[3,30] This diverse set of protein binding partners allows CS to affect cell state through the modulation of intracellular signaling pathways. Several transmembrane receptors including receptor protein tyrosine phosphatases, RPTPσ and LAR, and Nogo receptors, NgR1 and NgR3 have been identified as CS-E binding proteins that inhibit axon regeneration.[31] In Chapter 2, EphA4 was identified as a receptor of CS. The receptor tyrosine kinase EphA4 receptor has various roles in the development and regulation of the nervous system, and inhibiting axon regeneration after injury to the CNS. We found that EphA4 binds with high affinity to the glycosaminoglycan chains of CSPGs. This work presents a computational analysis of EphA4 interactions with the sulfated motifs CS-A, CS-C, CS-D, and CS-E. The identification and characterization of CS interactions with cell surface receptors advances our understanding of inhibition of axon regeneration following injury to the CNS where CS-E expression is upregulated, and provides us with the opportunity to develop therapies for the recovery of axon growth after injury to the nervous system.

Eph receptor activation by ephrin ligands occurs through a receptor clustering mechanism that results in tyrosine phosphorylation of the intracellular kinase domain.[6] We identify a similar mechanism of activation by CS-E and demonstrate its ability to cluster cell surface EphA4. Importantly, receptor clustering by CS-E results in elevated levels of tyrosine phosphorylation of EphA4, suggesting CS-E induces the formation of active EphA4 signaling clusters. This work performed computational docking to identify potential CS binding Eph receptors. The relative strengths of the predicted binding energies

are EphB4 > EphA8 > EphA1 > EphA3 > EphB1 > EphB3 > EphA7 > EphA5 > EphA4 > EphA6 > EphB2 > EphB6 > EphA2. Carbohydrate induced Eph receptor clustering could be a general mechanism of Eph receptor activation with implications for axon guidance and regeneration, regulation of synaptic plasticity, and cancer metastasis.

Methods

GAG-Dock Summary. These methods are outlined futher.[14] This involves a two-step process for each GAG-protein complex, we first identify likely GAG binding sites on the target protein using coarse docking and then we re-dock using find docking to identify strongly bound poses. In the first step, for "coarse-docking" we dock a single GAG conformation to the entire protein surface to identify likely binding sites. This configuration is chosen by minimizing the ligand in the solvent. Here, docking to the 'alanized' structure allows us to quickly scan the entire protein for putative GAG binding sites by optimizing the long-range Coulomb interactions. In the second step, for "fine-grained" we re-dock to the best coarse regions to identify specific, strongly bound poses. In this step, we sample ligand conformations more completely allowing rotations about single bonds to accommodate the intrinsic flexibility of the GAG ligand. We selected 12 conformations to have low energies while remaining diverse, as described under ligand preparation. Then do rigid docking of this ensemble of 12 GAG ligand conformations. Finally, all final energies for all poses for all 12 conformations are ranked together by total energy and the best 100 are minimization before identifying the top docked structure for each GAG-protein complex. These methods are detailed further below and in the SI.

System Preparation All Eph receptors were prepared in the manner as follows. The extracellular portion was modeled using SWISS-MODEL with EphA4-EfnA5 (PDBID: 4M4R4A) co-crystal structure used as the template.[32,33] The structures were minimized in vacuo using the DREIDING force field.[34] The following protein sequences were used for modeling: EphA1 (uniprot ID Q60750), EphA2 (uniprot ID Q03145), EphA3 (uniprot ID P29319), EphA4 (uniprot ID Q03137), EphA5 (uniprot ID Q60629), EphA6 (uniprot ID

Q62413), EphA7 (uniprot ID Q61772), EphA8 (uniprot ID O09127), EphB1 (uniprot ID Q8CBF3), EphB2 (uniprot ID P54763), EphB3 (uniprot ID P54754), EphB4 (uniprot ID P54761), and EphB6 (uniprot ID O08644).

References

1. Carulli, D., Laabs, T., Geller, H. M. & Fawcett, J. W. Chondroitin sulfate proteoglycans in neural development and regeneration. *Curr. Opin. Neurobiol.* **15,** 116–120 (2005).
2. Bartus, K., James, N. D., Bosch, K. D. & Bradbury, E. J. Chondroitin sulphate proteoglycans: key modulators of spinal cord and brain plasticity. *Exp. Neurol.* **235,** 5–17 (2012).
3. Miller, G. M. & Hsieh-Wilson, L. C. Sugar-dependent modulation of neuronal development, regeneration, and plasticity by chondroitin sulfate proteoglycans. *Exp. Neurol.* **274,** 115–125 (2015).
4. Xu, D. & Esko, J. D. Demystifying heparan sulfate-protein interactions. *Annu. Rev. Biochem.* **83,** 129–157 (2014).
5. Lisabeth, E. M., Falivelli, G. & Pasquale, E. B. Eph receptor signaling and ephrins. *Cold Spring Harb. Perspect. Biol.* **5,** (2013).
6. Kullander, K. & Klein, R. Mechanisms and functions of Eph and ephrin signalling. *Nat. Rev. Mol. Cell Biol.* **3,** 475–486 (2002).
7. Murai, K. K. & Pasquale, E. B. Eph receptors, ephrins, and synaptic function. *Neuroscientist* **10,** 304–314 (2004).
8. Lai, K.-O. & Ip, N. Y. Synapse development and plasticity: roles of ephrin/Eph receptor signaling. *Curr. Opin. Neurobiol.* **19,** 275–283 (2009).
9. Du, J., Fu, C. & Sretavan, D. W. Eph/ephrin signaling as a potential therapeutic target after central nervous system injury. *Curr. Pharm. Des.* **13,** 2507–2518 (2007).
10. Barquilla, A. & Pasquale, E. B. Eph receptors and ephrins: therapeutic opportunities.

Annu. Rev. Pharmacol. Toxicol. **55,** 465–487 (2015).

11. Coulthard, M. G. *et al.* Eph/Ephrin signaling in injury and inflammation. *Am. J. Pathol.* **181,** 1493–1503 (2012).
12. Goldshmit, Y., McLenachan, S. & Turnley, A. Roles of Eph receptors and ephrins in the normal and damaged adult CNS. *Brain Res. Rev.* **52,** 327–345 (2006).
13. Goldshmit, Y., Galea, M. P., Wise, G., Bartlett, P. F. & Turnley, A. M. Axonal regeneration and lack of astrocytic gliosis in EphA4-deficient mice. *J. Neurosci.* **24,** 10064–10073 (2004).
14. Adam R. Griffith, Claude J. Rogers, Gregory M. Miller, b Ravinder Abrol, Linda C. Hsieh-Wilson, W. A. G. I. Predicting glycosaminoglycan-surface protein interactions: Implications for studying axonal growth. *Proc. Natl. Acad. Sci. U.S.A.* (2017).
15. Sobel, R. A. Ephrin A receptors and ligands in lesions and normal-appearing white matter in multiple sclerosis. *Brain Pathol.* **15,** 35–45 (2005).
16. Hafner, C. *et al.* Differential gene expression of Eph receptors and ephrins in benign human tissues and cancers. *Clin. Chem.* **50,** 490–499 (2004).
17. Biervert, C., Horvath, E. & Fahrig, T. Semiquantitative expression analysis of ephrine-receptor tyrosine kinase mRNA's in a rat model of traumatic brain injury. *Neurosci. Lett.* **315,** 25–28 (2001).
18. Willson, C. A. *et al.* Upregulation of EphA receptor expression in the injured adult rat spinal cord. *Cell Transplant.* **11,** 229–239 (2002).
19. Irizarry-Ramírez, M. *et al.* Upregulation of EphA3 receptor after spinal cord injury. *J. Neurotrauma* **22,** 929–935 (2005).

20. King, C. E. *et al.* Transient up-regulation of retinal EphA3 and EphA5, but not ephrin-A2, coincides with re-establishment of a topographic map during optic nerve regeneration in goldfish. *Exp. Neurol.* **183,** 593–599 (2003).

21. Moreno-Flores, M. T. & Wandosell, F. Up-regulation of Eph tyrosine kinase receptors after excitotoxic injury in adult hippocampus. *Neuroscience* **91,** 193–201 (1999).

22. Goldshmit, Y. *et al.* EphA4 blockers promote axonal regeneration and functional recovery following spinal cord injury in mice. *PLoS One* **6,** 1–12 (2011).

23. Fabes, J., Anderson, P., Brennan, C. & Bolsover, S. Regeneration-enhancing effects of EphA4 blocking peptide following corticospinal tract injury in adult rat spinal cord. *Eur. J. Neurosci.* **26,** 2496–2505 (2007).

24. Rodger, J. *et al.* Expression of ephrin-A2 in the superior colliculus and EphA5 in the retina following optic nerve section in adult rat. *Eur. J. Neurosci.* **14,** 1929–1936 (2001).

25. Rodger, J. *et al.* Eph/ephrin expression in the adult rat visual system following localized retinal lesions: Localized and transneuronal up-regulation in the retina and superior colliculus. *Eur. J. Neurosci.* **22,** 1840–1852 (2005).

26. Figueroa, J. D. *et al.* Inhibition of EphA7 up-regulation after spinal cord injury reduces apoptosis and promotes locomotor recovery. *J. Neurosci. Res.* **84,** 1438–1451 (2006).

27. Rogers, C. J. Discovery of New Roles for Chondroitin Sulfate in Neurotrophin Signaling and Retinotopic Development. (California Institute of Technology, 2012).

28. Miranda, J. D. *et al.* Induction of Eph B3 after spinal cord injury. *Exp. Neurol.* **156,**

218–222 (1999).

29. Willson, C. A., Miranda, J. D., Foster, R. D., Onifer, S. M. & Whittemore, S. R. Transection of the adult rat spinal cord upregulates EphB3 receptor and ligand expression. *Cell Transpl.* **12,** 279–290 (2003).

30. Silver, J. & Miller, J. H. Regeneration beyond the glial scar. *Nat. Rev. Neurosci.* **5,** 146–156 (2004).

31. Sharma, K., Selzer, M. E. & Li, S. Scar-mediated inhibition and CSPG receptors in the CNS. *Exp. Neurol.* **237,** 370–378 (2012).

32. Xu, K. *et al.* Insights into Eph receptor tyrosine kinase activation from crystal structures of the EphA4 ectodomain and its complex with ephrin-A5. *Proc. Natl. Acad. Sci.* **110,** 14634–14639 (2013).

33. Bordoli, L. *et al.* Protein structure homology modeling using SWISS-MODEL workspace. *Nat. Protoc.* **4,** 1–13 (2009).

34. Mayo, S. L., Olafson, B. D. & Goddard, W. A. DREIDING: a generic force field for molecular simulations. *J. phys. Chem* **94,** 8897–8909 (1990).

Appendix A: Retinal Axon Guidance by Synthetic Chondroitin Sulfate Polymers

Chondroitin sulfate proteoglycans (CSPGs) are critically important for the proper development of the nervous system.[1,2] These proteoglycans can serve as positive and negative guidance cues, attracting or repelling extending axons and direct axons to their correct downstream synaptic targets.[3] The precise targeting of extending axons is essential for the formation of a correctly function mature nervous system. Our lab previously demonstrated the importance of the CS-E motif towards the guidance of extending retinal ganglion neurons. CS-E polysaccharides repulse retinal axons originating from ventral tissue, but has no effect on retinal axons from dorsal tissue.[4] Here, the ability of CS mimetic polymers to guide extending retinal axons was tested using the stripe assay. These mimetic polymers have been shown to recapitulate the biological activity of natural CS.[5] For example, CS-E mimetic polymers inhibit dorsal root ganglion neuron growth similar to CS-E polysaccharides isolated from natural sources.

The stripe assay is a common test for retinal axon guidance.[6] In this assay, CS—E polysaccharides or CS-E mimetic polymers were mixed with bovine serum albumin labeled with Alexa Fluor-488 (BSA-488) are flowed through a microfluidic device containing 50 μm wide channels spaced 50 μm apart (Fig. A.1a). This process results in efficient immobilization of the putative guidance molecule and BSA-488 in stripes on a glass coverslip (Fig. A.1b). Following stripe printing, whole retina, dissected from E7 chick, are flat-mounted for tissue slicing along the dorsal-ventral axis (Fig. A.1c). Tissues strips are placed on the glass coverslip perpendicular to the printed stripes (Fig A.1d). Extending

axons grow preferentially on the more permissive stripes, the experimental or control stripes.

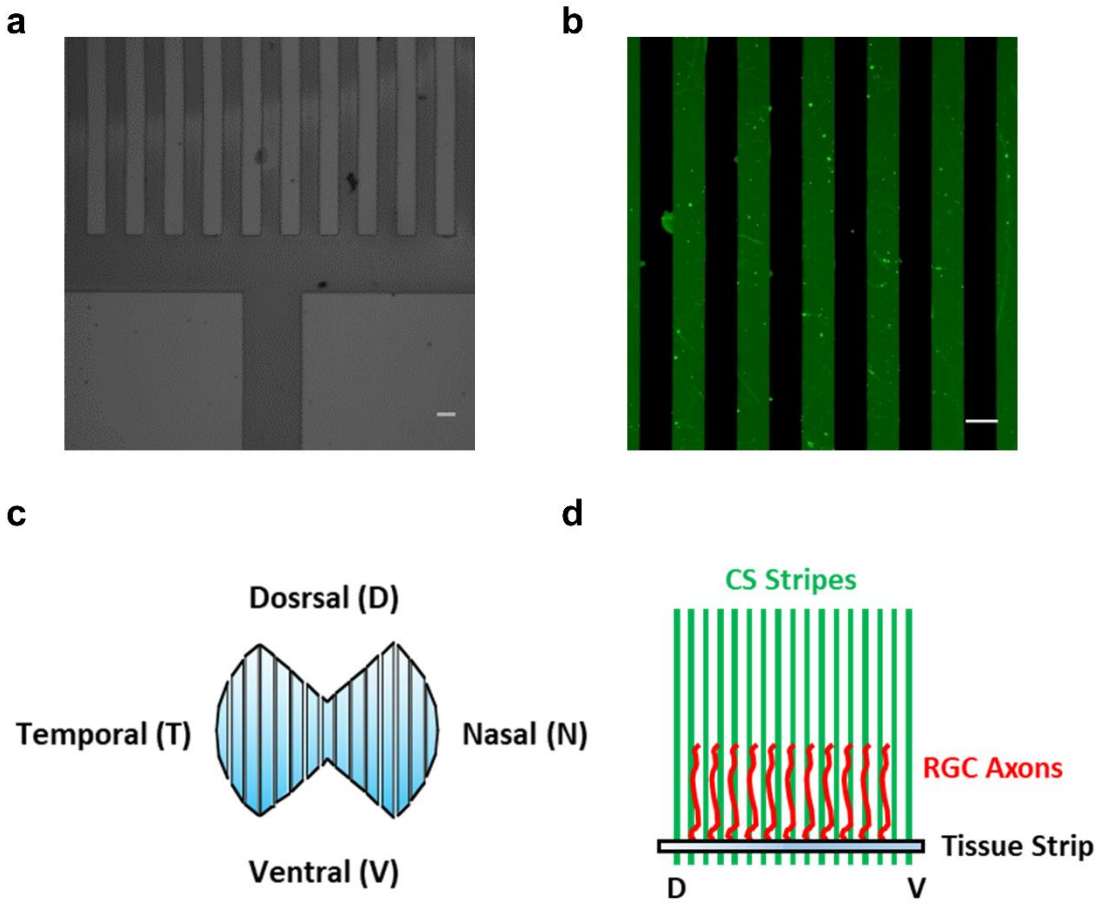

Figure A.1: Stripe Assay, assessment of Axon guidance of retinal neurons. Axon guidance molecules are immobilized in stripes on glass coverslips, retinal tissue explants are mounted perpendicular to the printed stripes, and as axons extend they are attracted, or repelled from the printed stripes. (**a**) Microfluidic devices containing 50 µm wide channels space 50 µm apart. Devices are placed on a glass coverslip, and a solution containing the putative axon guidance molecule, and bovine serum albumin labeled with alexaflour-488 (BSA-488), is flowed through the device and immobilized on the glass coverslip (scale bar, 50µm). (**b**) Representative stripes containing BSA-488 and CS polysaccharides immobilized to glass coverslip (scale bar, 50µm). (**c**) Chick retinal tissue post dissection is flat-mounted for slicing along the dorsal-ventral axis. (**d**) Schematic of stripe assay, dorsal-ventral tissue strips are mounted on pre-printed stripes containing BSA-488 and CS polysaccharides. Retinal tissue explants are cultured for 48 hr, fixed, and stained with Rhodamine B isothiocyanate.

To assess the guidance properties of CS mimetic polymers, the stripe assay was performed using CS-E polysaccharides or CS-E mimetic polymers. Both were efficiently immobilized on glass coverslips. As noted, previous work demonstrated ventral retinal axons, but not dorsal axons, are guided by CS-E polysaccharides.[4] These results were reproduced using CS-E polysaccharides in this study (Fig. A.2a). Tissue originating from the dorsal portion of the retina grow non-discriminately across CS-E polysaccharide printed stripes. While extending ventral axons are guided parallel to the printed CS-E polysaccharide stripes. CS-E polymers also guided ventral axons (Fig. A.2b). Extending ventral axons are guided as they grow on stripes printed with CS-E polymers. However, ventral axons are also guided by CS-E polymers. These results suggest the guidance activity of CS-E polymers does not fully recapitulate the activity of natural polysaccharides. Nerveless, CS-E mimetic polymers elicit a similar response towards the guidance of extending retinal axons.

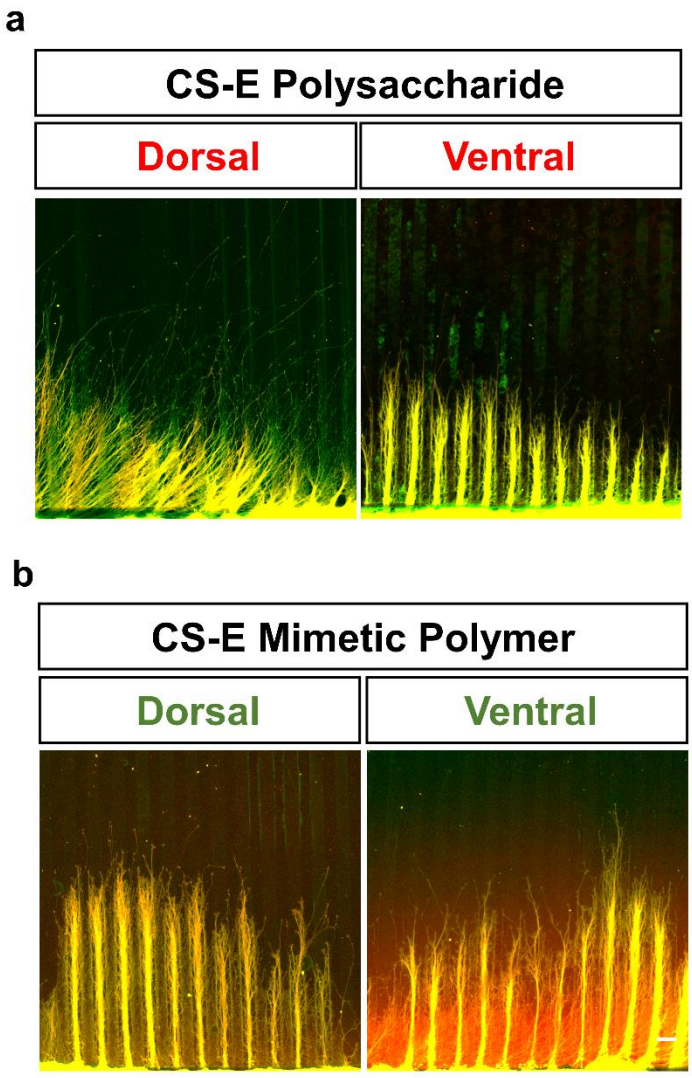

Figure A.2: Retinal Axon Guidance by Cs Mimetic Polymers The stripe assay was used to test axon guidance of retinal neurons by CS mimetic polymers. (**a**) Representative images of stripe assay with immobilized CS-E polysaccharides. Ventral retinal axons, but not dorsal, avoid stripes printed with CS-E polysaccharides. (**b**) Representative images of stripe assay with immobilized CS-E mimetic polymer. Dorsal and ventral axons both are guided by printed CS-E mimetic polymers (scale bar, 100μm).

Methods

Stripe Assay Square 22 x 22 mm acid washed glass coverslips were coated with poly-D-lysine (0.1 mg/mL in PBS). The coverslips were wash three times with PBS and three times with water, and allowed to air dry in the hood. Sterile microfluidic devices were mounted on the glass coverslips and connected to a syringe pump through the inlet and outlet valves.[6] The printing solution (containing chondroitin sulfate polysaccharide or mimetic polymer 0-20 μg/mL, laminin 10 μg/mL, BSA-488 10μg/mL, and 0.05% tween in PBS) was flowed through the device at a rate of 50 μL/h overnight. Microfluidic devices were removed from coverslips, and coverslips were washed three times with PBS and coated with laminin (10 μg/mL in PBS) for 2 h at room temperature, and then washed three times with PBS. Retina were dissected, flat-mounted, sliced, and cultured as previously described.[4] Retinal tissue was cultured on the printed coverslips for 36 h, before fixing and staining with rhodamine B isothiocyanate. Coverslips were imaged using an LSM 700, and images were prepared using ImageJ.

References

1. Bashaw, G. J. & Klein, R. Signaling from axon guidance receptors. *Cold Spring Harb. Perspect. Biol.* **2,** a001941 (2010).
2. Beller, J. A. & Snow, D. M. Proteoglycans: road signs for neurite outgrowth. *Neural Regen. Res.* **9,** 343 (2014).
3. Miller, G. M. & Hsieh-Wilson, L. C. Sugar-dependent modulation of neuronal development, regeneration, and plasticity by chondroitin sulfate proteoglycans. *Exp. Neurol.* **274,** 115–125 (2015).
4. Rogers, C. J. Discovery of New Roles for Chondroitin Sulfate in Neurotrophin Signaling and Retinotopic Development. (California Institute of Technology, 2012).
5. Brown, J. M. *et al.* A sulfated carbohydrate epitope inhibits axon regeneration after injury. *Proc. Natl. Acad. Sci.* **109,** 4768–4773 (2012).
6. Knöll, B., Weinl, C., Nordheim, A. & Bonhoeffer, F. Stripe assay to examine axonal guidance and cell migration. *Nat. Protoc.* **2,** 1216–1224 (2007).

Appendix B: Disaccharide Analysis of the Visual Cortex of Sulfotransferase Knockout Mice

CSPGs are also major components of perineuronal nets (PNNs), where they play crucial roles in the maturation of synapses and the closure of critical periods by limiting synaptic plasticity.[1–4] PNNs, which consist of CSPGs, tenascin, link-proteins and hyaluronic acid, surround the cell body and extend along the dendrites of inhibitory neurons expressing the calcium-binding protein parvalbumin (PV). They serve to restrict synaptic plasticity and stabilize the network of existing neuronal connections.[1–4] The CSPGs in PNNs, and in particular, their CS sugar chains, are essential to the structure and function of PNNs. Digestion of the CS sugars by ChABC in the visual cortex reactivated critical period plasticity following monocular deprivation in adult mice.[5,6]

Specific sulfation motifs on CSPGs have been shown to regulate PNN formation and critical period plasticity.[4] The sulfation patterns of CSPGs are tightly regulated during postnatal development in the mouse visual cortex. While 6-*O* sulfation of CS (CS-C) decreases, 4-*O* sulfation (CS-A) increases as the critical period comes to a close, resulting in an increase in the 4-*O* to 6-*O* sulfate (4S/6S) ratio.[7] Transgenic mice overexpressing C6ST-1 retain a low 4S/6S ratio and develop fewer PNNs around PV neurons.[7] Their PNNs are rich in CS-C and display a diffuse structure that is unable to tightly enwrap thalamocortical synaptic contacts. Importantly, the mice also exhibit persistent cortical plasticity into adulthood. When subjected to monocular deprivation, adult mice overexpressing C6ST-1 show ocular dominance plasticity similar to juvenile wild-type mice. Thus, the change from low to high 4S/6S sulfation ratio on CSPGs coincides with

the close of the critical period when plasticity is restricted, and reducing this ratio can modulate PNN structure and enhance cortical plasticity.

To explore the role of the CS-A and CS-E motifs in regulating neuronal plasticity, we utilized *Chst15* (CS-E knockout), and *Chst11* (CS-A knockout) mice.[8,9] The *Chst11* mouse is a conditional knockout in the brain under the nestin promoter, while the *Chst15* mouse is a constitutive knockout. Here, the disaccharide content of the visual cortex was analyzed for *Chst11* knockout, *Chst15* knockout, and wild type mice at the postnatal day 0, 7, 14, 28, and 60. Glycosaminoglycan side chains were isolated form the visual cortex and digested with chondroitinase, and disaccharides were labeled with 2-aminoacridone and quantified by HPLC.[10] The analysis is summarized in Figures B.1, B.2, and B.3. Interestingly, *Chst11* knockout mice have significantly less total CS (Fig. B.2a). This is consistent with reports that this sulfotransferase is involved in chain elongation as *Chst11* knockout cells produced shorter CS chains than wild type.[11] The *Chst11* knockout mouse has significantly reduced levels of CS-A, and increased levels of CS-C and unsulfated CS. Likewise, *Chst11* and *Chst15* knockout mice have no detectable levels of CS-E. These initial findings confirm the loss of specific sulfation patterns in sulfotransferase knockout mice. Namely, these mice lack the CS-A and CS-E motifs, sulfation patterns important for regulating neuronal plasticity, and provide a platform for studying the roles of these sulfation motifs in neuronal plasticity.

	Unsaturated disaccharide [pmol/mg (mol %)]					
	ΔDi-0S	ΔDi-6S	ΔDi-4S	ΔDi-diS$_D$	ΔDi-diS$_E$	Total
Wild-type						
P0	70.7 ± 8.7 (17.3)	115.6 ± 12.3 (28.3)	205.5 ± 16.8 (50.3)	7.8 ± 1.1 (1.9)	9.0 ± 1.2 (2.2)	408.6 ± 22.6 (100)
P7	56.3 ± 6.5 (13.5)	93.4 ± 9.6 (22.4)	254.3 ± 15.3 (61.0)	5.8 ± 0.8 (1.4)	7.1 ± 0.7 (1.7)	416.9 ± 19.2 (100)
P14	32.3 ± 4.6 (8.4)	38.8 ± 5.3 (10.1)	302.0 ± 19.5 (78.6)	6.1 ± 0.9 (1.6)	5.0 ± 0.6 (1.3)	384.2 ± 20.8 (100)
P28	30.3 ± 5.1 (8.2)	8.9 ± 3.1 (2.4)	320.7 ± 20.1 (86.8)	4.4 ± 0.7 (1.2)	5.2 ± 0.9 (1.4)	369.5 ± 21.0 (100)
P60	27.6 ± 4.0 (7.6)	9.8 ± 2.8 (2.7)	318.9 ± 18.0 (87.9)	2.5 ± 0.4 (0.7)	4.0 ± 0.5 (0.7)	362.8 ± 18.7 (100)
Chst15-KO						
P0	74.6 ± 6.9 (18.8)	103.2 ± 9.8 (26.0)	210.7 ± 15.0 (53.1)	8.3 ± 0.5 (2.1)	N.D.	396.8 ± 19.2 (100)
P7	66.2 ± 7.1 (16.5)	97.5 ± 12.3 (24.3)	230.3 ± 17.8 (57.4)	7.2 ± 0.8 (1.8)	N.D.	401.3 ± 22.8 (100)
P14	27.0 ± 5.6 (6.8)	46.9 ± 7.6 (11.8)	320.9 ± 16.9 (80.7)	2.8 ± 0.9 (0.7)	N.D.	397.7 ± 19.4 (100)
P28	25.9 ± 4.9 (7.2)	9.3 ± 6.9 (2.6)	320.4 ± 21.3 (89.1)	4.0 ± 1.2 (1.1)	N.D.	359.6 ± 23.0 (100)
P60	22.5 ± 5.3 (6.5)	8.0 ± 8.1 (2.3)	316.5 ± 19.7 (91.4)	2.8 ± 1.4 (0.8)	N.D.	346.3 ± 22.1 (100)
NesChst11-KO						
P0	121.0 ± 9.3 (45.6)	119.7±8.7 (45.1)	14.3 ± 4.3 (5.4)	10.3 ± 1.5 (3.9)	N.D.	265.3 ± 13.5 (100)
P7	122.6 ± 8.6 (47.6)	109.4±12.3 (42.5)	16.7 ± 3.7 (6.5)	8.8 ± 1.2 (3.4)	N.D.	257.5 ± 15.5 (100)
P14	118.4 ± 10.2 (52.3)	83.7±11.9 (37.0)	17.4 ± 4.0 (7.7)	6.8 ± 1.0 (3.0)	N.D.	226.3 ± 16.2 (100)
P28	111.4 ± 7.5 (53.1)	73.2±9.8 (34.9)	17.2 ± 6.2 (8.2)	8.0 ± 0.9 (3.8)	N.D.	209.8 ± 13.8 (100)
P60	115.1 ± 8.1 (53.2)	76.4±10.6 (35.3)	18.6 ± 5.8 (8.6)	6.3 ± 1.3 (2.9)	N.D.	216.36 ± 14.6 (100)

Figure B.1: Disaccharide Analysis of Chst11 and Chst15 Knockout Mice. Glycosaminoglycans were isolated from the visual cortex of *Chst11* knockout*, Chst15* knockout, and wild type mice, digested with chondroitinase ABC, and disaccharides were analyzed by HPLC. The disaccharides are expressed as pmol/mg of dried tissue homogenate, and as a percentage of the total disaccharide content. This analysis was performed on tissue dissected from P0, P7, P14, P28, and P60 mice, and represent the average values from three mice. N.D. = not detected.

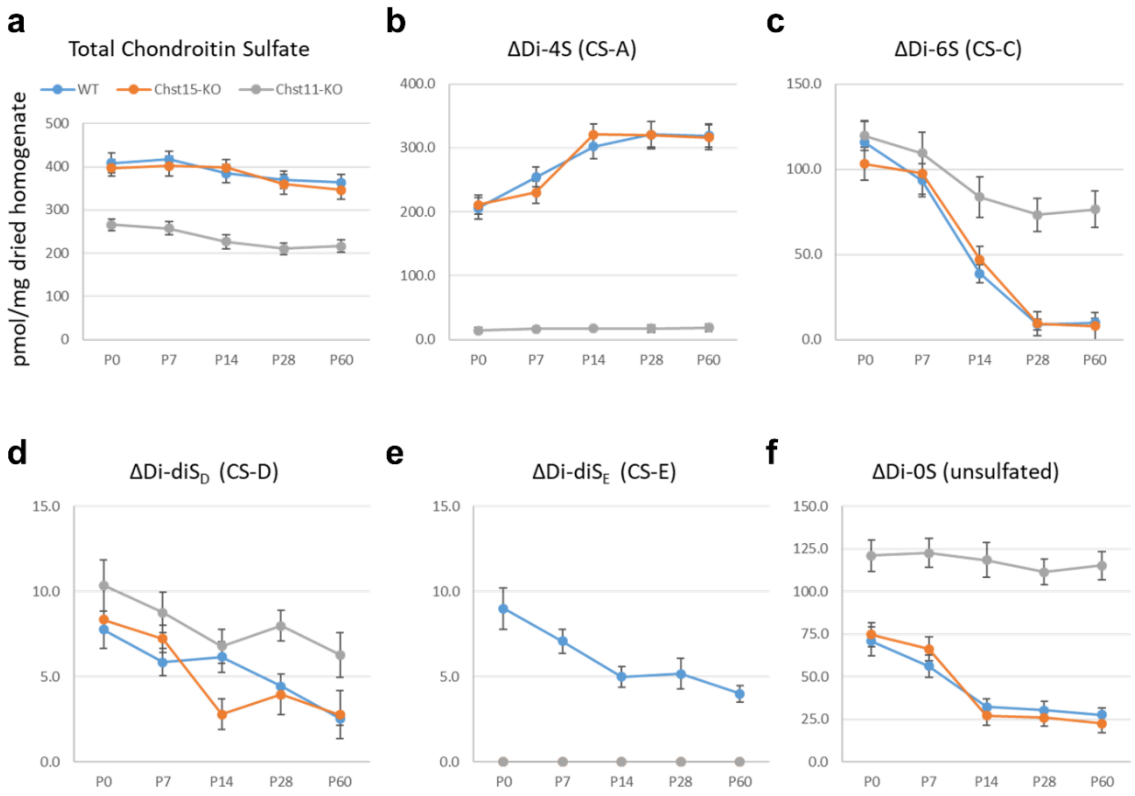

Figure B.2: Disaccharide Analysis of Visual Cortex. Glycosaminoglycans were isolated from the visual cortex of *Chst11 knockout*, *Chst15* knockout, and wild type mice, digested with chondroitinase ABC, and disaccharides were analyzed by HPLC. The disaccharides are expressed as pmol/mg of dried atissue homogenate. This analysis was performed on tissue dissected from P0, P7, P14, P28, and P60 mice, and represent the average values from three mice. (**a**) Total disaccharide content, (**b**) CS-A (ΔDi-4S), (**c**) CS-C (ΔDi-6S), (**d**) CS-D (ΔDi-diS$_D$), (**e**) CS-E (ΔDi-diS$_E$) content in the visual cortex. CS-E disaccharides were not detected in *Chst11* or *Chst15* knockout mice. *Chst11* knockout mice have less CS per mg of dried tissue homogenate than WT or *Chst15* knockout mice.

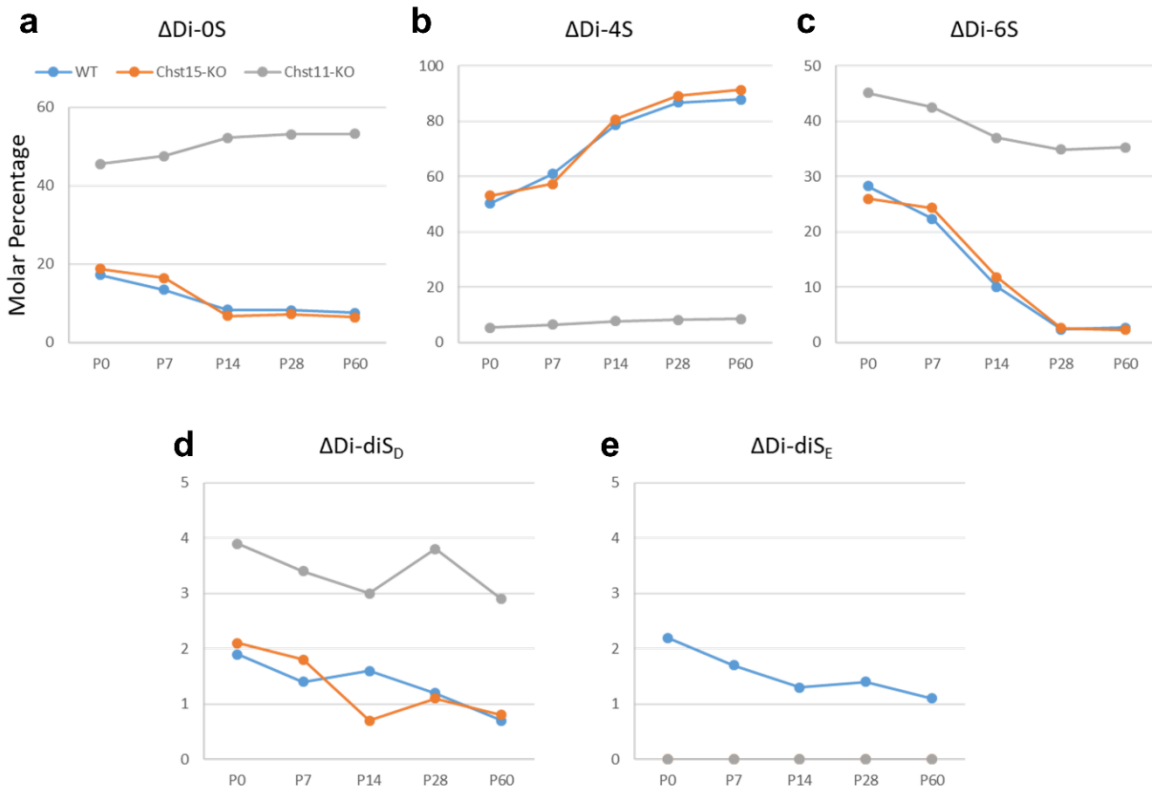

Figure B.3: Disaccharide Analysis of Visual Cortex as Molar Percentage. Glycosaminoglycans were isolated from the visual cortex of *Chst11 knockout*, *Chst15* knockout, and wild type mice, digested with chondroitinase ABC, and disaccharides were analyzed by HPLC. The disaccharides are expressed as pmol/mg of dried tissue homogenate. This analysis was performed on tissue dissected from P0, P7, P14, P28, and P60 mice, and represent the average values from three mice. (**a**) CS-A (ΔDi-4S), (**b**) CS-C (ΔDi-6S), (**c**) CS-D (ΔDi-diS$_D$), (**d**) CS-E (ΔDi-diS$_E$) content in the visual cortex. CS-E disaccharides were not detected in *Chst11* or *Chst15* knockout mice.

Methods

GAG Purification. The visual cortex was dissected, placed in a 2 mL dounce and homogenized in acetone. The sample was centrifuged at 4,000 x g for 2 min, supernatant discarded, and pellet washed three times with cold acetone, then allowed to air dry. The pellet was resuspended in digestion buffer (100 mM Tris pH 7.4, 20 mM $CaCl_2$, with 5 mg/mL Pronase; Sigma Aldirch). Samples were digested at 55 °C for 24 h. DNase was added and samples digested for 1 h at 37 °C. Samples were pelleted at 15,000 x g for 10 min, supernatant transferred to a 10,000 mw cutoff spin column and buffer exchanged to 50 mM Tris pH 7.4, 200 mM NaCl by repeated centrifugation and concentration of the sample. Samples were collected, made to 2 mL total volume, and passed over 0.5 mL of pre-equilibrated DEAE Sepharose resin. The resin was washed with 10 column volumes using 50 mM Tris pH 7.4, 200 mM NaCl. The GAGs were eluted with 6 column volumes of 16% NaCl, buffer exchanged to water using 10,000 mw cutoff spin column, and then lyophilized. GAGs were dissolved in 50 µL 25 mM Tris pH 8.0, 30 mM NaOAc. The uronic acid concentrations of the samples were determined using the carbazole assay.

Disaccharide Analysis. Disaccharide analysis was performed as previously reported.[10] The GAGs (50 µL) were diluted to 200 µL with the same buffer and digested with 50 mU of chondroitinase ABC (Seikagaku) at 37 °C for 24 h. The reaction was put into a 3,000 MWCO spin filter, centrifuged at 12,000 x g for 10 min, and the eluate was collected. This procedure was repeated twice more by adding 200 µL of water to the retentate. The eluates were pooled and lyophilized. For 2-aminoacridone (AMAC) labeling, 5 µL of a solution containing 0.1 M AMAC in 3:18 glacial acetic acid:DMSO was added to 1 µg of CS disaccharide and incubated for 15 min at room temperature. 5 uL of 1 M $NaBH_3CN$ was

added, and the reaction was incubated for 4 h at 45 °C. The reaction was quenched with 1:1 DMSO:water and analyzed by HPLC with a Poroshell 120 EC-C18 column (4.6 x 50 mm) with the following method at a flow rate of 1 mL/min and detection at 428 nm: linear gradient of 98% 60 mM NH4OAc and 2% MeCN to 70% 60 mM NH4OAc and 30% MeCN for 50 min, followed by 15 min of 98% 60 mM NH4OAc and 2% MeCN. P-values were determined using one-way ANOVA with Tukey's HSD post hoc analyses, and the results from three experiments were shown.

References:

1. Berardi, N., Pizzorusso, T., Ratto, G. M. & Maffei, L. Molecular basis of plasticity in the visual cortex. *Trends Neurosci.* **26,** 369–378 (2003).
2. Dityatev, A., Schachner, M. & Sonderegger, P. The dual role of the extracellular matrix in synaptic plasticity and homeostasis. *Nat. Rev. Neurosci.* **11,** 735–746 (2010).
3. Kwok, J. C., Dick, G., Wang, D. & Fawcett, J. W. Extracellular matrix and perineuronal nets in CNS repair. *Dev. Neurobiol.* **71,** 1073–1089 (2011).
4. Miyata, S. & Kitagawa, H. Mechanisms for modulation of neural plasticity and axon regeneration by chondroitin sulphate. *J. Biochem.* **157,** 13–22 (2015).
5. Pizzorusso, T. *et al.* Reactivation of ocular dominance plasticity in the adult visual cortex. *Science (80-.).* **298,** 1248–1251 (2002).
6. Pizzorusso, T. *et al.* Structural and functional recovery from early monocular deprivation in adult rats. *Proc. Natl. Acad. Sci.* **103,** 8517–8522 (2006).
7. Miyata, S., Komatsu, Y., Yoshimura, Y., Taya, C. & Kitagawa, H. Persistent cortical plasticity by upregulation of chondroitin 6-sulfation. *Nat. Neurosci.* **15,** 414–422 (2012).
8. Ohtake-Niimi, S. *et al.* Mice deficient in N-acetylgalactosamine 4-sulfate 6-O-sulfotransferase are unable to synthesize chondroitin/dermatan sulfate containing N-acetylgalactosamine 4, 6-bissulfate residues and exhibit decreased protease activity in bone marrow-derived mast cells. *J. Biol. Chem.* **285,** 20793–20805 (2010).
9. Bian, S. *et al.* Dermatan sulfotransferase Chst14/D4st1, but not chondroitin sulfotransferase Chst11/C4st1, regulates proliferation and neurogenesis of neural

progenitor cells. *J Cell Sci* **124,** 4051–4063 (2011).

10. Volpi, N., Galeotti, F., Yang, B. & Linhardt, R. J. Analysis of glycosaminoglycan-derived, precolumn, 2-aminoacridone–labeled disaccharides with LC-fluorescence and LC-MS detection. *Nat. Protoc.* **9,** 541–558 (2014).
11. Izumikawa, T., Okuura, Y., Koike, T., Sakoda, N. & Kitagawa, H. Chondroitin 4-O-sulfotransferase-1 regulates the chain length of chondroitin sulfate in co-operation with chondroitin N-acetylgalactosaminyltransferase-2. *Biochem. J.* **434,** 321–331 (2011).